4-2-2010

Polarization of Galvanic Point Anodes for Corrosion Prevention in Reinforced Concrete

Margareth Dugarte
University of South Florida

Polarization of Galvanic Point Anodes for Corrosion Prevention in Reinforced Concrete

by

Margareth Dugarte

A dissertation submitted in partial fulfillment
of the requirements for the degree of
Doctor of Philosophy
Department of Civil and Environmental Engineering
College of Engineering
University of South Florida

Major Professor: Alberto A. Sagüés, Ph.D.
Rajan Sen, Ph.D.
Andrés Tejada-Martinez, Ph.D.
Matthias Batzill, Ph.D.
Venkat Bhethanabotla, Ph.D.

Date of Approval:
April 2, 2010

Keywords: zinc, cathodic protection, patch repair, reinforcing steel, potential

ACKNOWLEDGMENTS

I would like to thank my advisor, Dr. Alberto Sagüés, whose guidance, supervision and support from the early stages to the concluding level of this project, allowed me to finish this dissertation. Appreciation is given to my examining committee chairperson Dr. Alex Volinsky and members, Dr. R. Sen, A. Tejada-Martinez, M. Batzill, and V. Bhethanabotla for their interest.

The author appreciates the financial support provided from the Florida Department of Transportation and the U.S. Department of Transportation for the research discussed in this dissertation.

I wish to thank my colleagues from Corrosion Laboratory at USF, Kingsley Lau, Ezeddin Busba, Andrea Sanchez, Adrienne Accardi, Mersedeh Akhoondan and Brandon Berke, they all assisted and encouraged me in various ways during my permanency in the laboratory. The author thanks Maria Constanza Suarez and Gary Spicer for their collaboration in the experimental phase of the project.

Finally, I would like to thank my husband, Ulises Orozco, who provided support throughout this dissertation process, as well as confidence and love. My parents, Daniel Dugarte and Yaneth Coll and my sisters, Elisama, Yamile and Mercelena, for their love, support, and patience over the last 5 years. This dissertation is dedicated to them.

TABLE OF CONTENTS

LIST OF TABLES

LIST OF FIGURES

POLARIZATION OF GALVANIC POINT ANODES FOR CORROSION PREVENTION IN REINFORCED CONCRETE

Margareth Dugarte

ABSTRACT

The polarization performance of two types of commercial galvanic point anodes for protection of reinforced steel around patch repairs was investigated. Experiments included measurement of the polarization history of the anode under constant current impressed by galvanostatic circuits and in reinforced concrete slabs. The tests revealed, for both types of anodes, a potential-current function (PF) indicating relatively little anodic polarization from an open circuit potential at low current levels, followed by an abrupt increase in potential as the current approached an apparent terminal value. Aging of the anodes was manifested by a continually decreasing current output in the concrete tests, and by increasingly more positive potentials in the galvanostatic tests. Those changes reflected an evolution of the PF generally toward more positive open circuit potentials and, more importantly, to the onset of elevated polarized potentials at increasingly lower current levels. There was considerable variability among the performance of replicate units of a given anode type. Modest to poor steel polarization levels were achieved in the test yard slabs. Modeling of a generic patch configuration was implemented with a one-dimensional approximation. The model calculated the throwing distance that could be achieved by a given number of anodes per unit perimeter of the patch, concrete thickness, concrete resistivity, amount of steel and amount of polarization

needed for cathodic prevention. The model projections and aging information suggest that anode performance in likely application scenarios may seriously degrade after only a few years of operation, even if a relatively optimistic 100 mV corrosion prevention criterion were assumed. Less conservative criteria have been proposed in the literature but are yet to be substantiated. Other investigations suggest a significantly more conservative corrosion prevention may apply instead. The latter case would question the ability of the point anodes to provide adequate corrosion prevention.

1. INTRODUCTION

1.1 Background

Corrosion of reinforcing steel in concrete is of major concern due to the associated cost and possible structural degradation. It has been estimated to cost billions of dollars per year to restore or replace damaged structures, and corrosion can result in failure of structural elements. The direct cost of corrosion in infrastructure is about $22.6 billion per year according to recent studies by the Federal Highway Administration. Indirect societal costs can be considerably higher [FHWA 2002].

There are approximately 600,000 highway bridges in the U.S and more than 15% of them are affected by corrosion damage [FHWA 2002]. These statistics underscore the impact of corrosion on the economy of developed nations. The associated safety and financial liability issues warrant the need for development of techniques and procedures to effectively control corrosion. The corrosion control of reinforcing steel in concrete is then a significance maintenance practice that government agencies and industry have address to reduce adverse impact.

Chloride-induced corrosion of steel in concrete is one of the major causes of bridge deck and marine substructure deterioration. The presence of chlorides results from exposure to sea water in coastal locations and application of de-icing salts on roadways in northern states. When chlorides reach the steel surface active corrosion ensures forming expansive corrosion products that crack the concrete cover. The concrete delamination, cracking and spalling if left

unmitigated can require costly maintenance of even eventually cause structural failure. Repairs often consist of removing the cracked concrete and replacing it with chloride-free concrete. It takes only a small amount of corrosion metal loss (e.g. ~0.1 mm (0.004 in)) at the reinforcing steel bar (rebar) surface to create corrosion products sufficient to generate internal stresses that crack the concrete [Torres-Acosta 2004]. Thus, repairs often do not involve rebar replacement, as the remaining steel cross section is still adequate. However, patch repairs limited to the portions of the structure that showed conspicuous cracking may have detrimental consequences. As is often the case, zones adjacent to the patch have already had substantial chloride contamination. As will be discussed in the following, corrosion can rapidly develop there promoted by the newly placed patch, and small ("point") anodes at the periphery of the new patch are often recommended as a means to alleviate that problem. This investigation focuses in evaluating the performance of those anodes in concrete repair applications.

1.2 Literature Review

1.2.1 Corrosion of Steel in Concrete

Steel in concrete is normally in the passive condition (protected against corrosion by a nanoscale-thick oxide film) formed due to the highly alkaline nature of the pore water (pH 12.5 to 13). However, the film is disrupted by events such as a decrease in the pH of the pore water due to carbonation, or intrusion of chloride ions from the external environment. The latter modality tends to result in earlier distress in bridge applications and will be considered here. Corrosion starts when the chloride concentration at the rebar surface exceeds a critical value known as the chloride corrosion threshold (C_T). Much of the information available on the value of C_T concerns atmospherically exposed concrete. In that case the potential E between an isolated plain rebar steel segment and the immediately surrounding concrete tends to be, when passive, in the range -100

to -200 mV in the Copper/Copper Sulfate Electrode (CSE). In those conditions C_T is typically >~0.4% of the mass of cement per unit value in the concrete [Li 2001]. The value of C_T depends on many variables such as the rebar material [Hurley 2006], the pH of the concrete pore water [Li 2001, Gouda 1970, Hausmann 1967] and the presence or voids [Glass 2007]. Of importance to the present work, C_T has been found to depend also on the value of E for the passive steel in a manner that reflects the well known dependence between pitting potential and chloride content in other systems [Szklarska-Smialowska 1986]. The evidence available to date for steel in concrete is limited, but it suggests that if all other factors remain the same, C_T tends to increase manifold when E decreases from ~-150 to ~-600mV CSE. There is uncertainty as to the precise amount o polarization needed for a given effect [Presuel-Moreno 2005A, Alonso 2000, 2002; Izquierdo 2004, Pedeferri 1996].

There are four components present for corrosion of steel reinforcement in concrete to occur: the concrete pore water or electrolyte, oxidation of iron ($Fe \rightarrow Fe^{++} + 2e-$), oxygen reduction in presence of water ($O_2 + 2H_2O + 4e- \rightarrow 4\ OH^-$), and an electronic path between anodic and cathodic regions in the steel rebar assembly. The value of E for an isolated rebar segment is determined by the interplay between cathodic electron-consuming reactions (principally the reduction of dissolved oxygen in the pore water indicated above) and anodic electron-producing reactions (such as the dissolution of iron from the rebar indicated above). In the passive condition the rate of iron dissolution, or passive corrosion rate, is very small [Sagüés 2003] and the resulting mixed potential [Fontana 1986] for the system is in the relatively less negative value range given earlier. After C_T is exceeded, the rate of the anodic reaction increases dramatically. The resulting mixed potential of steel that is corroding actively in atmospherically exposed chloride-contaminated concrete drops, typically to values E_{ACT} in the ~-300 mV to -600 mV SCE range [Bentur 1997, Broomfield 1997, Li 2001].

1.2.2 Cathodic Protection and Cathodic Prevention

These modes of corrosion control and their differences and associated terminology are reviewed here as they pertain to the scope of this investigation.

Cathodic protection in concrete is a method for decreasing the corrosion rate of steel that is already in the actively corroding stage. The decrease is achieved by lowering the steel potential to a value below that which existed in the freely corroding condition. The rate of corrosion is that of the net anodic reaction, which decreases strongly as the potential becomes more negative following usual electrochemical kinetic laws [Fontana 1986]. Assuming on first approximation Tafel kinetics and neglecting the effect of the metal deposition reaction, a decrease in potential by an amount equal to one Tafel slope (typically in the order of 0.1V [Jones 1996] would lower the corrosion rate by about 90%. It is then not surprising that practical criteria for achieving cathodic protection, based on operating experience, specify a polarization level of 100 mV below the freely corroding potential as a criterion for effective application of cathodic protection [Funahashi 1991]. In addition to direct action on anodic kinetics, the electric field driving the cathodic polarization current tends over time to respectively decrease and increase the concentrations of chloride and hydroxide ions at the rebar surface. Depending on the electric field strength [Glass 1997], those changes may actually restore passivity on the rebar surface.

Cathodic prevention is based on the entirely different concept from that of cathodic protection. In cathodic prevention the potential of the passive steel is shifted from its natural value in the negative direction *before* the onset of active corrosion, to substantially delay or prevent the initiation of such corrosion when the passive film is still in place. The change to a more negative potential has the effect, noted above, of increasing the value of C_T so that the steel can withstand significantly greater chloride content in the surrounding concrete before sustained passivity breakdown takes place. In other words, this preventive

cathodic polarization extends (sometimes indefinitely) the time period before any corrosion starts. The mechanism responsible for this effect is not precisely known, but it may involve phenomena observed in other systems such as improved resistance of the passive film to chloride ions [Macdonald 1992], or destabilization of incipient pits [Frankel 1998] as the polarization becomes less anodic. Such processes involve conditions quite different from those present on fully active rebar, so criteria such as the 100 mV shift for cathodic protection [Funahashi 1991] do not necessarily apply to cathodic prevention cases. As indicated earlier, there is uncertainty as to the value of the potential at which the passive rebar needs to be held to achieve a given increase in C_T, an issue that will be addressed later in this document. There is agreement however that the current density needed to cathodically shift the potential by a given amount from the freely corroding condition is significantly less for passive than for active rebar [Glass 1997, Pedeferri 1996]. Thus, if the required potential shifts were comparable, cathodic prevention would be comparatively easier to implement than cathodic protection. For example, the lesser driving potential of a galvanic system may suffice in a cathodic prevention application, while an impressed current system may be needed for cathodic protection.

The polarization needed for cathodic protection or prevention may be achieved either with impressed current or galvanic systems [Broomfield 1997]. Typical reported (independent confirmation may be needed) steel protection current densities range between 2 to 20 mA/m^2 for cathodic protection and a little as 0.2 to 2 mA/m^2 for cathodic prevention [[Glass 1995]. In either case an anode or system of anodes in contact with the concrete is the physical source of the polarizing current, which travels through the concrete to the rebar assembly. Given a certain polarization criterion value, the effectiveness of both cathodic protection and prevention depends also on how far away from the anode the polarization criterion is satisfied. That reach is called the throwing distance. The throwing distance and its decrease with age are important descriptors of the capability of a protection or prevention system.

1.2.3 Corrosion Macrocells and Effect of Patch Repairs

If a rebar segment is not isolated but is instead part of a larger rebar assembly, then because of electrochemical coupling the local value of E at the rebar segment is elevated or decreased if the potential in the surrounding zones is higher or lower respectively than that of the segment if it were isolated. This *macrocell* coupling effect is stronger if the electrical conductivity of the concrete is high (low resistivity) [Sagüés 1990, 2003, Broomfield 1997, Kranc 1994, Kranc 2001, Raupach 1996].

An important consequence of macrocell coupling is that any passive steel surrounding an actively corroding rebar zone may develop E values significantly more negative than if the rebar assembly were discontinuous. As a result, the corroding zone where corrosion had started at an earlier date, is effectively acting as a galvanic anode providing a degree of cathodic prevention to the surrounding passive steel. Thus, C_T in that surrounding steel is increased and active corrosion would not take place there for some time, even if chloride contamination at the rebar depth were already substantial. Such situation takes place in reinforced concrete structures, such as for example a bridge deck in deicing salt service, where chloride contamination was more or less widely distributed and increased with service time. Eventually active corrosion starts at a location where chloride buildup was fastest. The steel surrounding that zone, while still in the passive condition, may be nevertheless in contact with concrete with high chloride content. Corrosion there could have started soon afterwards without the prevention effect mentioned. Models providing visualizations of this effect have been presented elsewhere [Sagüés 1998, 2009A, 2009B].

The zone experiencing corrosion may be patch-repaired by removing the chloride contaminated concrete there and replacing it with fresh, chloride-free concrete. As a result the previously active steel in the patch becomes passive and corrosion stops there. However, that transition to the passive condition also

elevates the potential of the steel in the patch from its former highly negative value to one that can be several hundred mV more positive. Consequently, the cathodic prevention effect on the surrounding zone is lost. The newly lowered value of C_T in the surrounding zone then may be less than the existing local chloride concentration, and active corrosion could promptly start. This detrimental consequence is called a *ring* or *halo* damage around the patch [Broomfield 1997]. In those cases, prevention may be restored by inserting a sacrificial galvanic anode (e.g. made of zinc, which develops a highly negative potential) in the patch-repair zone. That anode takes up the function of the previously corroding rebar and prevents corrosion from starting both in the patch area and its surroundings.

1.2.4 Anodes for Controlling Corrosion Around Patch Repairs

Small galvanic anodes ("point anodes") are available commercially for casting in patch repairs, for the intended purpose of forestalling the halo damage effect [Bennett 2002, Sergi 2001,Whitmore 2003,Bennett 2006]. The anodes usually consist of a zinc alloy piece with steel connecting wires, and embedded in a mortar disk. Electronic connection to the rebar is necessary for these anodes to work, and it is made by tying the wires to the rebar in the patch. The mortar around the zinc alloy is formulated to obtain high pore water pH, increase water retention, or otherwise promote a regime where the formation of a passive film on the alloy is hindered and the alloy stays in an active condition. The mortar may also be engineered to mitigate the effect of expansive anode corrosion products. The alloy composition itself may also be adjusted to promote activity. In such condition the isolated (open circuit) value of E for Zn alloys is highly negative (e.g. ~-1,000 mV CSE). Macrocell coupling with the rebar in both the patch and the surrounding zone then could allow for appreciable lowering of E and restoration of a cathodic prevention regime to a condition comparable to or greater than that existing before the repair. Proprietary patch concrete mixtures

are also marketed to increase the conductivity around the anode and maximize macrocell coupling with the ring zone.

Point anodes as described above were the subject of developmental work and commercial production in Europe during the previous decade [Sergi 2001] followed by introduction in North America by two different companies. Typical production units are illustrated in Figure 1. Much of the marketing of those units has been aimed at residential or parking building applications, but recently there is increasing consideration for highway applications. Of special interest is the mitigation of corrosion around repaired bridge deck spalls patches in inland as well as marine substructure components.

1.2.5 Open Issues to be Addressed

The possibility of large scale applications in highway systems brings up several important performance and durability issues needing resolution. Among those, at the beginning of this investigation there was little documented information on the quantitative relationship between the operating potential of point anodes and the amount of current delivered as function of that potential - the polarization function (PF) of the anode.

There was also a need to know how the ability of the anode to provide protective current would be degraded with service time and the total amount of protective charge that could be delivered. It was also unknown over how long of a distance away from the repair patch the corrosion prevention effect may be obtained for a given potential-current anode function, anode age, and especially anode placement density so that a means of assessing the number of anodes needed (and hence cost) for a given desired effect could be assessed by the potential user.

1.3 Objectives

The main objective of this study is therefore to evaluate galvanic point anodes to determine their performance and applicability for concrete repairs. Based on the needs indicated in the previous section, the present investigation focused on durability and effectiveness as the two key factors deserving attention.

1.3.1 Regarding Durability

a. Determine for selected commercially available point anodes the operating potential/current delivery function, and its dependence on relevant service variables and on service time.

b. Establish anode cumulative capacity (total usable charge delivered) and associated ultimate service life capability.

1.3.2 Regarding Effectiveness

a. Assess the anode ability to achieve cathodic prevention over a usable distance (throwing distance) under realistic service conditions and as a function of the number of anodes needed, so as to establish the means of conducting cost/benefits analyses by potential users.

2. INVESTIGATION METHODOLOGY

2.1 Approach

To achieve the investigation objectives the following two tasks were performed: laboratory experiments addressing durability issues, and modeling addressing effectiveness.

2.1.1 Laboratory Experiments

The polarization behavior of the anodes was examined by two types of tests in concrete. In one experiment the anodes were under constant current impressed by galvanostatic circuits, while in the other the anodes operated in natural macrocell conditions coupled to reinforcing steel in outdoor exposure test slabs.

2.1.2 Modeling

Modeling of a generic patch configuration was implemented to project the performance of point anodes for patch repairs applications as function of service time. The model computations are intended to evaluate the extent of steel polarization that could be achieved by these anodes in situations representative of highway applications. The findings will serve to fill gaps in design criteria for galvanic point anode systems, and enable rational selection and application of corrosion prevention methods that best use limited public fiscal resources.

2.2 Products Selected for Evaluation

In this investigation two types of point anodes in regular commercial production, each from a different manufacturer, were evaluated. These products are designated by the code names C and W. The manufacturers provided the anodes used for the laboratory tests directly to the University of South Florida, identifying those anodes as regular production units. Two sets of anodes from each manufacturer were evaluated. The first set (1st) was provided in 2004 and the second set (2nd) in 2007. The anode model name for each manufacturer was the same for both sets.

For C anodes the mortar pellet surrounding the anode proper was circular (Figure 1) and had an external diameter ~63 mm and thickness ~27 mm. The mortar mass was ~100 g. The zinc alloy anode proper met ASTM B 418-95a Type I requirements according to the manufacturer. The pellet was of highly alkaline mortar, reported by the manufacturer to have pH=14 or greater. The product Material Safety Data Sheet for this product model name identifies cement (no type specified) and lithium hydroxide as major constituents. Destructive examination of a unit of the 1st set revealed an internal solid zinc alloy disk (Figure 2) 44 mm in diameter and 12 mm thick. The zinc alloy mass (after subtracting that estimated for internal steel wires) was 103 g. The steel wires for external connection (~1.5 mm diameter) were embedded in the zinc alloy medallion and extending outwards. Examination of a unit of the 2nd set revealed a ribbed zinc alloy disk (Figure 2) 43 mm in diameter, 19 mm maximum thickness and 115 g alloy mass, with external connection wires as those in the 1st set.

For W anodes the mortar pellet surrounding the anode proper was roughly rectangular (Figure 1), 77 by 60 mm on the sides and 33 mm thick. The mortar mass was ~ 170 g. The zinc alloy met ASTM B418-01 requirements according to the manufacturer. The pellet was of mortar reported by the manufacturer to

contain humectants and proprietary zinc activators. The product Material Safety Data Sheet for this product model name identifies Portland cement and lithium bromide among major constituents, and calcium salt (a synonym for calcium hypochlorite but no clarification given), calcium nitrate and lithium nitrate among minor constituents. Destructive examination of one unit from the 1st set revealed an internal zinc alloy element consisting of four piled rectangular expanded metal mesh squares, 34 mm on the side, with a combined height of 18 mm. A plastic sponge separated the squares into two pairs (Figure 3). The total zinc alloy mass was 48 g. Two steel wires (~1.5 mm diameter) for external connection were wrapped tightly against the expanded metal squares. Examination of three units from the 2nd set (Figure 3) revealed in all cases an internal zinc alloy element consisting of three piled rectangular expanded mesh squares, 34 mm on the side, with a combined height of 14 mm. There was no plastic sponge separating the squares. The total zinc alloy mass averaged over the 3 units was 40 g. Two steel wires (~1.5 mm diameter) for external connection were wrapped tightly against the expanded metal squares.

Figure 1 - External appearance of anode types (C on top, W on bottom).

Figure 2 - Type C anode specimens. Zinc alloy anode appearance after embedded mortar was stripped; otherwise as-received. Left, 1st set; Right, 2nd set.

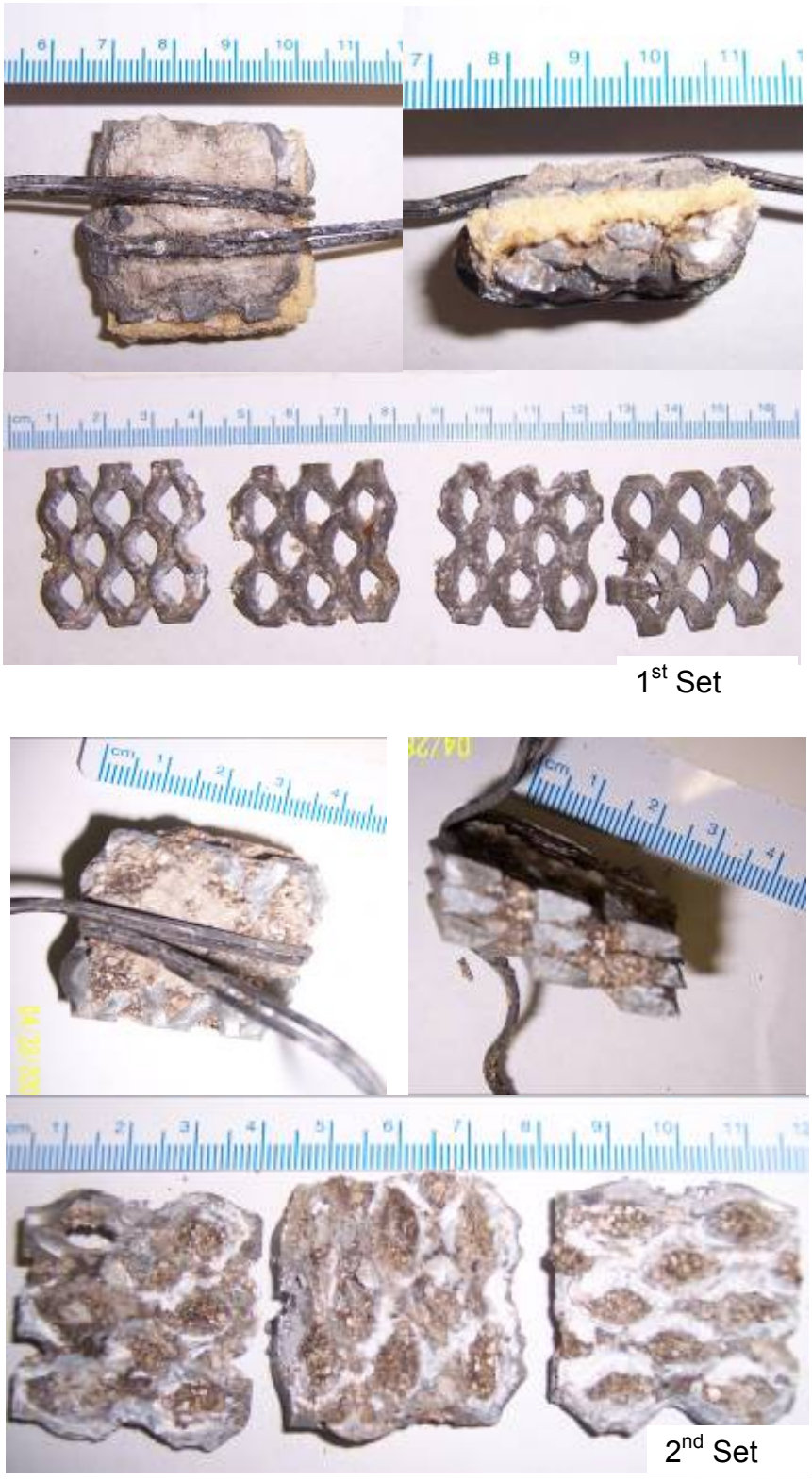

Figure 3 - Type W anode specimens. Zinc alloy anode appearance after embedded mortar was stripped. Top 1st set. Bottom 2nd set. (Mortar only partially stripped).

2.3 General Aspects of the Anode Evaluation Approach

The investigation aims in large part to characterize anode performance by determining the potential/current delivery function (PF) of the anode, and its dependence on relevant service variables (e.g. moisture content and alkaline content of surrounding concrete) and on service time. Implicit in this approach is determining the ability of the anode metal to remain in the active condition over long periods of time, as well as the cumulative capacity of the anode (total usable charge delivered) and associated ultimate service life capability.

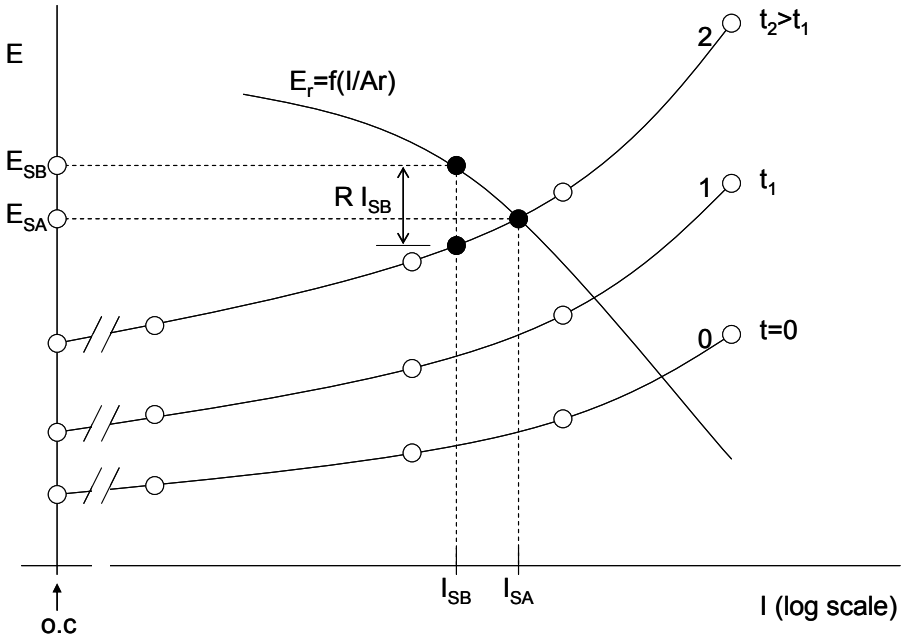

Figure 4 - Idealized potential-current diagram of the evaluation approach.

Figure 4 shows the concepts involved and their application [Sagüés 2005]. Consider an anode being evaluated when initially placed in service. The anode is expected to develop under open circuit (OC) condition, a potential in the order of -1V CSE. If connected with a passive rebar assembly, the anode delivers some current and polarization causes the anode potential (as measured against a

reference electrode placed in close proximity to the anode) to become less negative than in the OC condition. The polarization increases with larger current demand, as described by Curve 0 which is effectively the PF of the anode at the beginning of its service life. Curve 0 would also result from joining the locus of separate points corresponding to a number of similar newly placed anodes acting independently at different current demands. If current delivery of each anode were kept constant for a long time, the anode performance is expected to degrade somewhat from causes such as zinc consumption (with consequent decrease in effective surface area) and accumulation of corrosion products that may impede the passage of ionic current or even promote passivation of the anode surface causing eventually failure to deliver protection. The manifestation of such degradation would be a shift to more positive values in the anode potential, likely to a greater extent at longer services times and higher currents, as illustrated by PF Curves 1 (time = t_1) and 2 (time = $t_2 > t_1$). Those curves can be obtained experimentally by operating the anodes while connected to an external galvanostatic control circuit. Both the ability of the anode to remain active and the cumulative capacity of the anode can then be characterized from the curves at each current regime and at different time intervals.

A diagram thus obtained (family of PF curves as function of time) for a given anode type and environment, including mortar type and humidity condition, can serve as a standardized descriptor of the anode performance for those conditions. If a galvanic control circuit is used, this procedure eliminates the variability that appears when evaluating anodes, as it is often done [Sergi 2001], by coupling to a passive rebar assembly embedded in the same mortar or concrete. The variability in such cases stems from the current demand by the rebar assembly, which may sometimes be sustained at high levels for long periods of time, or drop rapidly early in the life of the test depending on the initial condition of the steel surface or small variations in the pore water composition or concrete moisture.

The curves in a PF diagram obtained from a sacrificial anode may be used to obtain a bounding indication of how much protective action may be expected from a rebar assembly for which there is information on its polarization characteristics. As an illustration, the polarization information can take the form of the long term potential-cathodic current density polarization curve $E_r=f(i)$ for the reinforcing steel, determined by prior measurements as illustrated in Figure 4. Thus if the anode placement density is such that each anode is to protect an area A_r of rebar surface area, the curve $E_r=f(I/A_r)$ describing the polarization characteristics of that area [Sagüés 2003] can be superimposed directly on the PF diagram to determine how much rebar polarization may be achieved at different aging conditions (Figure 4). If the resistivity of the concrete path between anode and rebar is very small, the rebar receives a current I_{SA} and is polarized down to potential E_{SA}, which may then be compared with the minimum requirements for corrosion prevention in the specific application considered. E_{SA} is the best polarization level to be expected; if concrete resistivity is finite so an effective circuit resistance R applies, the current is less (I_{SB}) and the rebar polarization is only down to E_{SB}. The amount of polarization is proportionally less if the area to be polarized is greater, as the effect is the same as moving the rebar polarization curve to the right. This type of analysis, to project the extent of useful anode action based on the results of the test, can be extended to more complex system geometries by appropriate current distribution modeling [Presuel-Moreno 2005B, Sagüés 2003]. Those concepts have been applied in more detail in Chapter 5 of the present document, dealing with performance modeling of sacrificial anodes in a reinforced concrete structure.

Some content in this dissertation has been published in reports to the sponsoring agency (Dugarte and Sagues, 2010), and has been in part reproduced here.

2.4 Anodes in Galvanostatic Regime in Concrete

These sets of experiments were conducted using the above principles, where anode specimens were evaluated under various galvanostatic regimes in controlled humidity chambers.

2.4.1 Materials and Preparation

These tests involved the two anodes types to be evaluated (1st set only), in two different embedding media, two relative humidity (RH) regimes, four galvanostatic regimes, and were conducted in triplicate for each condition for a total of 96 specimens. These specimens were exposed for approximately 4 years.

The basic test specimen arrangement (Figure 5) consisted of a prism 20 cm x 20 cm x 10 cm) with a test anode placed near the center. An embedded activated titanium rod (ATR) reference electrode [Castro 1996] (periodically calibrated against a Copper Sulfate Electrode (CSE)) was placed against one of the external mortar faces of the anode. Alternatively, an externally placed CSE is used with appropriate compensation for electrolyte resistance if potential measurements are done with current *on*. An activated titanium mesh of the type used for impressed current cathodic protection of steel in concrete was cast underneath one of the main faces of the prism. The specimens were kept in controlled containers at the desired relative humidity. Connecting wires from anode and mesh led to a galvanostatic system capable of handling multiple independent channels.

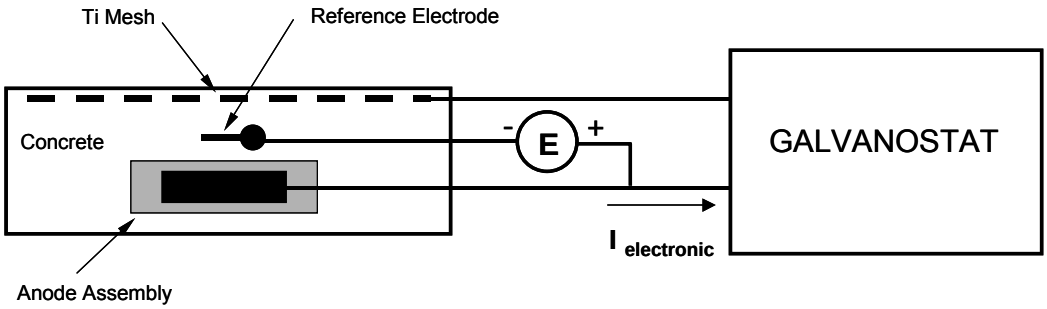

Figure 5 - Anode test arrangement (sketch). Anode was placed centrally in specimen.

2.4.2 Test Conditions

A summary of materials and test conditions is given in Table 1. A picture of the 95% RH chamber with test specimens is shown in Figure 6.

Figure 6 - The 95% RH test chamber.

Table 1 - Materials and test conditions for anodes in galvanostatic regime in concrete.

Anodes evaluated	C and W - 1st Set only.
Embedding media	• A Portland-cement with polymers commercial product marketed for patch repairs[A]. Mixed per manufacturer's instructions, using 2 liter water per 50 lb bag of product plus 15 lb 3/8" Aggregate. • Ordinary Repair Concrete (ORC), 0.41 w/c, 658 lb per cubic yard. Type II cement, 3/8" Aggregate.
Test environments	95% R.H. and 60% R.H. – target values; typically controlled to +-5%
Galvanostatic regime	0, 30, 100 and 300 μA anodic current
Replication	Triplicate
Total test blocks	96

2.4.3 Data Measurement for Performance Evaluation

The potential E_{IO} of the anodes is reported in the CSE scale in the instant-Off condition (~ 1 sec after current interruption) either measured directly against a CSE electrode placed on the block side, or against the internal activated Titanium rod calibrated against a CSE. Potential is reported as function of time t, with t=0 chosen to correspond to the moment of energizing of the anodes subject to galvanostatic control, which was 48 days after casting for the 95% R.H. tests and 81 days after casting for the 60% R.H tests.

[A] Provided by the manufacturer of the W anodes.

The instant-Off potential, E_{IO}, values of triplicate specimens were averaged. If the power-on potential of any specimen reached ~0V (i.e., clearly incapable of any protective action) at a given test time, testing of that specimen was discontinued and the E_{IO} average value from that time on was computed only for the remaining specimens of that trio.

2.5 Anodes Coupled to Reinforcing Steel in Concrete

These experiments determined the combined anode-rebar performance in outdoor exposure test yard slabs. These tests were intended to supplement the information provided by the galvanostatic experiments by examining an anode aging trajectory closer to that expected in actual applications, and to have an opportunity to reveal possible effects of diurnal and seasonal variations in temperature and humidity that would have not been experienced in the laboratory tests. In addition, the reinforced concrete tests would serve to provide information on steel polarization data, and to offer a means to validate modeling predictions such as those described in the next paragraph. The outdoor tests served also to compare the behavior of the first and second sets of anodes from each manufacturer. For these tests and for the reasons indicated earlier, additional test strategies were needed to separate the information that pertains solely to the anode performance. One of those strategies was to insert resistors of various sizes between the anode and the rebar assembly in a test system and monitor the resulting potential/current trajectory of the anode, thus yielding an alternative way of obtaining a PF diagram for the sacrificial anode samples at various stages of aging.

2.5.1 Materials and Preparation

Figure 7 shows the test slab configuration. The steel rebars were regular production No.7 (nominal diameter 7/8 in (22mm)) bars complying to ASTM A-615 Grade 60, with dark gray mill scale on the surface. Each rebar had a nominal 293 cm^2 surface area, resulting in a 0.80 nominal ratio of steel area to concrete footprint area. The yard slabs were built using the same Ordinary Repair Concrete formulation as for the concrete blocks in the galvanostatic experiments, except that the shaded portion near the center contained admixed sodium chloride to obtain 5.9 Kg/m^3 (10 pounds per cubic yard (pcy)) chloride ion. Each slab contained two anodes of the each set provided by the manufacturers, placed as shown. Rebars were numbered from 1 to 12, starting from the left on Figure 7. Both anodes were of either Type C in triplicate slabs numbered 1, 3 and 5 or Type W in triplicate slabs numbered 2, 4 and 6.

2.5.2 Test Conditions

Six concrete slabs with embedded sacrificial point anodes as indicated in Figure 7 were cured in the molds for one week and then demolded and placed horizontally, elevated 1 ft above ground, in the outdoor test yard at USF. The demolding date was designated as the start of the exposure period (t=0). While curing, the main anode was kept provisionally wired to the four rebars in the Cl^- rich zone. Since placement in the yard and until connections boxes were in place, the entire rebar assembly and the main anode were kept interconnected with provisional wiring. Due to casting difficulties the concrete in the chloride-rich zone was at places poorly consolidated and exhibited some honeycombing. After placement in the yard the affected slabs were fitted with partial forms and a cement-water grout was poured as needed to fill in the voids in the honeycombed spots.

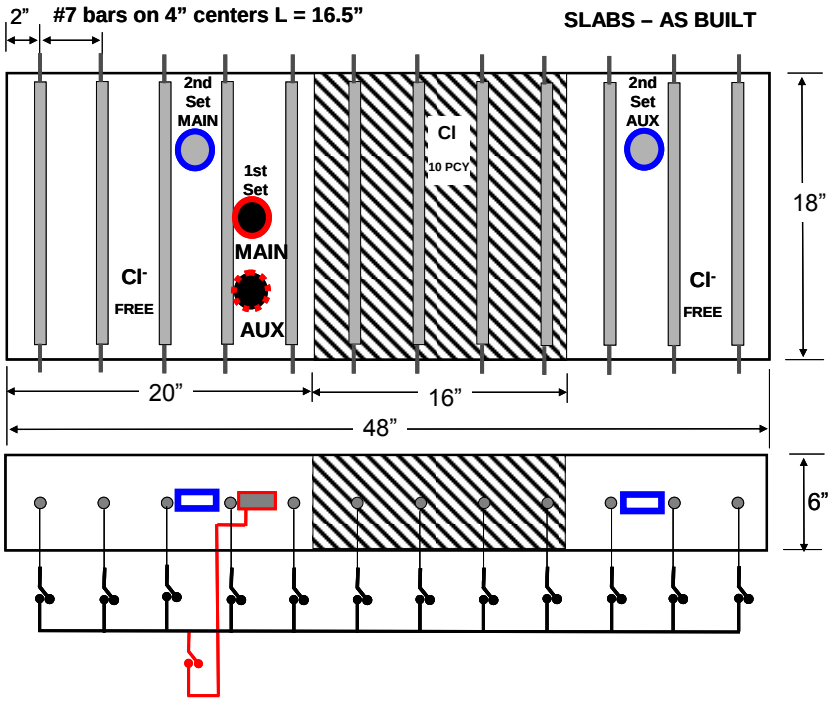

Figure 7 - Yard slab test configuration showing 1st and 2nd set anode positions. Dimensions in inches. Rebars are numbered starting with No. 1 at left.

The anode on the slab centerline (Main) was normally always connected to the rest of the rebar assembly. The other anode (Auxiliary) was disconnected except when indicated. After 1045 days of operation of the 1st set of anodes an additional pair of externally wired duplicate anodes, from the 2nd set provided by the manufacturers, was placed in each slab as shown and keeping the same slab assignment for each type of anode. The 2nd set of anodes was placed by first drilling two partially overlapping 2-in (5 cm) diameter core holes in the space indicated, inserting the anode in the opening and filling it with a proprietary mortar compound for placing point anodes as a retrofit in hardened concrete, applied per manufacturer's instructions. The connection to the previous Main anode was then switched to the Main anode of the 2nd set; all other anodes remained normally disconnected.

2.5.3 Data Measurements

Externally wired switches permitted performing instant-Off potential measurements and measurements of current delivery to individual rebars. All rebars and the main anode were normally interconnected. ATR electrodes were placed 12 mm away from the surface of each of the rebars. Figure 8 shows an installed slab.

Figure 8 - Installed yard slab with connection box.

Measurements conducted typically on a weekly schedule included (a) anode and individual rebar currents; (b) potential of the anode-rebar assembly with anode energized (" Current-On" potential) with respect to a CSE placed on the concrete on top of each individual rebar as well as over the anode position, and also with respect to each of the embedded ATR electrodes; and (c) potential measured 1 second after disconnection ("Instant-Off potential) and immediate reconnection afterwards of each individual rebar as well as the anode, using both the CSE and the ATR electrodes. Air temperature (and internal concrete temperature after the 2nd set of anodes was installed) was measured each time

those tests were performed. The following measurements and calibration tests procedures were conducted typically on a monthly or less frequent schedule.

2.5.3.1 Concrete Resistivity

A Nilsson Model 400 Soil resistivity meter (square wave alternating current (*ac*), 97 Hz). In this meter, current is applied with current terminals designated C1 and C2, and potentials are measured between terminals P1 and P2. The meter was employed with a 4-point configuration that determined the concrete resistivity as function of distance along the main axis of the slab. All slab switches were temporarily placed in the open position. The rebars at each end of the assembly (No. 1 and 12) were connected to the meter terminals C1 and C2 respectively. The potential connections were made consecutively to pairs of rebars starting with meter terminal P1 to rebar No.1 and terminal P2 to rebar No.2, then P1 to rebar No. 2 and P2 to rebar No.3 and so on. The resulting resistance for each of the other measurements was multiplied by a cell factor (68.6 cm, equal to the cross sectional area of the slab divided by the center-to-center rebar distance) to obtain the concrete resistivity for the concrete slice between each the pair of rebars. The raw measurement for the rebar pairs 1-2 and 11-12 were divided by a correction factor of 1.2 to account for uneven current distribution at the injection current rebars[B]. The *ac* current path was uneven due to the presence of the main and auxiliary anodes between rebars No.4 and 5 for the 1st set of anodes, and in addition between rebars No. 3 and 4 and 10 and 11 after the 2nd set of anodes was placed. Thus, the resistivity of the chloride-free concrete is reported as the average of that obtained for rebar pairs 1-2 (corrected), 2-3, 3-4, 10-11 and 11-12 (corrected). After the introduction of the 2nd set of anodes, the values for pair 3-4 and 10-11 were not used for that

[B] The cell factor was obtained as the average, for all slabs and for all test times up to the introduction of the 2nd set of anodes, of the raw resistivity value for rebar pair 1-2 divided by that for pair 2-3, and similarly for pairs 11-12 and 10-11.

resistivity calculation. The resistivity for the concrete in the chloride-containing concrete region is reported as the average for rebar pairs 5-6, 7-8 and 8-9.

2.5.3.2 Anode to Rebar Resistance

These measurements were conducted at irregular intervals. The anode was temporarily disconnected from the rebar assembly to which it was normally connected. The soil resistivity meter was then used as a 2-point resistance measuring device, with one terminal connected to the anode and the other to the rebar assembly to which the anode was normally connected.

2.5.3.3 Steel Depolarization

This test started with an instant-Off potential determination, after which the anode was left disconnected and remained so while the potentials of the anode and individual rebars ("Off potential) were measured 1h, 4h and 24h following disconnection. The anode was reconnected afterwards. The result of the depolarization test was normally reported as the difference between the 4h Off potentials and the Instant-Off potentials at the beginning of the test. Results for the other intervals were archived and discussed when appropriate.

2.5.3.4 Slow Anode Cyclic Polarization

This test was conducted to obtain an approximation of the anode PF diagram at various aging periods. The tests were conducted as slowly as practical to approximate stabilization of the anode at each of the potential/current points determined. Moreover, the tests were conducted first changing conditions in one direction and then again in the return direction. The extent to which any hysteresis effects appeared was an indication of how much the results obtained deviated from long term steady conditions. The test began after a regular set of Instant-Off measurements was conducted and is exemplified by the following

sequence. The connection between the anode and the rebar assembly was then opened and restored after introducing a 500 ohm resistor in the current path. After a typically 24 h wait period the current and Instant-Off potential of the anode was determined and the resistor was replaced by another about 2 times greater in value. The procedure was repeated in subsequent days. When a resistor value >=30 kohm was reached, the next daily step was in the open circuit condition so as to document the unpolarized potential of the anode. The subsequent daily steps were conducted with the same series of resistors but in reverse order, until reaching the direct connection condition. The test typically was completed over a period of 1-2 weeks. The Instant-Off potential vs current data with the forward and reverser data were reported as the PF curve of the anode at the aging condition corresponding to the beginning of the test.

2.5.4 Corrections and Adjustments

This section concerns corrections to measured variables in the yard slab inherent to the conditions of the experiment. The purpose of the present section was to explore and analyze important sources of uncertainly in the potential measurements of reinforcing steel in concrete and temperature compensation in order to make the appropriate corrections. It is noted that the temperature corrections were intended primarily to assist in smoothing the data available to reveal long term trends. First the temperature correction is analyzed, followed by a similar analysis of the potential correction. A third section deals with the resistivity corrections.

2.5.4.1 Potential and Current -Temperature Corrections

Potential measurements conducted with a CSE on aged concrete surfaces are subject to artifacts including junction potentials induced by the gradient in OH^- concentration due to carbonation or leachout of pore water [Myrdal 1996]. To

correct for those effects small (typically 1 cm^2) portions of the upper slab surface of each slab were periodically chipped off or abraded to expose a fresh concrete surface next to each of the positions used for regular measurements. Potential measurements taken with the CSE tip on the fresh surface were compared with measurements performed on an adjacent undisturbed surface. The difference was tallied as function of time and prorated accordingly to build a potential correction (averaged for all slabs) that was globally applied to the raw potential data. Cross-checks against the internal ATR electrodes (not subject to the surface effects) validated that approach. All reported anode potential values in this document have been corrected accordingly.

In addition to the systematic deviations noted above, potential measurements conducted on the concrete surface even in the absence of appreciable temperature variations (discussed below) were subject to scatter from e.g. surface moisture variations and degree of contact with the electrode sensing tip. Rebar potential measurements spanned a narrower range than that of anode potentials, so the obscuring effects of random scatter were considerable when attempting to construct a global steel polarization curve as shown in Section 3.2.2. In contrast, potential measurements of steel against the embedded ATR electrodes were found to be appreciably more stable. Consequently, the potentials reported in this document for constructing the steel polarization function were based on the measurements against the embedded ATR, corrected by calibration performed at selected times against an external CSE. The calibration was conducted by carefully controlling surface conditions and performing repeated measurements to minimize random error in the average of those measurements. As the steel potential measurements were instant-Off values with only the current to a single rebar interrupted at a time, a compensation procedure was developed to account in the calibration for residual ohmic drop between the respective potential measuring points of the CSE and the corresponding ATR.

Temperature of the test yard slabs spanned a wide range, from ~5 to ~35 ^{o}C. Measured values of galvanic currents, concrete resistivity and potentials showed appreciable day to day and seasonal fluctuations that correlated well with variations in temperature. Those fluctuations obscured long term trends due solely to anode aging and other system evolution, and added scatter to determinations of anode PFs. Consequently, the data were analyzed to extract parameters that could serve to approximately compensate for the temperature variation effects. Following prior approaches documented in the literature [Virmani 1983, Pour-Ghaz 2009] the anode current, I, was assumed to follow an apparent Arrhenius relationship

$$I(T_1) = I(T_2) \exp [- H_A R^{-1} (T_1^{-1}-T_2^{-1})] \quad (1)$$

Where T_1 is the temperature for which all measurements are to be reported (chosen to be 298^{o}K, 25^{o}C which was the approximate average temperature of the yard slabs at the time of the day measurements were conducted), T_2 is the temperature at the moment the measurement was performed, H_A is the apparent activation energy and R is the gas constant.

The value of H_A was obtained from the best fit slope of a modified Arrhenius plot of the current-temperature data for each anode type of the 2nd set of anodes. The modification consisted of plotting the value (Δln I)/R as function of ΔT^{-1}, where the differences are the change in measurement results for each slab of a given type of anode from the previous test date. The slope of the straight line best fitting the combined results for that anode was reported as the average effective activation energy. This approach emphasizes the changes due to temperature variations, which are relatively short-term, and minimizes error in estimating H_A introduced otherwise by the longer-term changes due to system aging and not related to temperature. Values of H_A=53 kJ/mole and 32 kJ/mole were thus obtained for the C and W anodes respectively. Accurate concrete temperature records were kept only during the last half of the evaluation of the

1st set of anodes, when anode current values were generally small which tended to result in larger relative experimental scatter. Trial calculations showed that the resulting uncertainty in H_A determination was considerably greater than that for the 2nd set of anodes. Consequently, it was decided instead to apply globally the H_A values obtained for the 2nd set of anodes to the 1st set as well, recognizing that its correction is only roughly evaluated due to reduced confidence in both temperature and activation energy values.

The temperature compensation described above for the anode current is only a rough approximation that ignores the complex interaction of the combined electrochemical processes at the anode and the rebar assembly, plus the effect of variation of electrolyte resistance with temperature. For example, the correction did not take into account the value of the potential at the time the current was measured. This simplified approach was adopted as it was felt that the uncertainty inherent in the instant-Off anode potential (where a relatively large ohmic potential drop is eliminated but never exactly) did not merit further precision.

A more sophisticated approach was used for temperature correction of the (mostly) cathodic current on the rebar, for which the instant-Off potential can be determined more accurately. Following a simplified absolute reaction rate kinetics approach (see for example Kaesche 2003 and observations by Tanaka (1964)), the cathodic rebar current density was corrected for temperature taking into account the potential E as well by:

$$I(T_1, E) = I(T_2,E) \exp [- (H'_A+P E) R^{-1} (T_1^{-1}-T_2^{-1})] \qquad (2)$$

Where H'_A is a nominal corrected activation energy term and P is a parameter that adjusts for the value of the steel potential when the current measurement was made. The approach neglects also the complicating effect of any anodic reaction that took place on the rebar surface.

The values of H'_A and P were obtained by a best fit procedure to be presented elsewhere [Dugarte 2010] that takes into account the cathodic current density, temperature and potential changes between measurements performed at consecutive test dates. The resulting average values of H'_A and P were 40 kJ/mole and 10.4 kCoul/mole respectively, with no significantly different results from steel in the slabs that contained C or W anodes. Because of the small value of the products PE compared with H'A, the final correction is not much different that what would have been obtained with a simpler relationship such as Eq.(1) with only the nominal activation energy term.

2.5.4.2 Resistivity –Temperature Corrections

A procedure similar to that used for the anodic current temperature correction was used to obtain the apparent activation energies for the concrete resistivity, with a resulting value of 24 kJ/mole for the concrete in the chloride-free zone. These apparent activation energy values and Eq.(1) were then applied to the entire data set. All anode current and concrete resistivity results reported in the following are temperature-compensated by that procedure.

It is noted that the temperature corrections were intended primarily for data smoothing to assist in revealing trends in other system variables. Further analysis of this issue, including mechanistic interpretation of the apparent activation energies values obtained is left for future continuation work [Dugarte 2010].

3. RESULTS

3.1 Results, Anodes in Galvanostatic Regime in Concrete

For the following, it is recalled these experiments were performed only with the 1st set of anodes provided by the manufacturers.

The average Instant-Off potentials E_{IO} from individual anodes of a given replicate trio were again averaged over 200 day periods from 0-200 days to 800-1200 days, and the results are illustrated in Figures 9 and 10 for the 95% and 60% RH humidity conditions respectively. The 0 mV vs CSE condition was reached in the high RH chamber for only a few of the specimens, most in the 300 μA regime and then relatively late in the test. In contrast, in the low RH chamber the condition was reached relatively soon in more specimens and at lower current levels (10 and 30 μA), effectively terminating the test early for those cases.

The initial open circuit potentials (OCP) of the anodes ranged from values approaching that commonly expected for active zinc (~-1V vs CSE) to sometimes markedly more positive values. In general both C and W anodes showed a more negative OCP in the proprietary mix medium than in the ordinary repair concrete, in both the high and low RH chambers. At 95% RH and for both embedding media the C anodes had more negative initial OCP than the W anodes. In contrast, at low RH the initial OCP of both anodes were comparable and not so negative (~ -500 mV). Scatter in the OCP values was significant, obscuring determination by these measurements of a possible variation of OCP with time such as the increasing trend suggested in the introduction.

The results for tests with galvanostatic current control typically showed clear increases in E_{IO} with increasing current and time, culminating often in reaching the test-termination condition as noted above. At 95% RH the C anodes tended to polarize more, and faster with time, than the W anodes thus offsetting much of the difference in OCP between both types of anodes. At 60% RH both types of anodes (but more so the C anodes) tended to reach the test-termination condition faster than at 95% RH. By 1200 days of exposure at 60% RH a majority of the anodes of both types had reached the test termination condition at all three impressed current levels.

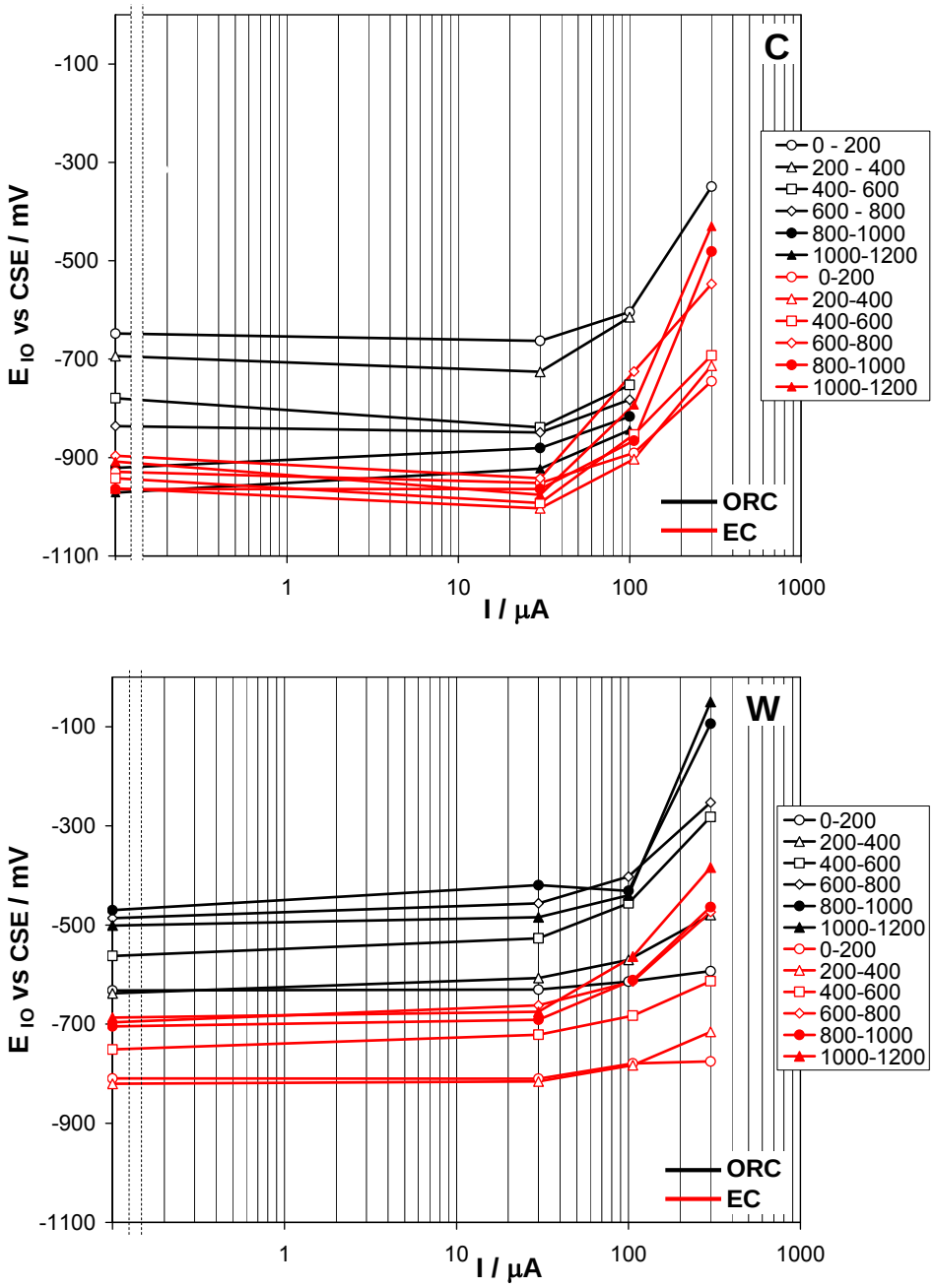

Figure 9 - E_{IO} evolution for both test media and anode types exposed in the 95% RH chamber. Average results from multiple replicate anodes over each period (in days of exposure) indicated in the legend.

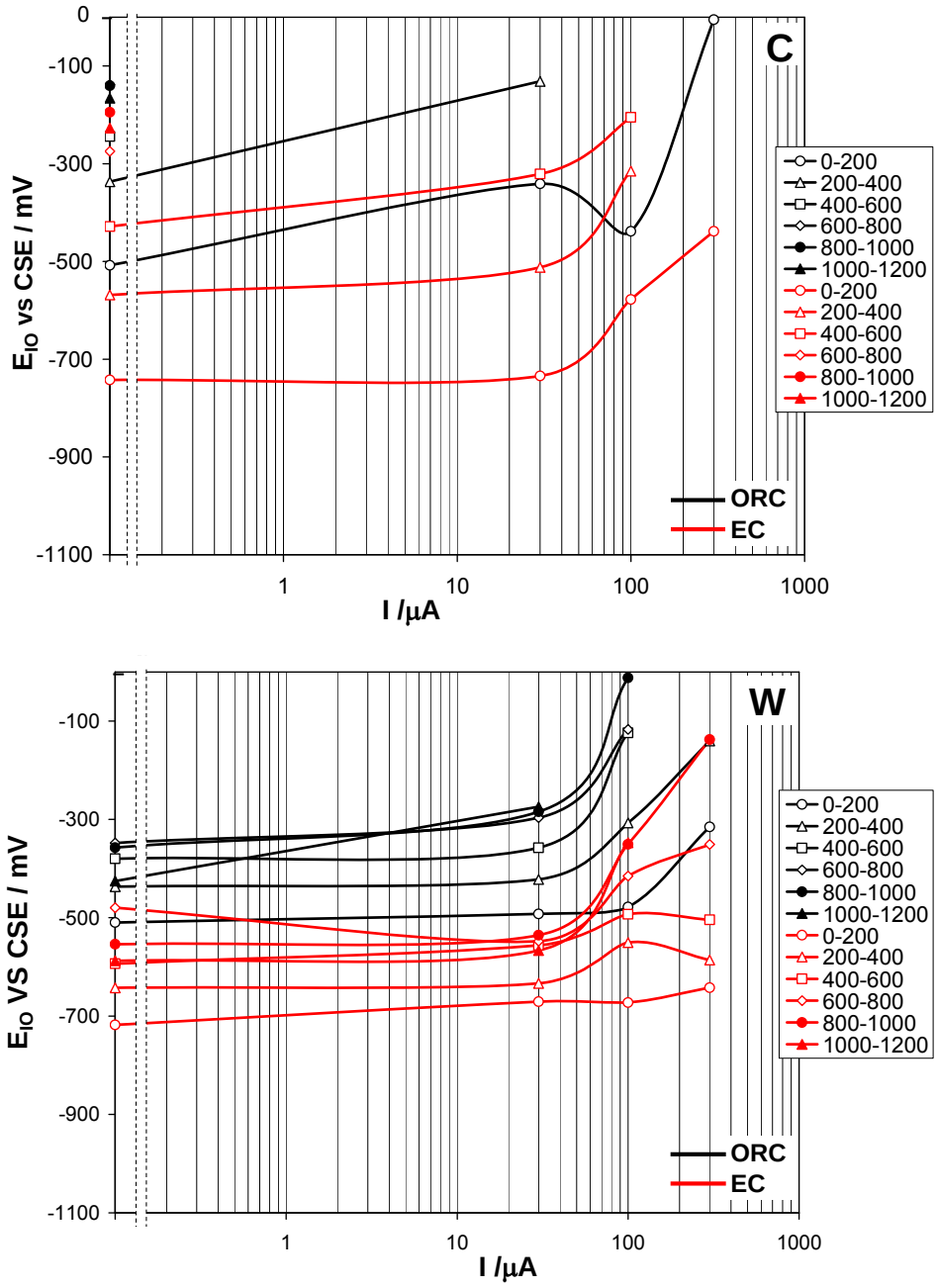

Figure 10 - E_{IO} evolution for both test media and anode types exposed in the 60% RH chamber. Average results from multiple replicate anodes over each period (in days of exposure) indicated in the legend.

3.2 Results, Anodes Coupled to Reinforcing Steel in Concrete

For the following, it is recalled that these experiments were performed with anodes from both the 1st and the 2nd sets provided by the manufacturers. The manufacturer product designations were the same in each case. The test schedule differed between both sets of anodes in that for the 1st set the 4 rebars in the chloride-contaminated region were connected from day 0 to day 477 and disconnected from thereon until day 1045 when testing of the 1st set ended. For the 2nd set tests, that started immediately afterwards, those rebars were never connected. Unless otherwise indicated, time reported in the following corresponds to the period starting at the beginning of the placement of the respective set of anodes. This report covers the evolution of the 1st and 2nd set of anodes through their first 1045 and 590 days respectively.

Results from both series of experiments in the yard slabs are presented as follows.

3.2.1 Anode Polarization

The current delivered by the anodes to the entire rebar assembly as a function of exposure time is shown in Figure 11 for both sets tested. In both instances there were high initial currents (sometimes > 3 mA) that decayed generally steadily to values in the range of 200-500 μA after about 1.5 years for the C anodes of either set, and for the W anodes of the 2nd set. Notably, the performance of the 1st set of W anodes deteriorated much faster than the rest, to values about one order of magnitude lower than those of the C anodes (e.g. 20-90 μA) at the end of the same period. For the 1st set of anodes of both types, there was a momentary lull in the long term decreasing trend after the active rebars were disconnected, but the trend was resumed afterwards. It is noted that for much of the test period the current delivered by anode C-1 of the1st set was consistently significantly greater than that of its peers in the same set.

The evolution of Instant-Off potentials with time for both sets of anodes is shown in Figure 12. Initially potentials for all anodes in both sets were quite negative, ~-700 mV. For the 1st set the potential rapidly increased early on for both anodes, to reach a roughly steady regime at ~-400 mV CSE. Disconnection of the active rebars at day 477 was followed by an increase of ~100 mV for the W anodes but little change for the C anodes. Of the latter, anode C-1, which had the highest currents as noted above had also the more negative potential, which began to drift toward even lower values (~ -600 mV) later in the exposure period. Both anode types in the 2nd set (with only passive rebars) showed a relatively slow increasing potential trend with time, reaching average potentials of ~-450 mV and ~-600 CSE for W and C anodes respectively by the end of the test period.

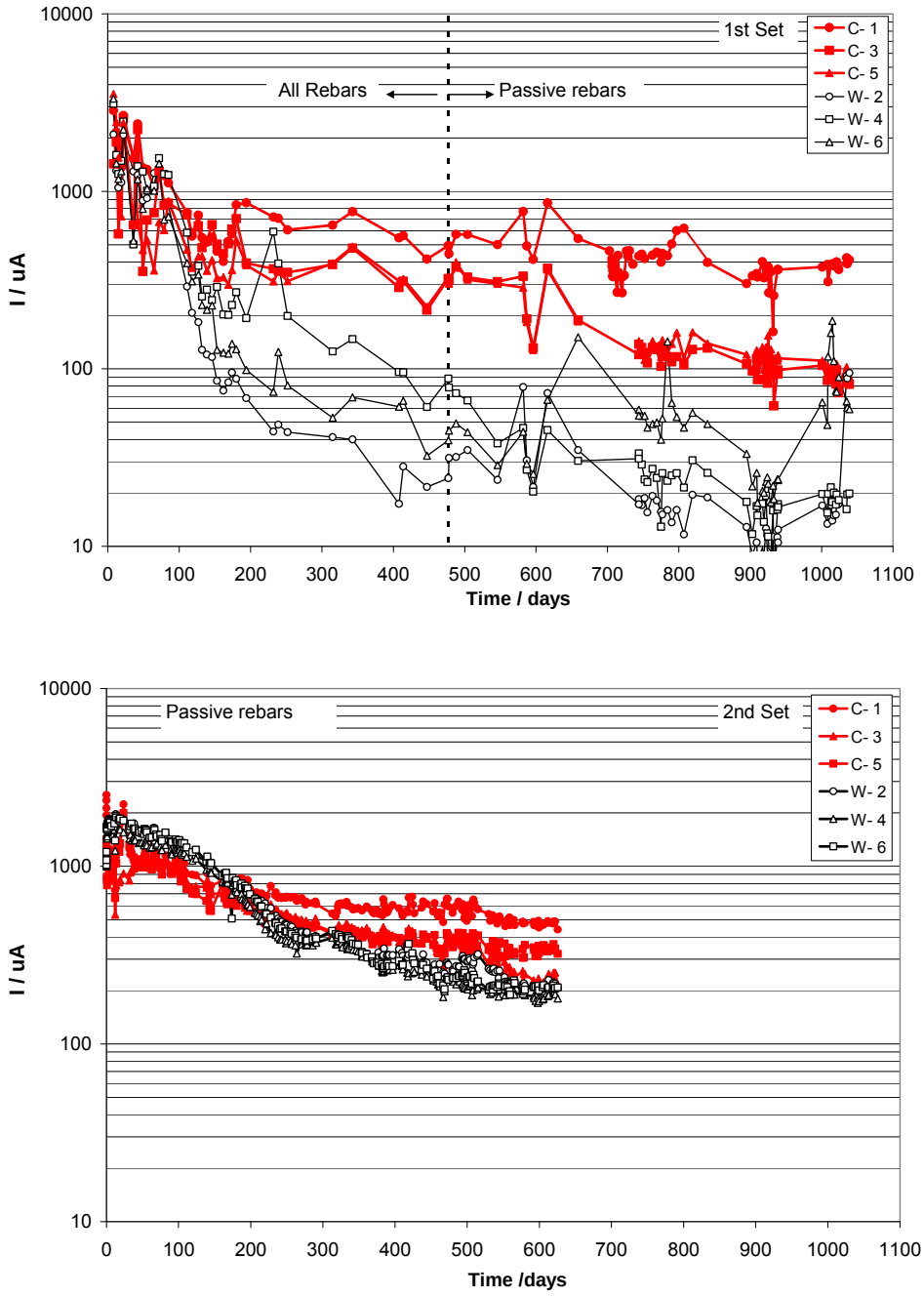

Figure 11 - Anode current evolution with time for both sets of anodes. Results of anodes in individual test yard slabs.

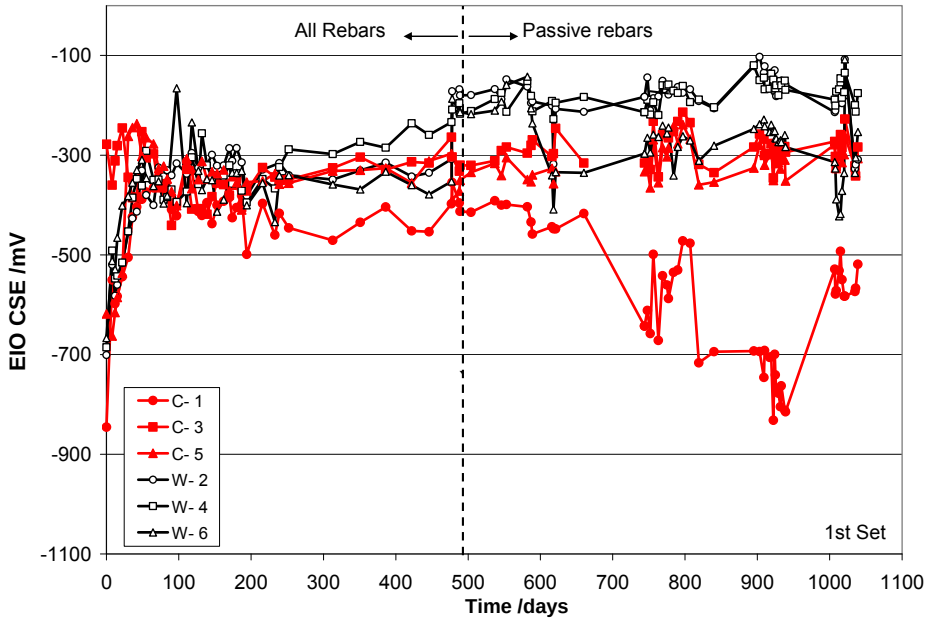

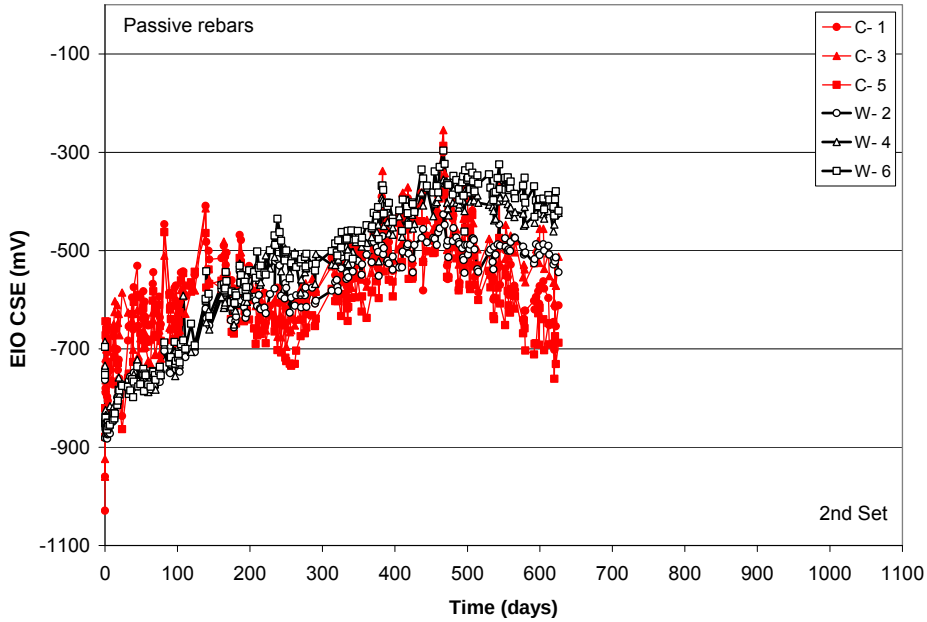

Figure 12 - Anode potential (Instant-Off) evolution with time for both sets of anodes. Results of anodes in individual test yard slabs.

The trends of potential evolution with time of the auxiliary anodes, which were normally in an open circuit condition, are shown in Figure 13. For the 1st set, with one exception (C-1), the auxiliary anode potentials of both types started at values ~100 to 200 mV lower than those of the energized anodes, but increased at a much slower rate, reaching on average a plateau at ~-600 mV after about 1.5 years. The auxiliary anode in Slab 1 (C-1) stayed however at more negative potentials over much of the test period. The 2nd set of anodes showed also a slow increasing potential trend, but with starting values that were markedly more negative (~ -900 to -1200 mV) than those of the 1st set.

The current and potential evolution of the energized anodes is shown in Figures 14 and 15 as function of the cumulative amount of galvanic charge, Q, delivered by each anode up to the moment of each measurement. The value of Q was obtained by summation of the product of anode current-duration of all the previous test intervals up to the moment of measurement. The larger the value of Q, the larger is the amount of anode metal consumption due to the galvanic current, so Q serves as one descriptor for the extent of anode aging. For the 1st set of anodes there was a striking decrease in current output of the W anodes Q reached ~10 k Coul to 20 k Coul. Two of the C anodes in the 1st set showed markedly decreased current delivery at Q ~10 k Coul to 20 k Coul, but anode C-1 was delivering ~500 μA even at Q ~ 60 k Coul.

Anodes in the 2nd set showed a more uniform decrease in current delivery with increasing Q, up to ~ 35 k Coul by the end of the test period. Unlike in the 1st set, performance of the W anodes did not show early deterioration and was comparable up to the end of the test interval to that of the type C anodes in both sets. Potential evolution trends as function of Q were obscured in the 1st set, especially for the C anodes. The 2nd set showed a clearer trend, with potentials of both types of anodes increasing somewhat uniformly as Q increased.

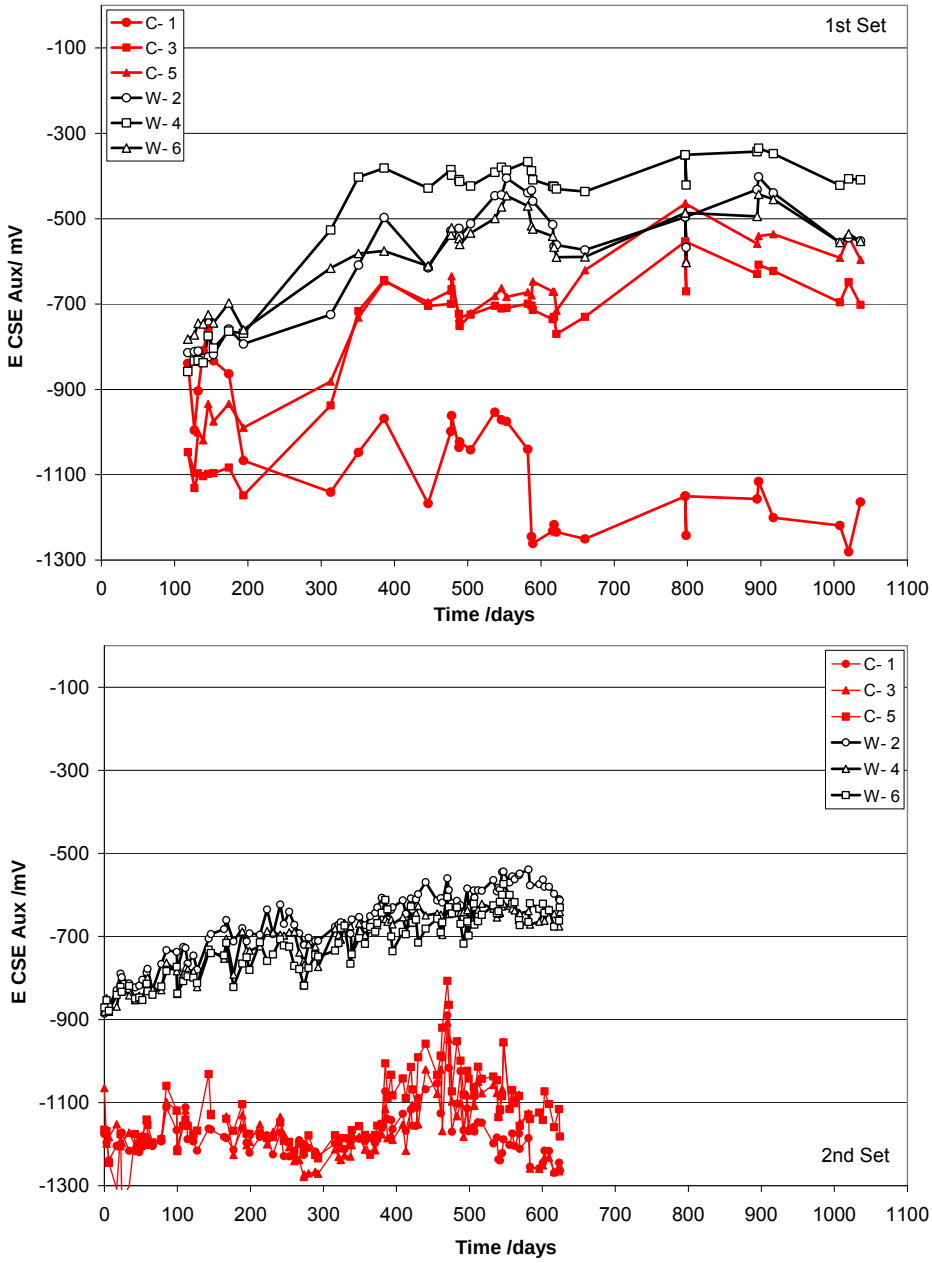

Figure 13 - Auxiliary anode potential evolution with time for both sets of anodes. Results of anodes in individual test yard slabs.

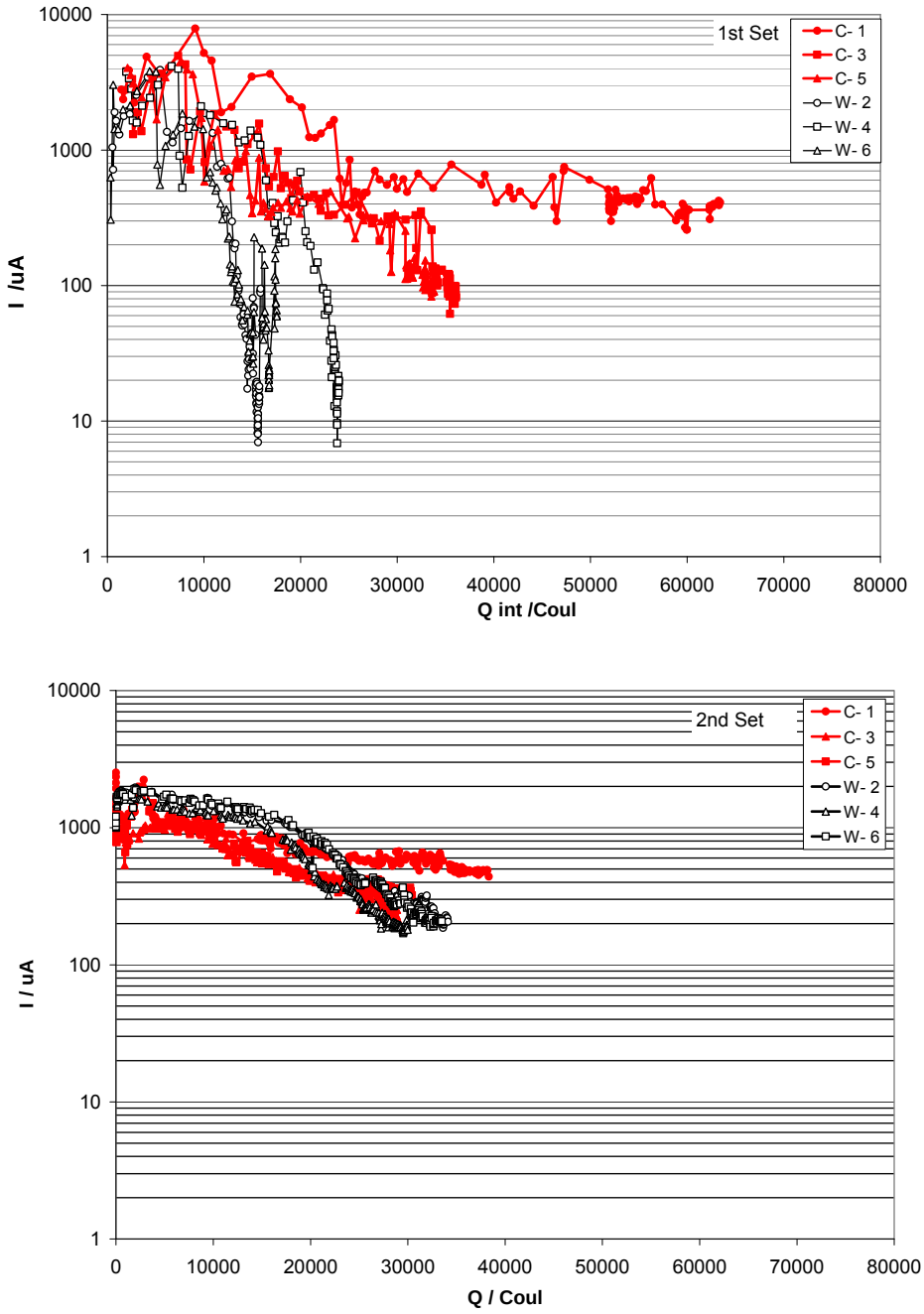

Figure 14 - Anode current as function of integrated anodic charge delivered for both sets of anodes.

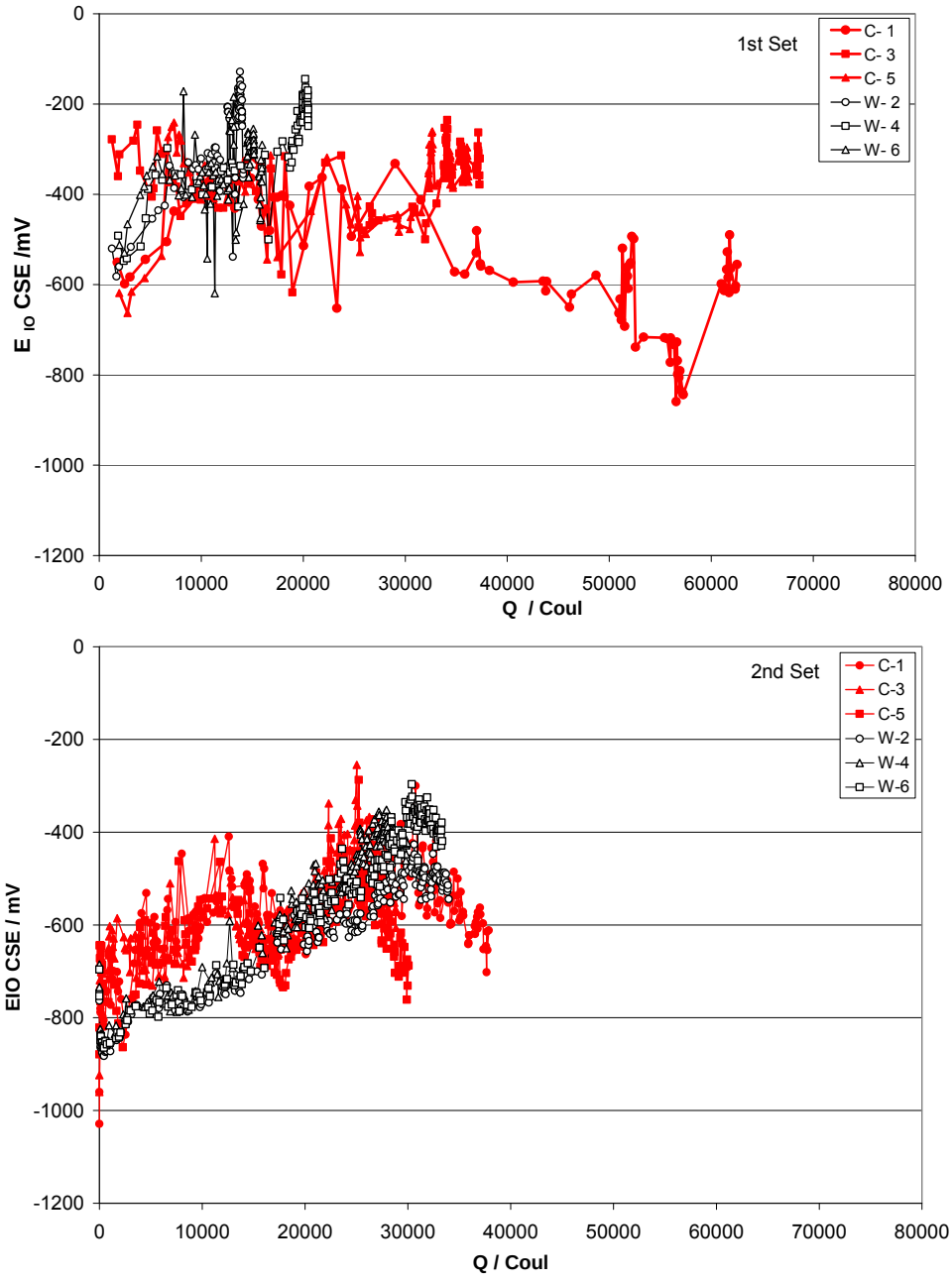

Figure 15 - Anode Potential as function of integrated anodic charge delivered for both sets of anodes.

The potential-current trajectory of the anodes in the test yard slabs is shown in Figures 16-17. Each symbol correspond to the average Instant-Off potential and corresponding current reading for each anode, over a 100-day period starting with anode placement. The smallest symbol indicates the 0-100 day interval with increasingly large symbols for the subsequent intervals. With the exception of data for anode C-1 near the end of the test period, the trajectories correspond roughly to lines with a negative slope, small for the 1st set of anodes and steep for the 2nd set. The general direction of the trajectories (C-1 for 1st set excepted) is indicated by arrows.

Results from the slow cyclic polarization tests for the 1st set of anodes are illustrated in Figures 18 and 19. For this set the tests were conducted only near the end of the exposure period, so the curves reflect significant performance derating due to aging. The curves for the C anodes show little hysteresis, with the forward and return curves nearly overlapping, while the results for the W anodes tended to some hysteresis. The results show significant unit-to-unit variability, but the shape of the curves generally resembles that of the galvanostatic test results, with a relatively abrupt increase in anodic polarization once a given current level is reached.

The slow cyclic polarization test results for the 2nd set of anodes are given in Figure 20 and 21. The 2nd set tests of both C and W anodes tended to have as a whole small hysteresis, comparable to that observed for the C anodes in the 1st set tests. Therefore, for graphic simplicity only the average values of the forward and reverse parts of the test are presented. Tests were conducted at anode ages of 1, 4 and 13 months. The starting point of each curve generally matched the corresponding position in the potential-current trajectory (Figure 16 and 17) for the respective anode type. The results show increasing anodic polarization with anode age, with the C anodes having a more negative OCP (the zero current condition) than the W anodes, but with a more abrupt polarization increase with increasing anodic current. Unlike the case of the 1st set, the results

from replicate anodes of a given type and aging condition showed relatively little variability.

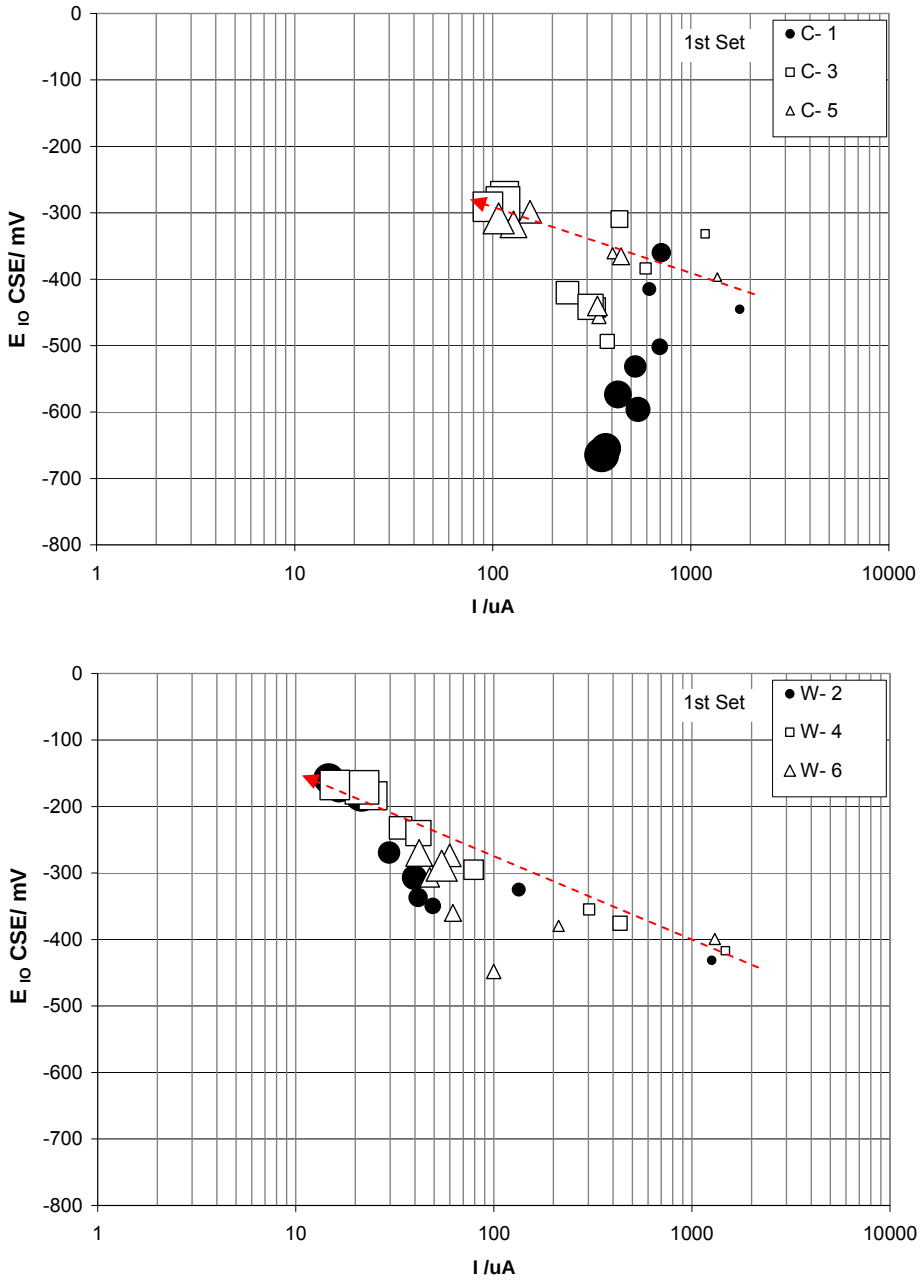

Figure 16 - Potential-Current trajectory for 1st set of anodes in test yard slabs. Largest symbols indicate greater age. See text for explanation of other symbols and on behavior of anode C-1.

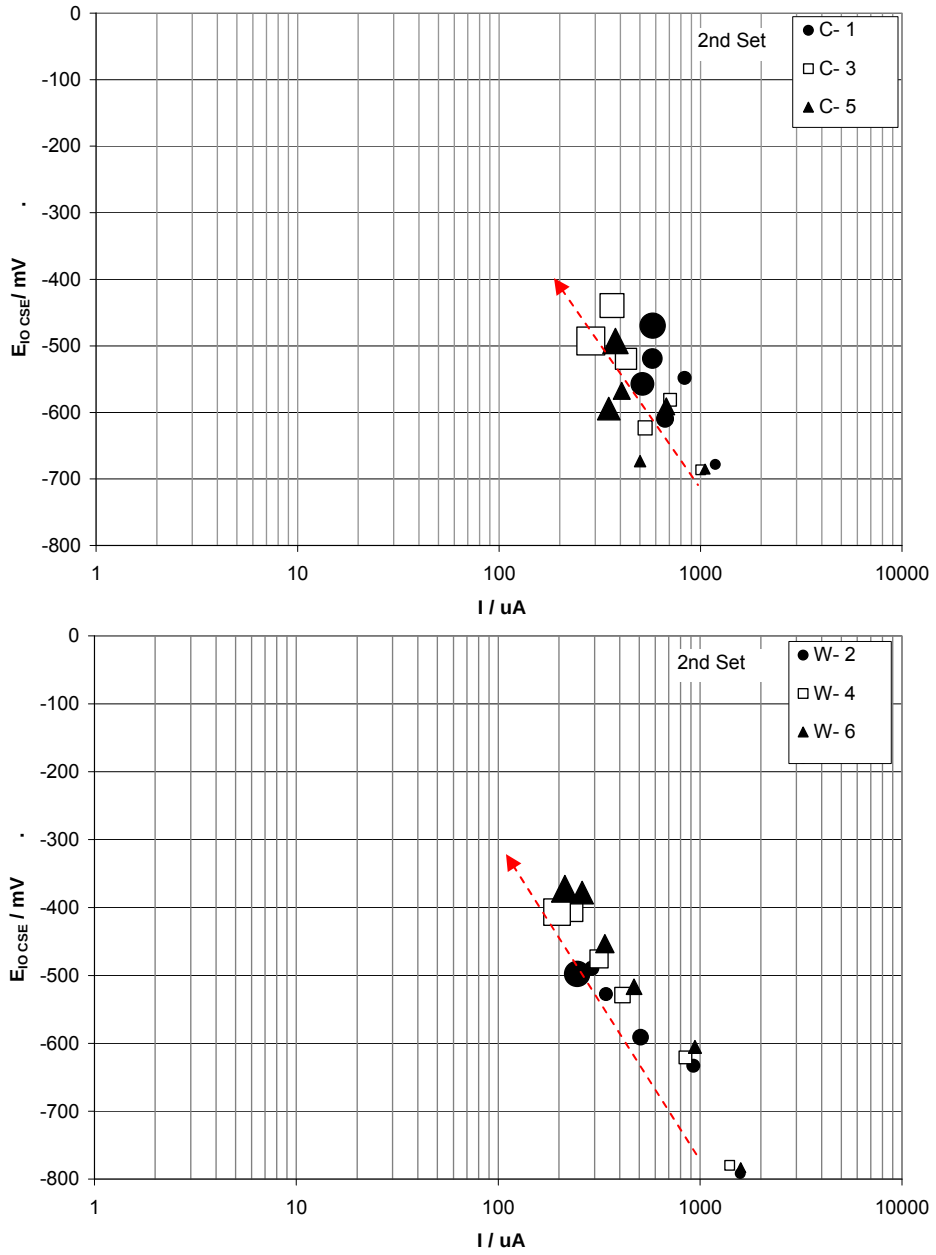

Figure 17 - Potential-Current trajectory for 2nd set of anodes in test yard slabs. Largest symbols indicate greater age. See text for explanation of other symbols.

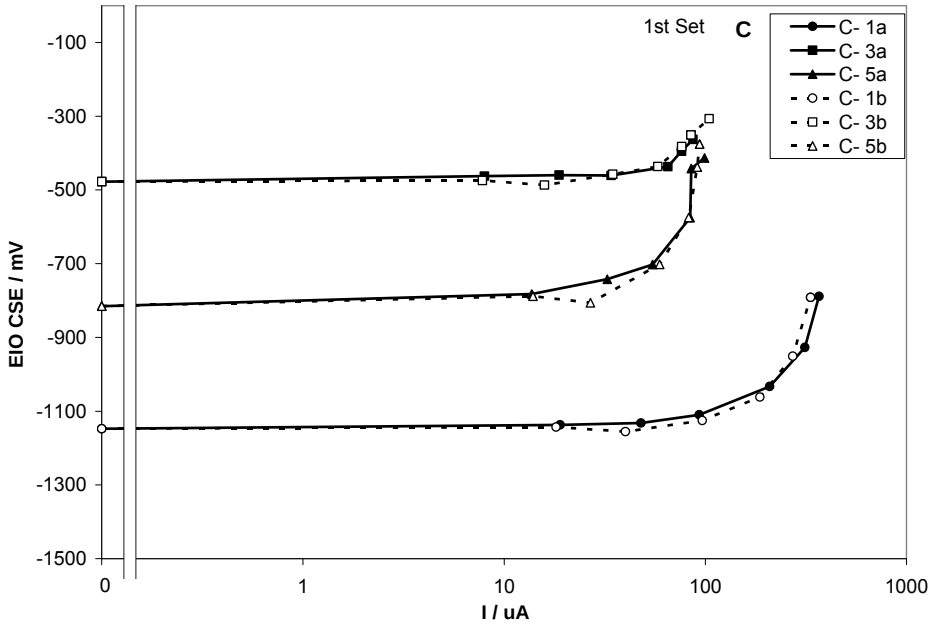

Figure 18 - E_{IO}-log I curves of the 1st set of C anodes in test yard slabs. Polarization curves in the forward (a) and return directions (b)

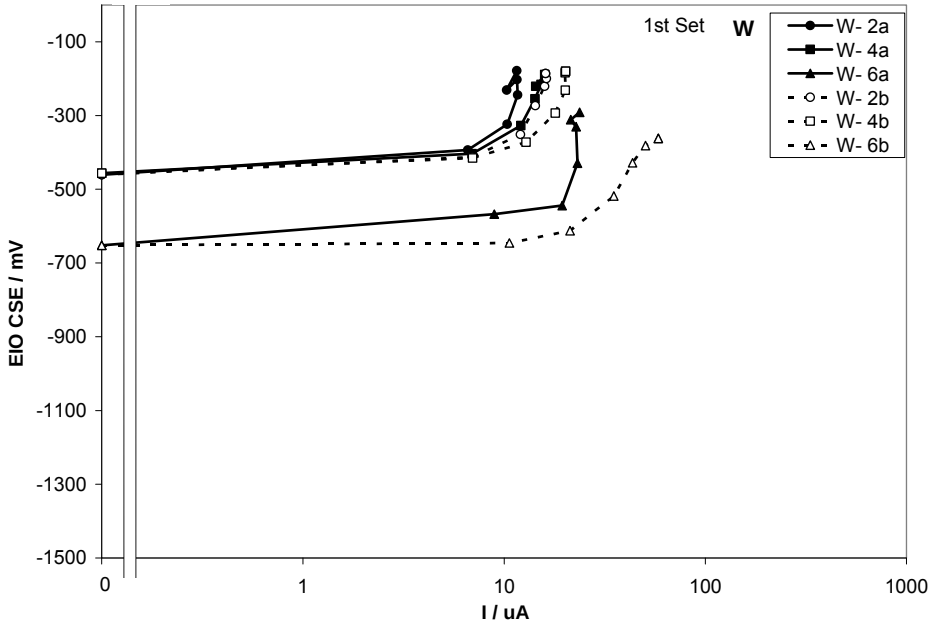

Figure 19 - E_{IO}-log I curves of the 1st set of W anodes in test yard slabs. Polarization curves in the forward (a) and return directions (b).

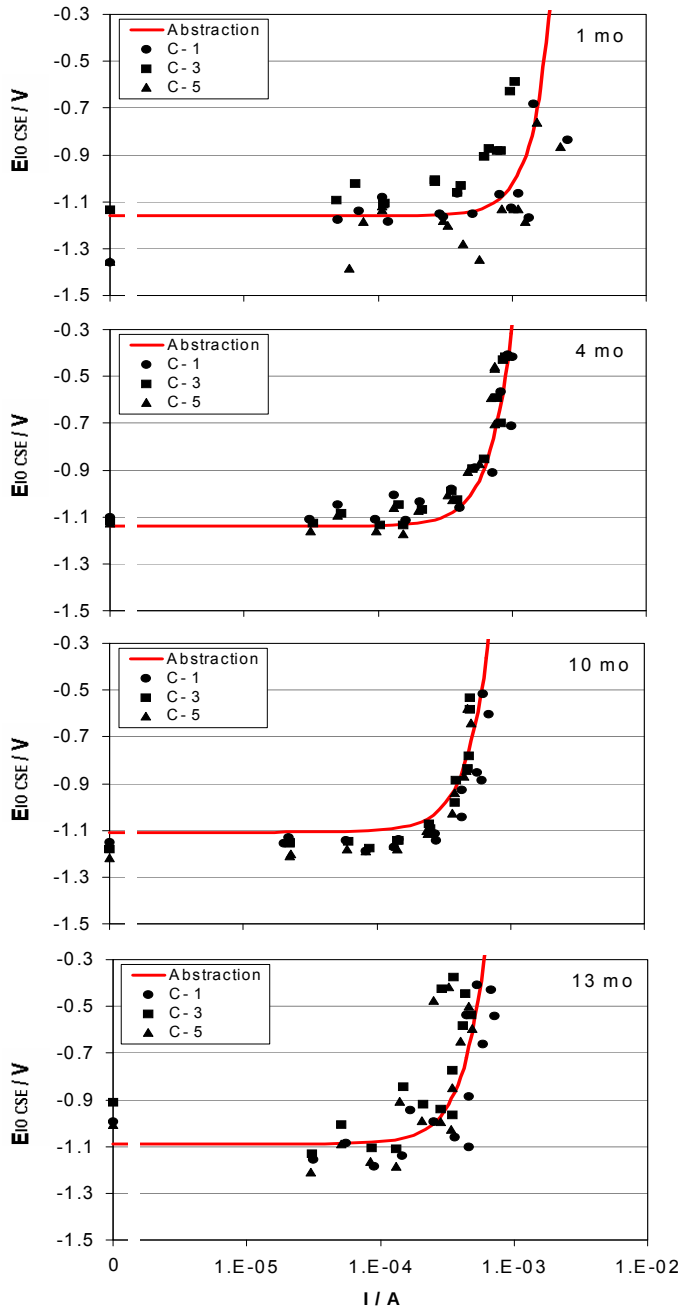

Figure 20 - E_{IO}-log I slow cyclic polarization data for 2nd set of Type C anodes. Data for each of the corresponding test yard slabs (1,3,5), at approximate indicated anode age. Both forward and return data are displayed for each symbol.

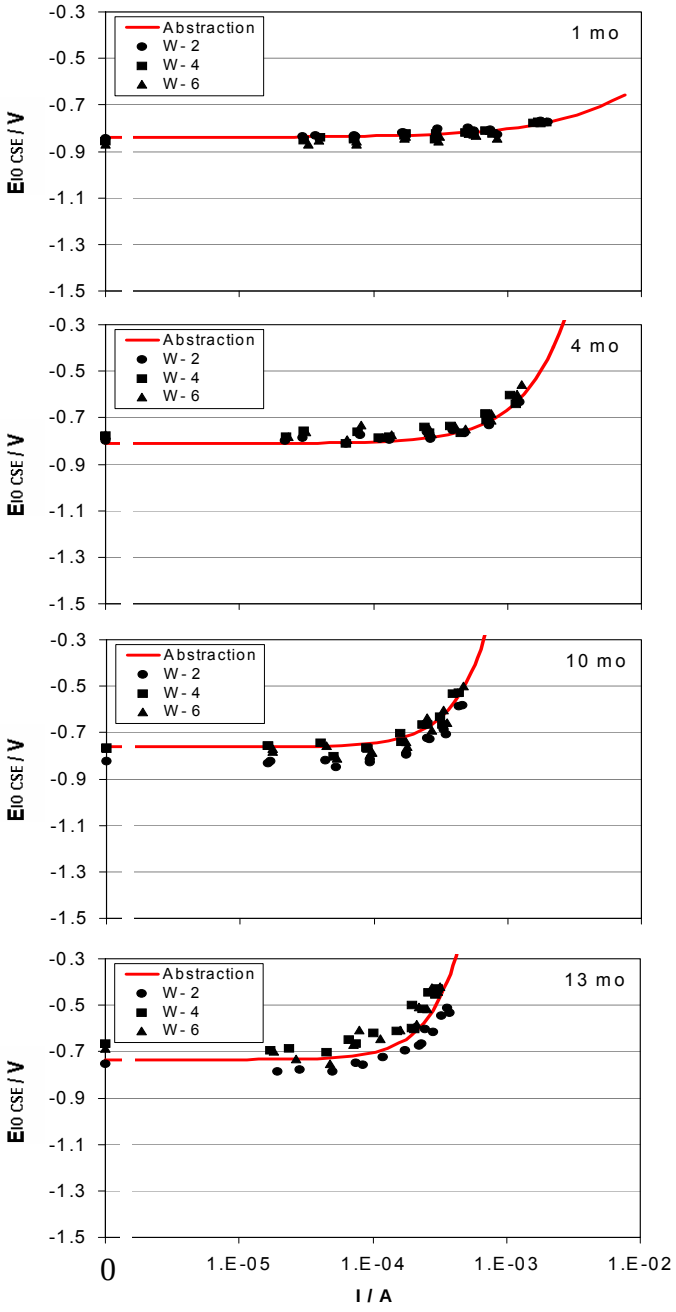

Figure 21 - E_{IO}-log I slow cyclic polarization data for 2nd set of Type W anodes. Data for each of the corresponding test yard slabs (2, 4, 6), at approximate indicated anode age. Both forward and return data are displayed for each symbol.

3.2.2 Rebar Polarization

The amount of current delivered by the 1st set of anodes to the rebars at different positions in the slab at various times is shown in Figures 22 and 23, for stages early and late respectively during the period when all bars were connected (before day 477). Cathodic (protective/preventive condition) current is assigned a positive sign. Currents values are the average of the three slabs of each type of anode. Both types of anode delivered about the same level of current at that time. All the passive rebars were subject to a net cathodic current, and it was greatest for the bars immediately next to the anode. In contrast, some of the active bars in the chloride contaminated zone had negative current indicating that they were acting as net anodes. That effect persisted until the time in which the active bars were disconnected. After disconnection of the active bars (Figure 24) the current to the remaining bars, all-passive, was always cathodic. The bars closest to the anode received the highest current, which decayed for rebars further away. A corresponding pattern was observed at the far end of the slab.

Four-hour depolarization test results of the rebars performed during the evaluation for the 1st set of anodes, while all rebars were connected, are shown in Figures 25-28. The depolarization level achieved was poor or nil on much of the rebar assembly both early on (Figure 25) and after 14 months (Figure 26). Depolarization levels improved somewhat for the C anode yard slabs when both the main and the auxiliary anode were temporarily connected together (Figure 27), but only on the side of the slab containing the anodes and still yielding modest to poor results there. After disconnection of the active rebars (Figure 28, top) the extent of depolarization increased markedly for the C anode yard slabs, exceeding 100 mV on average for the slabs closest to the anodes. By that time the performance of the 1st set of W anodes had degraded dramatically and only poor depolarization levels were reached in those slabs even with an all-passive connected assembly. Later on, (Figure 28, bottom, for day 1000) the average

performance of the C anodes had degraded significantly and average depolarization levels did not reach 100 mV even next to the anode.

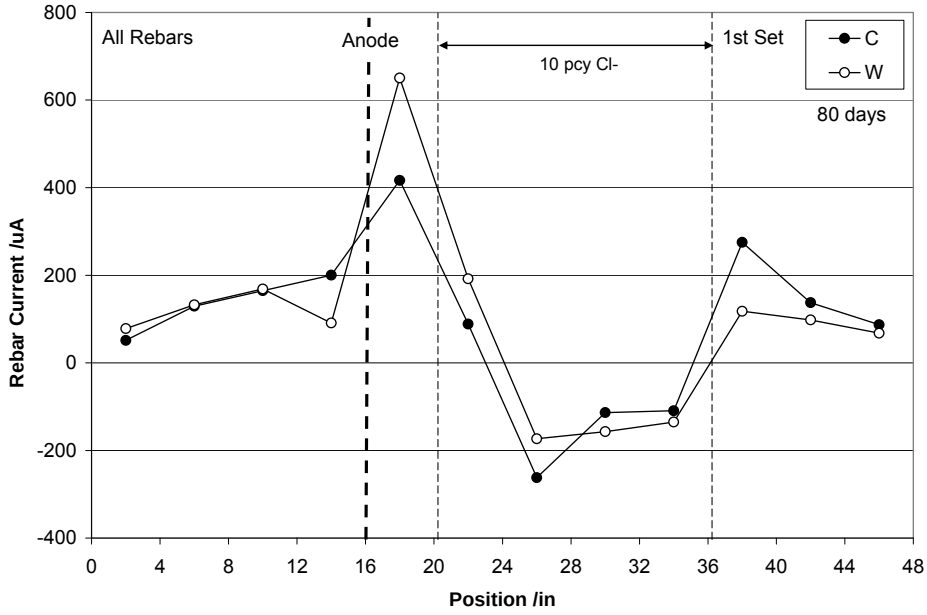

Figure 22 - Rebar current along the yard slab main direction early in the exposure period (80 days). 1st set of anodes. All rebars connected (average of triplicate slabs).

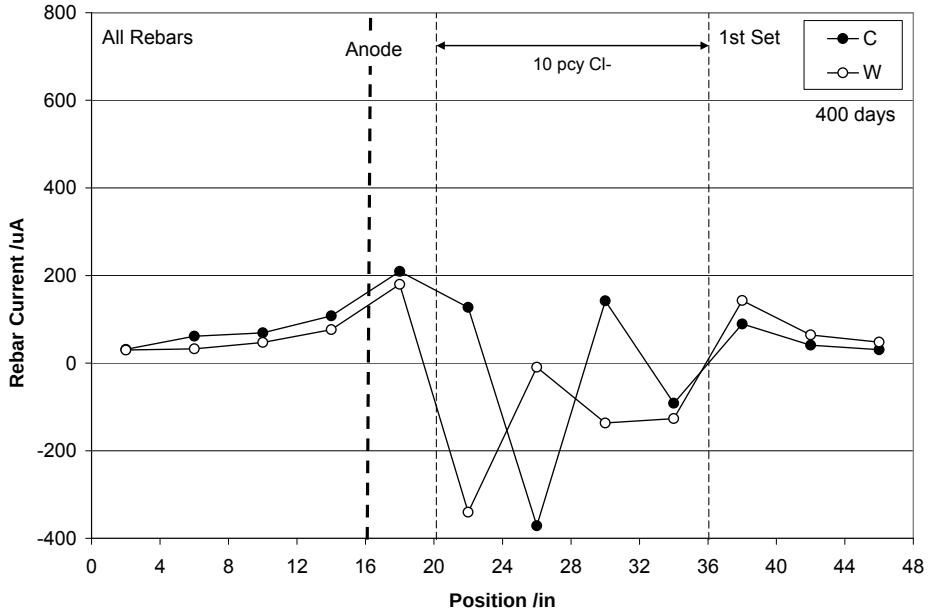

Figure 23 - Rebar current along the yard slab main direction later in the exposure period (400 days). 1st set of anodes (average of triplicate slabs).

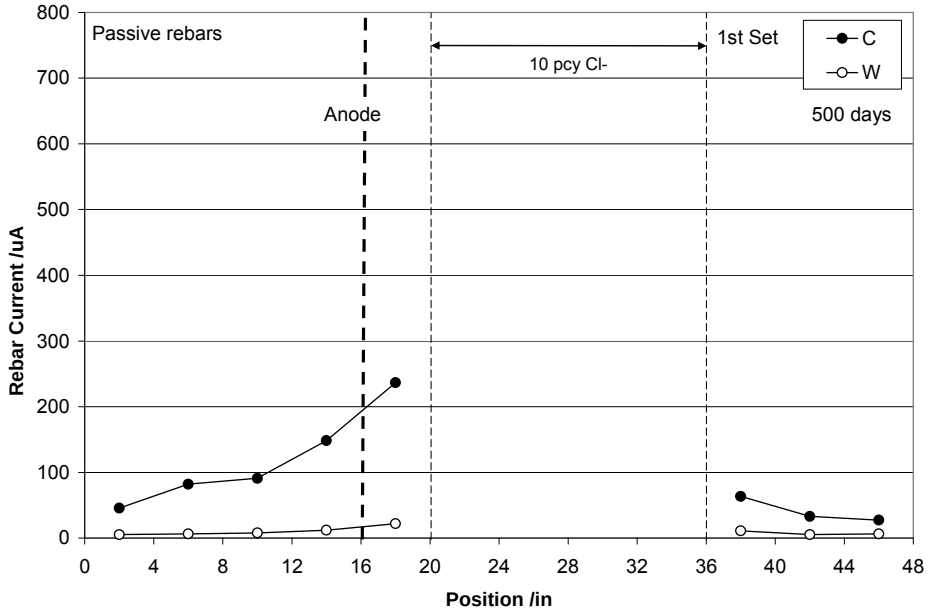

Figure 24 - Rebar current along the yard slab main direction shortly after the 4 rebars in the chloride-contaminated zone were disconnected. 1st set of anodes (average of triplicate slabs).

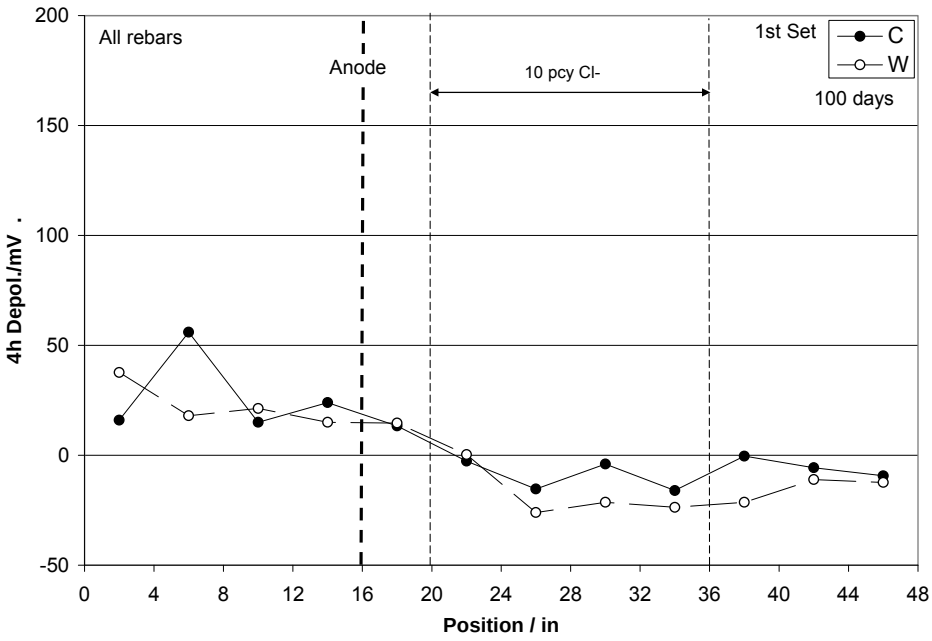

Figure 25 - Four-hour rebar depolarization after 4 months of normal exposure. 1st set of anodes. Average results of triplicate slabs.

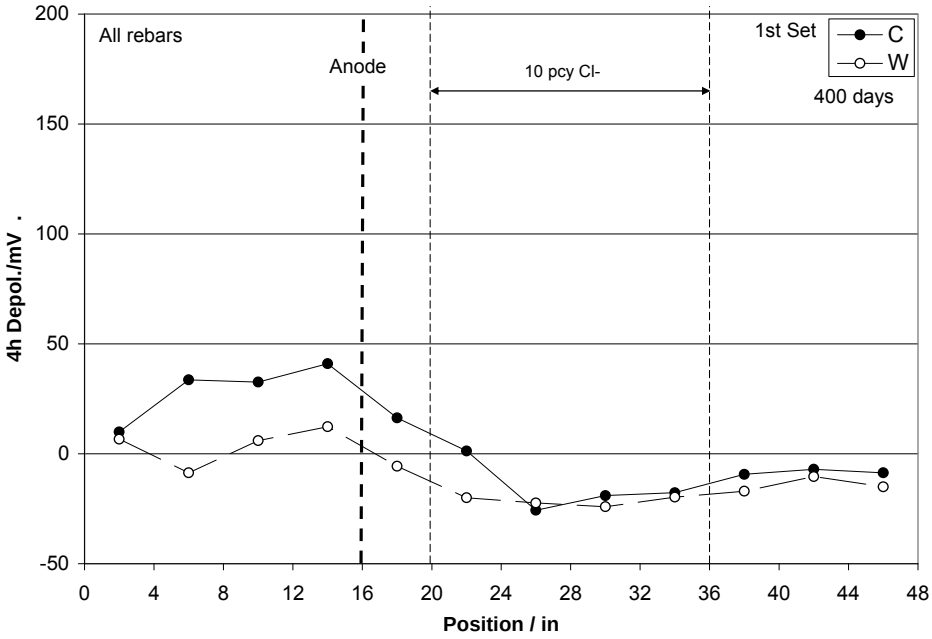

Figure 26 - Four-hour rebar depolarization after 14 months of normal exposure. 1st set of anodes. Average results of triplicate slabs.

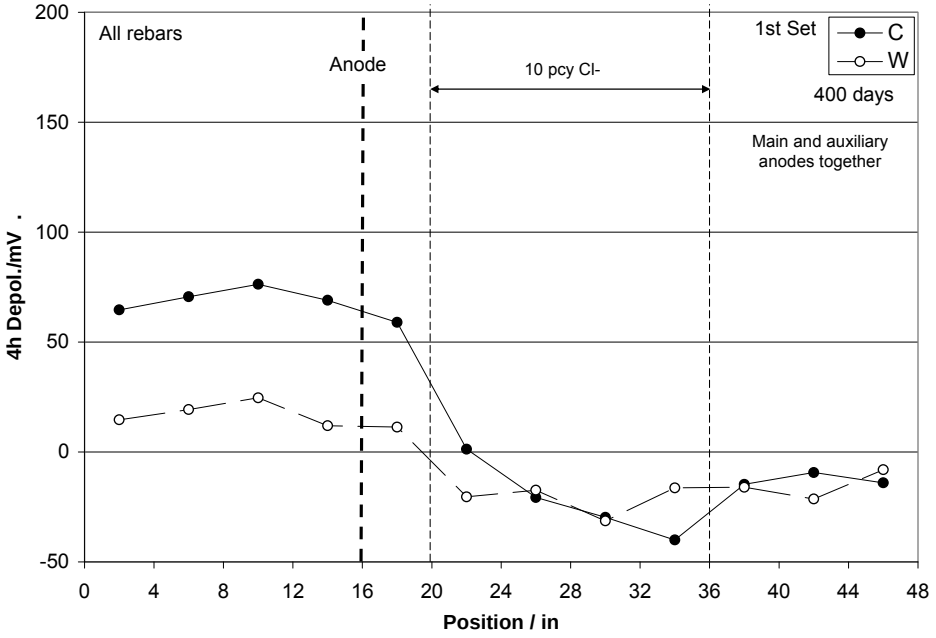

Figure 27 - Four-hour rebar depolarization after 14 months of normal exposure plus several days of jointly connecting the Main and Auxiliary anodes. 1st set of anodes. Average results of triplicate slabs.

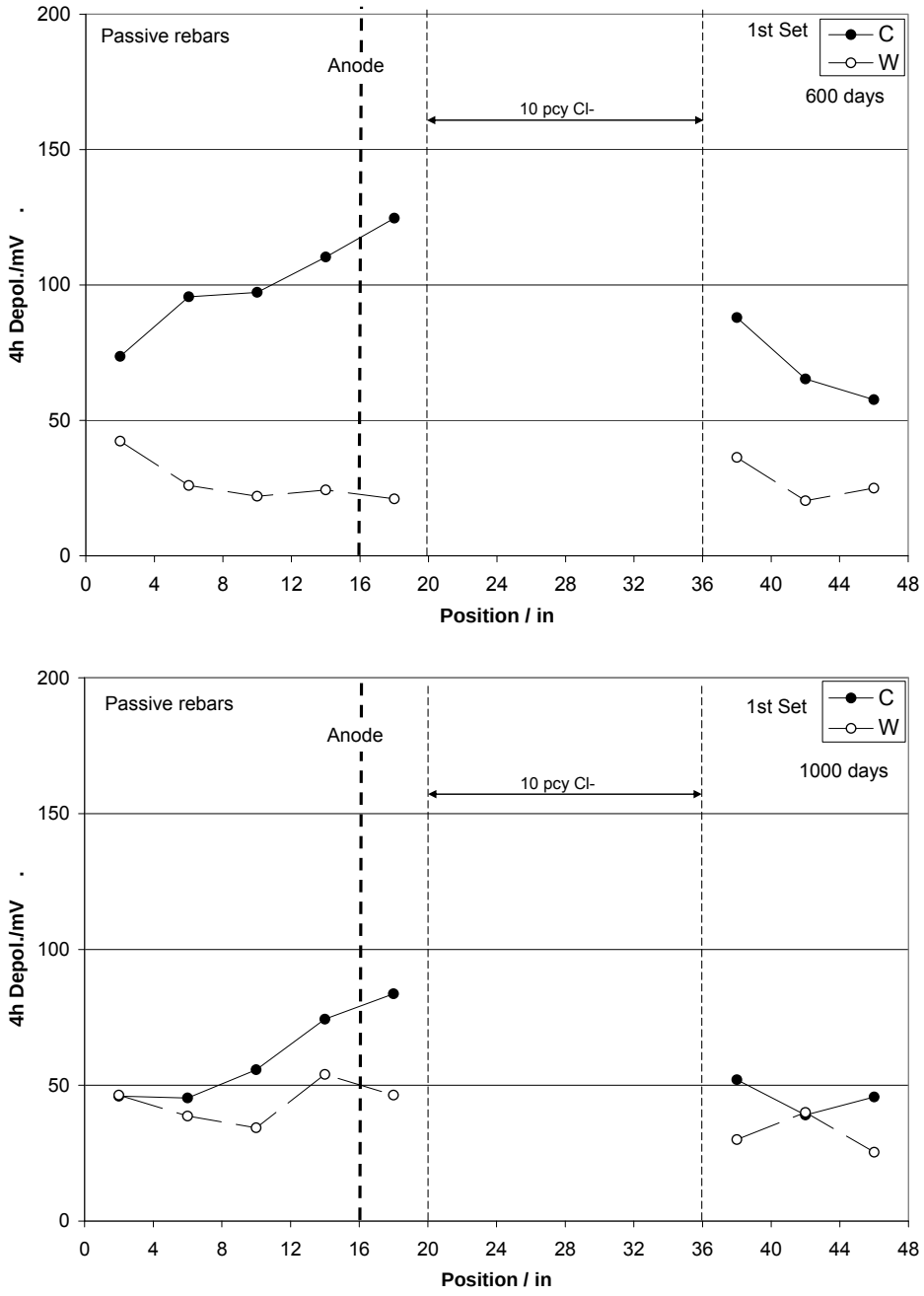

Figure 28 - Four-hour depolarization of passive rebars after disconnection of the rebars in the chloride contaminated zone. 1st set of anodes. Average results of triplicate slabs.

Figure 29 summarizes the depolarization measurement results for the 1st set of anodes for the different conditions and aging times evaluated. Rebar numbering starts at number 1 for the leftmost rebar as shown in the plan view of Figure 7.

Cathodic rebar currents and 4-h depolarization levels increased substantially when energizing the 2nd set of anodes, which always acted only on the passive rebars. The effect decreased moderately with time over the ~500 days test period. Both types of anodes performed comparably although the performance of the W anodes appears to have degraded somewhat faster (relative to the initial levels) than that of the C anodes. Figures 30-32 document these trends.

Each periodic measurement series of the test yard slabs yielded individual Instant-Off potential and current values for each of the passive rebars in every slab. At any given time those values covered a broad range depending on proximity of the rebar to the anode and condition of the anode, and the range varied further as the anodes aged. Since the rebar material was the same throughout and the concrete surrounding the rebar had (with exceptions noted below) the same composition, the combined results are expected to reflect the overall polarization behavior of the steel surface under those conditions. The graph in Figure 33, with results expressed as current densities by dividing current by the nominal rebar surface area confirms that expectation. There the data obtained from separate rebars in the six slabs, spanning a wide time period, generally delineate a cathodic polarization curve. The data in Figure 33 include results for rebars No. 1-5 and 10-12 for the 1st set of anodes, and rebars No. 1-4 and 11-12 for the 2nd set of anodes. Data for rebars No.5 and 10 while evaluating the 2nd set of anodes are not included since, as discussed elsewhere, there was some evidence of chloride levels having increased there significantly by that time , causing incipient rebar activation in some cases. As expected, the large majority of the recorded net rebar currents were cathodic. The data reflect

the typical scatter of test yard slab measurements, of which uncertainty in the potential value is expected to be a major contributor. The solid line represents a fit to the results based on an abstraction consisting of an activation-limited cathodic reaction current density and a potential-invariant passive dissolution anodic current density, as described in the Modeling section.

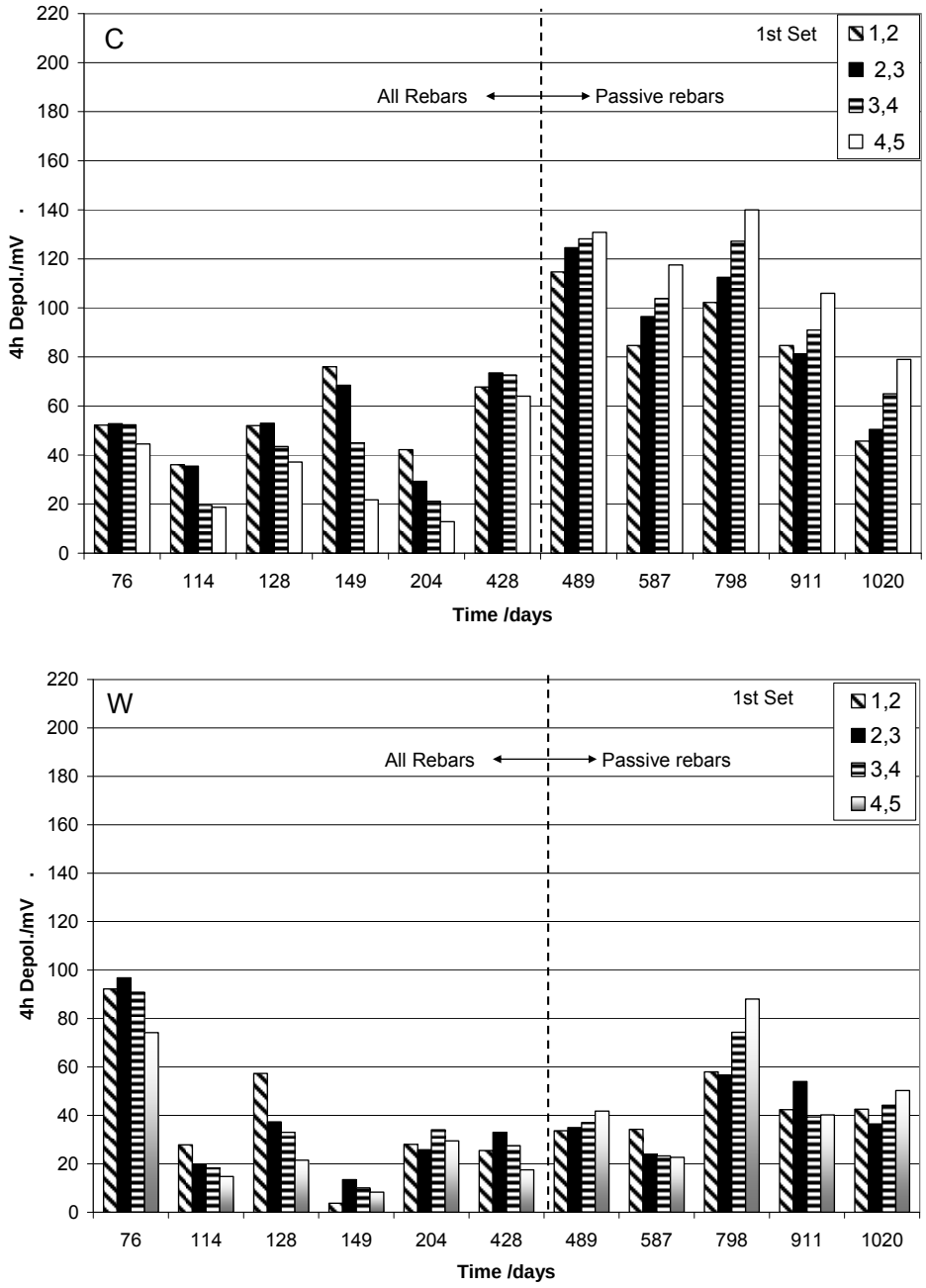

Figure 29 - Summary of 4-h depolarization test results for 1st set of anodes. Columns indicate average value for rebar pair indicated by numbers. Anode was located between rebars 4 and 5. Time indicates period since anode placement.

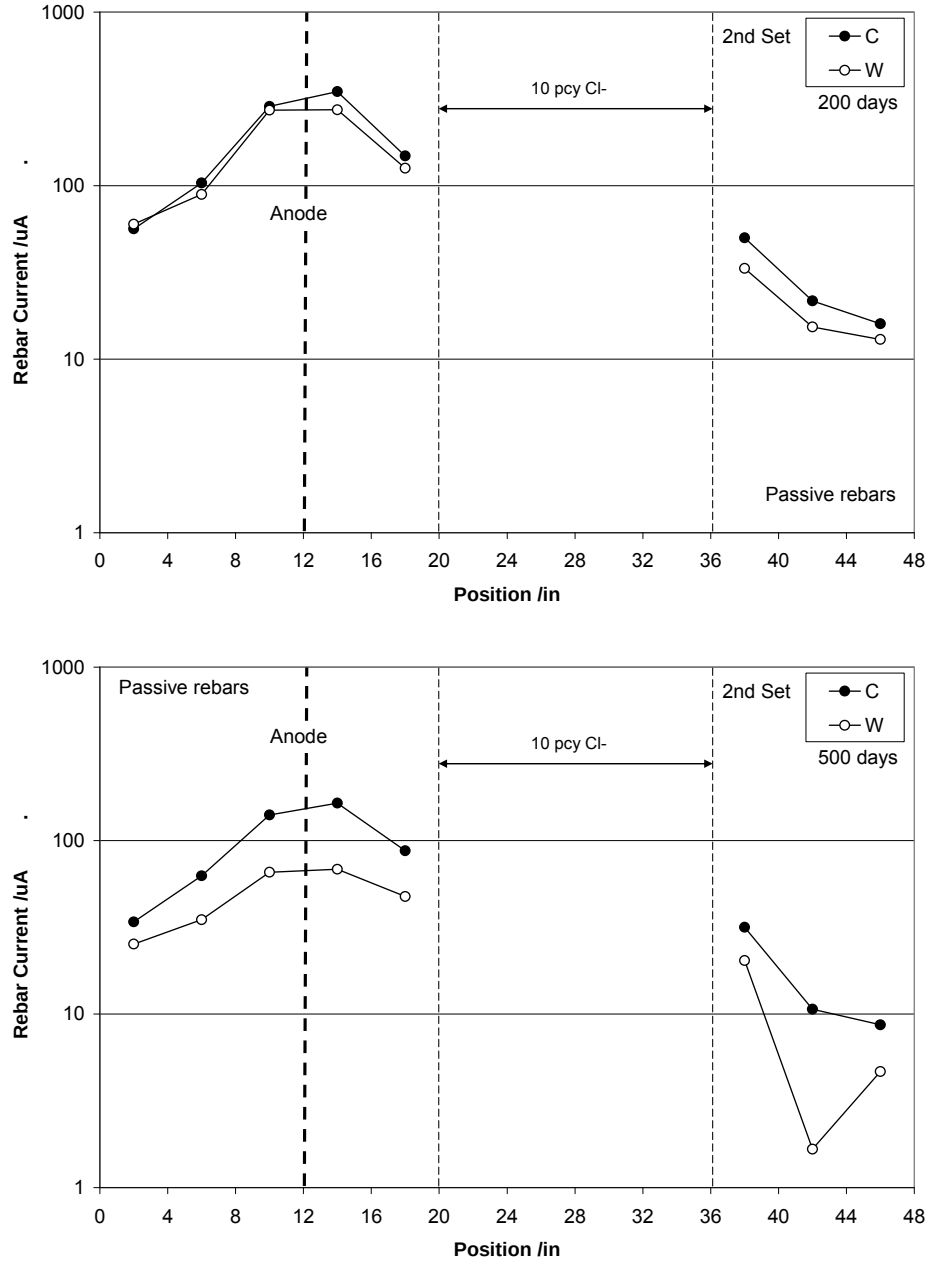

Figure 30 - Rebar current along the yard slab main direction at two different anode ages. 2nd set of anodes (average of triplicate slabs). Only passive rebars connected. Time indicates period since placement of 2nd set of anodes.

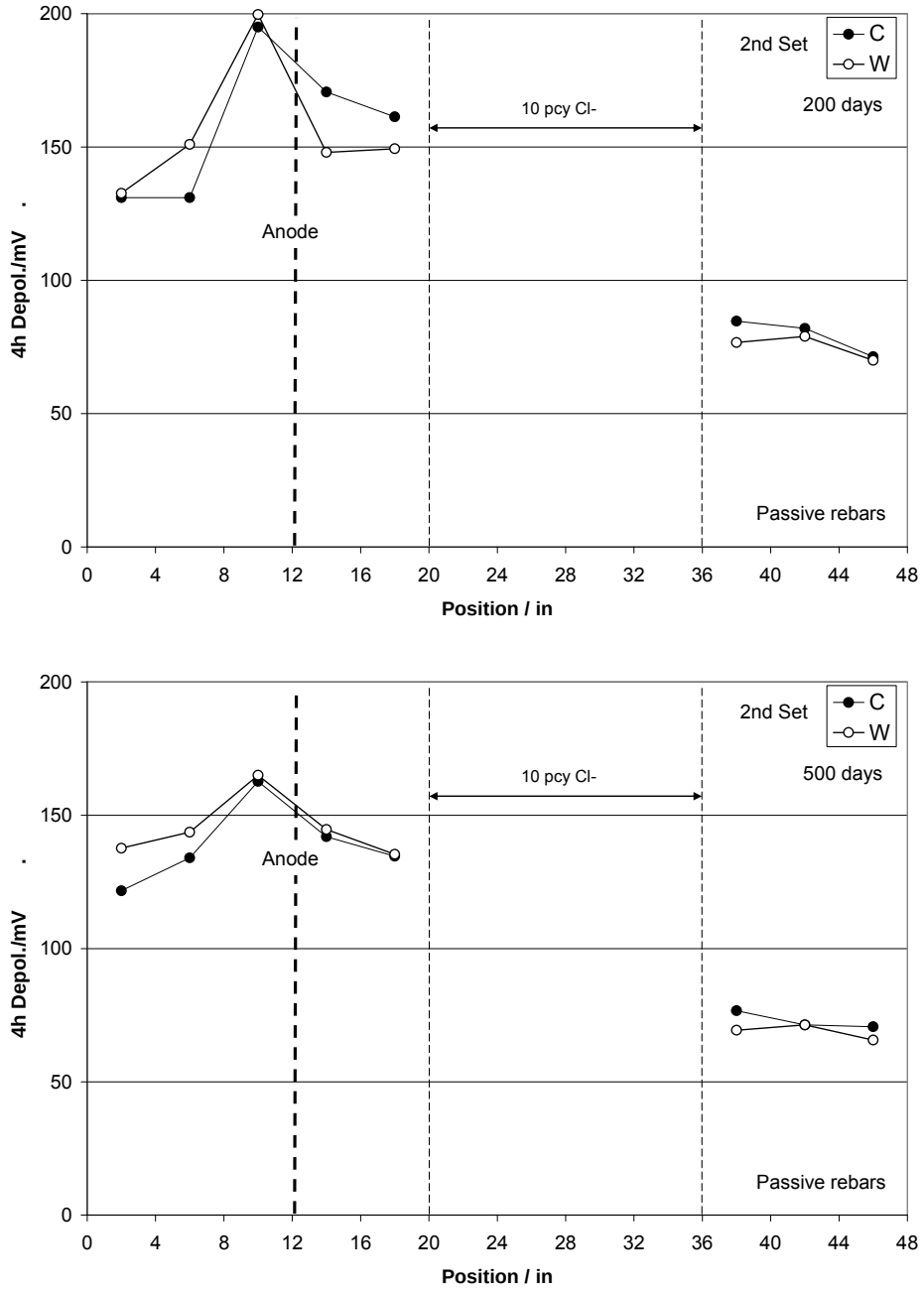

Figure 31 - Four-hour rebar depolarization after 14 months of normal exposure. 2nd set of anodes (average results of triplicate slabs). Only passive rebars connected. Time indicates period since placement of 2nd set of anodes.

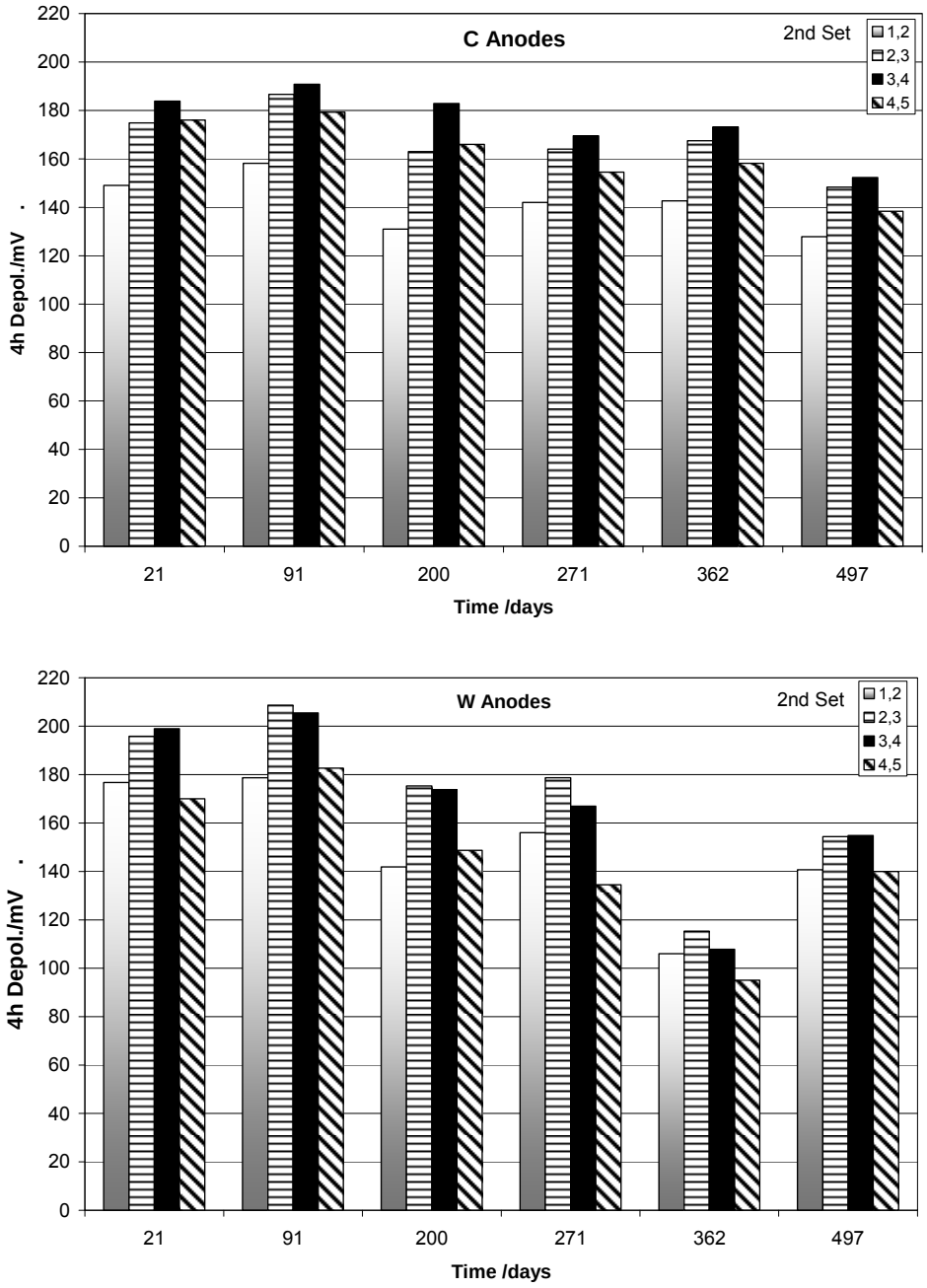

Figure 32 - Summary of 4-h depolarization test results for 2nd set of anodes. Columns indicate average value for rebar pair indicated by numbers. Anode was located between rebars 3 and 4. Time indicates period since placement of 2nd set of anodes. Only passive rebars connected.

3.2.3 Concrete Resistivity and Anode Resistance

Average values of concrete resistivity of the zones with and without admixed chloride of all slabs as function of time since casting the concrete are shown in Figure 34. The resistivity increased with age toward a long term average value approaching 25 kΩ-cm for the zone without chloride, and about half as much for the zone with admixed chloride. There was modest variability from slab to slab (standard deviation typically <20% of the average).

Anode to rebar assembly resistance measurements for the 2nd set of anodes, averaged for a period between ~1 and ~1.5 years after placement were ~240 and 290 Ω for the Type C and Type W anodes respectively. From calculations performed in the Modeling section, it is estimated that ~2/3 of the anode to rebar assembly resistance is due to the anode-concrete current spread resistance.

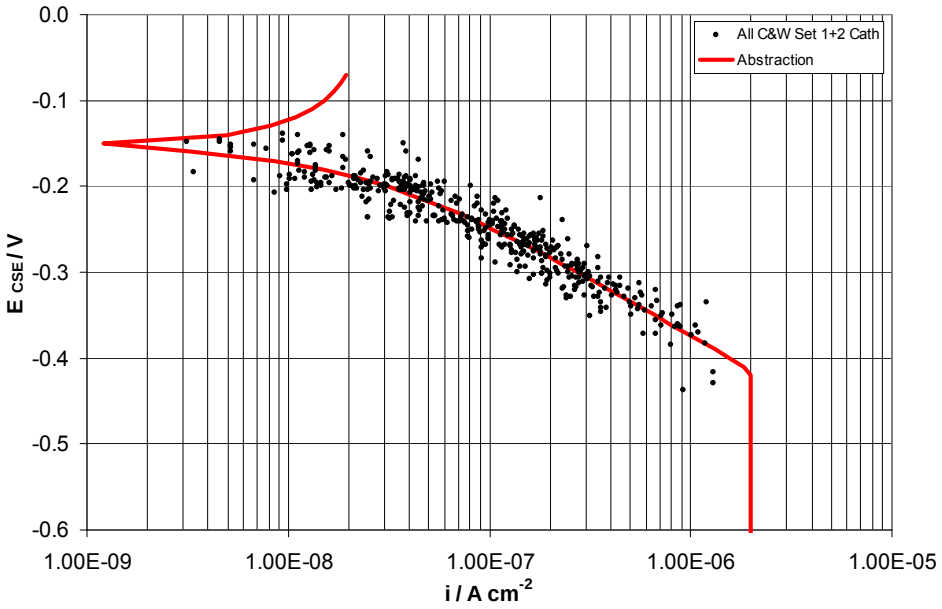

Figure 33 - Combined E_{IO}-log i representation of the individual Instant-Off potential and current density values for passive rebars. Data recorded during evaluation of both sets of anodes.

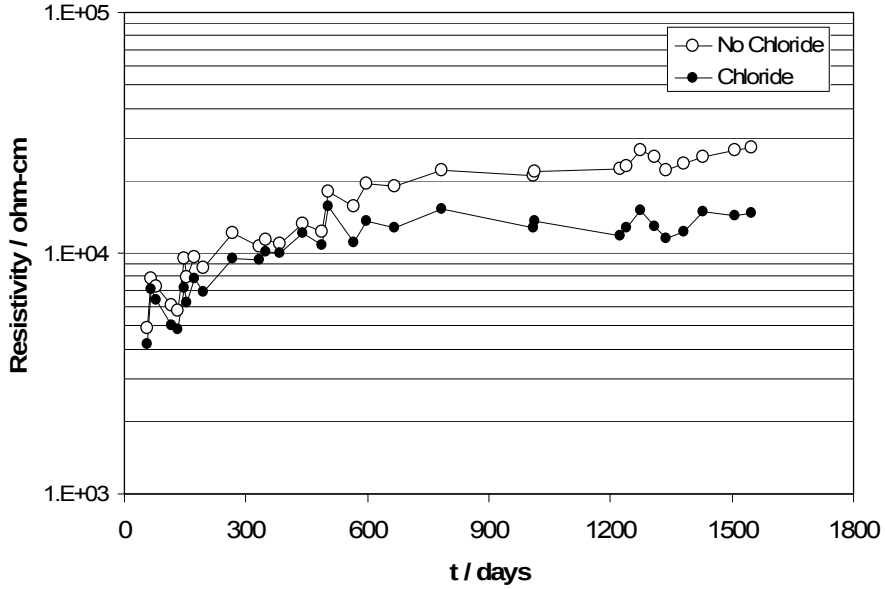

Figure 34 - Concrete resistivity of the zones with and without admixed chloride of all slabs as function of time since casting the concrete.

4. DISCUSSION

4.1 Anode Potential-Current Functions (PFs)

Both the galvanostatic RH chamber and the test yard slab revealed, for both types of anodes, comparably shaped PFs. The functions showed at low current levels relatively little anodic polarization away from the open circuit potential, followed by an abrupt (in terms of a logarithmic current scale) increase in polarization as the current approached an apparent terminal value. The curves resemble the behavior expected from a system that is approaching a transport-controlled limiting current density, or alternatively, the presence of a sizable ohmic resistance [Jones 1996]. As the curves were constructed using Instant-Off potentials, it could be argued that the presence of an ohmic solution resistance component would have been cancelled by the test method used. However, as noted elsewhere [Sagüés 1994] an Instant-Off (or a high frequency EIS) procedure may not completely cancel out all ohmic polarization components if the corrosion is localized to small parts of the metallic anode surface. That localization may affect various parts of the anode surface as time progresses, so this effect could not be completely ruled out even if autopsy tests were to show a cumulative, near uniform corrosion wastage of the metallic anode. A transport-limited polarization component could occur due to dynamic accumulation of anode corrosion products on its surface, which would effectively shift the equilibrium potential of the anode toward a more positive value as observed. These issues merit attention in continuation research.

For a given test condition and anode service history, the PFs showed notable variability among anodes of the same type in the 1st set of anodes

tested. Thus, in the aged condition two of the three type C 1st set anodes in the replicate test yard slabs had relatively elevated E_{OC} values and low apparent terminal currents, while the remaining anode showed much greater activity. Significant variability, although at much lower performance levels, existed also for the aged type W 1st set of anodes. Unit-to-unit performance variability among each type was much less for the 2nd set of anodes. In the test yard slab the 1st set of W anodes showed notably inconsistent behavior with that of the 2nd set, even though both sets were nominally the same product. The 1st set, as a group, performed much worse than the 2nd suggesting a production problem in the former. Consequently, in the following the discussion of the PFs of type W anodes will address principally the functions determined for the 2nd set, with the qualification that production uniformity may be an issue.

In general and at moderate aging levels and humid conditions, the C anodes tended to have more negative open circuit potentials, and faster polarization upon current delivery, than the W anodes. Nevertheless, both anodes tended to reach roughly the same operating point when coupled with passive steel in the test yard slabs. Similar behavior was observed in the galvanostatic tests at 95% RH. Initial trends in the 60% RH chamber (1st set of anodes only tested there) showed for both anode types comparable relative PF features to those seen in the other environments, but it should be recalled that early in that exposure the embedding medium likely still retained much of the initial free water. Later behavior in the 60% RH chamber was obscured by data scatter.

Aging of the anodes by delivering current in service was manifested in the test yard slab, for both types and sets of anodes, by the continually decreasing current output. Increasing ohmic resistance as concrete aged is expected to have been only a minor factor in this decay, since resistivity roughly stabilized in value after the first year, as shown in Figure 34. There was no indication either

of any important change in the polarizability of the steel bars that would have resulted in a strong decrease in cathodic current demand as time progressed.

As implied by the slow cyclic polarization test results, the current decreases most likely reflect primarily an evolution of the PF generally toward more positive open circuit potentials and, more importantly, to the onset of elevated polarized potentials at increasingly lower current levels. That situation is explained in Figure 35 where idealized PF curves are shown for a fresh anode (t=0) and for increasingly aged conditions (t_1, t_2). The anode is coupled to a rebar assembly that creates a cathodic current demand as indicated. For each condition the operating point of the anode is denoted by the open circle. The effective ohmic drop between the steel and the anode is given by the vertical space between the open and filled circles. As the anode ages, the operating point describes the trajectory indicated by the arrowed red line, with corresponding decrease in current delivery and increase in anode potential denoted also by red arrows. That interpretation is supported by the observation of such trajectories for both types and both sets of anodes in Figures 16 and 17.

The evolution of anode potential with time toward more positive values was much faster for the 1st set of anodes than for the 2nd (Figures 12, 16 and 17). This behavior is explained in the following as a consequence of the steel bars in the chloride contaminated zone having been connected to the anode for the first half of the evaluation period of the 1st set of anodes. Moreover, the Type C 1st set anode for Slab 1 (C-1) showed anomalous behavior in that its potential elevation trend was reversed at later exposure times (Figure 12). That anomalous behavior will be considered next as well.

The chloride contaminated zone contained 1.5% Cl^- ion by weight of cement, about 4 times the value of commonly assumed critical threshold values for corrosion initiation [Li 2001]. The steel bars there were externally connected to the anode already during casting and curing of each slab, and were kept so

over the first 477 days of testing. That coupling was however not sufficient to prevent corrosion initiation of the four rebars in that zone, which were found to be in the active condition from the start. Active rebar has low polarizability, and given the quite low concrete resistivity during the first year of operation (~7 to 10 k Ω-cm, Figure 34) and the large steel surface area involved, that group of four rebars was an important contributor in determining the potential over much of the system. Indeed, as shown in Figure 23, some of those rebars were net anodes even though they were only about 15 cm (6 in) from the point anode. Thus, except for a very short initial period (Figure 12), for much of the initial year or so of evaluation of the1st set of anodes the anode potential was more or less stabilized at a value not much below that of active reinforcing steel in chloride-contaminated concrete (e.g. ~-400 mV CSE). Consequently the potential-current trajectory for the first set normally spanned a shorter potential range than if the anode would have been in contact with a more polarizable (i.e. passive) assembly. That latter scenario applied to the second anode set, for which the rebars in the chloride zone were never connected. Accordingly, the potential-current trajectories for the 2nd set anodes were found to span a wider potential range (Figure 17) more fitting to the outcome described in Figure 33.

The auxiliary anodes did not have a galvanic current load so in principle their potential history should be indicative of the effects of self corrosion plus any changes in the composition of the proprietary mortar in the pellet surrounding the metallic core. With the exception of the auxiliary C anode in Slab 1, the potential changes were significant over time (hundreds of mV) and in the positive direction suggesting degradation. A possible cause for that evolution is diffusion into the surrounding concrete of the substances in the anode pellet that were responsible for zinc activation. For young concrete with the mixture proportions of the ORC in the humid outdoors environment used, diffusivity of ionic species typified by that of chloride ions is in the order of 10^{-8} to 10^{-7} cm^2/sec [Sagüés 1994], and likely nearer to the high end of the range based on the low values of resistivity

observed [Berke 1992]. Consequently characteristic diffusion distances of ionic species into the surrounding concrete after a year or so could amply exceed 1cm. That distance is in the order of the pellet thickness so substantial dissipation of anode activators with the test time interval would not be surprising. That dissipation could be an important contributor to anode performance derating over time, above and beyond any detrimental effects from galvanic current delivery.

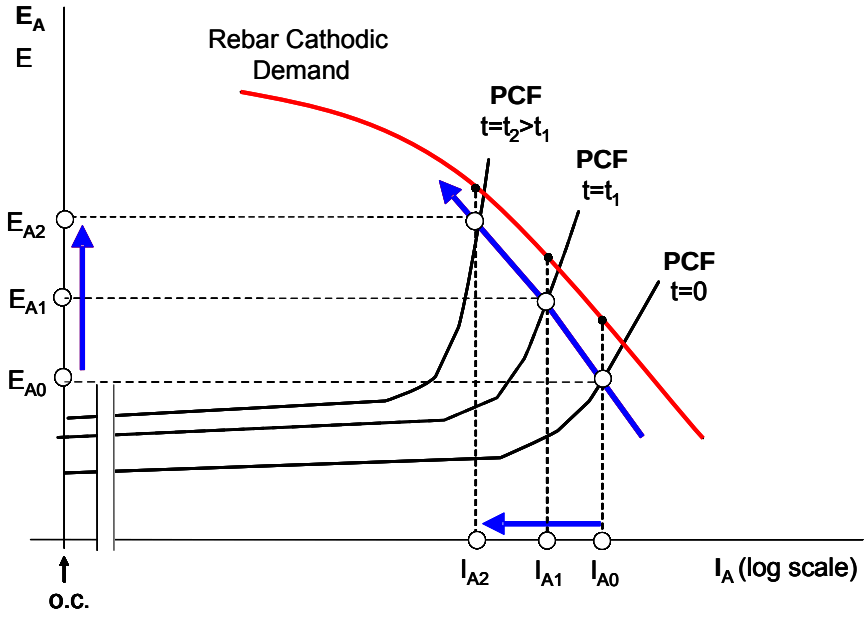

Figure 35 - Idealized evolution of anode PF with aging and effect on operating conditions. E_A, I_A: anode potential and current; o.c.: open circuit condition. Black circles indicate the polarization condition of the anode. Filled circles correspond to the effective rebar polarization condition, at a potential equal to that of the anode plus an ohmic drop difference. Arrows indicate trends as aging time increases

The more straightforward anode degradation effect expected from current delivery is loss of anode mass. Based on the measurements reported in Section 2.2, rounded-off values of 110g and 45 g will be assigned in the following to the initial anode metallic mass of Type C and W anodes respectively. Those masses correspond respectively to 1.68 and 0.69 mol of Zn, based on the atomic weight of Zn = 65.39 g/mol. Assuming dissolution as Zn^{+2} ions the maximum (also called the "theoretical") amount of galvanic charge Q_T that could be delivered can be calculated. The amount, equal to 2 F n_M, where F=96.49 k Coul/equivalent is Faraday's constant and n_M is the number of moles, is then Q_T=324 k Coul and Q_T =133 k Coul for C and W anodes respectively. Anode self corrosion and loss of physical continuity between parts of the anode or with the connecting wires often lower significantly the practical amount of possible charge delivery by actual cathodic protection anodes, e.g. to ~0.5 Q_T. Thus, even if other factors have not already had significant derating consequences, by the time the anodes evaluated here deliver about 160 k Coul (C) or 65 k Coul (W), they would be expected to be approaching the end of their effective service life.

As shown in Figure 14, all type W anodes in the 1st set tested in the yard slabs showed substantial loss of the ability to provide galvanic current after having delivered only 10 to 22 kCoul, or only ~7% to 15% of Q_T. Two of the C anodes in the 1st set experienced faster current derating at Q ~10% of Q_T, but anode C-1 in that set still retained appreciable current capacity at Q ~20% of Q_T. Performance of the W anodes in the 2nd set showed considerable improvement over the 1st, as current remained at substantial levels for all three anodes with Q approaching 25% of Q_T. The 2nd set of C anodes performed, up to the final data acquired at Q ~10% of Q_T, similarly to the earlier stages of the1st set when only moderate current decay was taking place.

The potential trends as function of Q shown in Figure 15 correlate well with the current trends only for the 2nd set of anodes, likely because of the obscuring effect of coupling to the active bars during the first part of the

evaluation of the 1st set. The 2nd set potential and current trends, if they were to be sustained over later aging stages, would suggest that current delivery for these test conditions would reach values well below 100 μA, and potentials approach ~-200 mV (thus providing little beneficial effect), at Q ~¼ to ⅓ Q_T for the Type C and W anodes respectively. Such projection would be somewhat, but not extraordinarily less than the behavior expected for many galvanic anode systems as indicated earlier.

The energized and the auxiliary 1st set Type C anodes in Slab 1 showed anomalous active behavior, as suggested by the highly negative potential of both anodes late in the test period, and by the high current and total charge delivery of the energized anode. This behavior is suggestive of anode activation beyond that expected from the effect of the anode pellet mortar and the initially chloride-free ORC medium. Such activation is likely to have occurred because of chloride transport from the chloride contaminated zone into the nearby concrete surrounding the anode. As indicated earlier, the characteristic chloride diffusion distance in the sound concrete could easily be >> 1 cm after 1year, and it may have been even higher locally due to the instances of poor consolidation noted earlier. Also as indicated earlier, there were also signs of incipient activation of rebars No. 5 and No. 10, (immediately on either side of the chloride zone) in some of the slabs during the last stages of testing. Those observations are further indication of substantial chloride diffusion into the previously chloride free concrete. Consequently, the behavior of the 1st set of C anodes in Slab 1 may be explained by that slab being the first where chloride intrusion into the previously chloride-free concrete reached a sufficient level to promote enhanced activation of that anode. This explanation will be further examined in continuation testing of the auxiliary and disconnected 1st set anodes of the other slabs to ascertain if signs of activation develop there as well in the future. It is noted that the 2nd set anodes were intentionally placed one extra rebar step further than the 1st set from the chloride transition line, to minimize the chances of extraneous activation from Cl^- ions diffused in from the chloride-rich zone.

4.2 Rebar Polarization

The poor rebar polarization levels achieved by the 1st set of anodes while all rebars in the yard slab were connected can be ascribed to the low polarizability of the active rebars, as discussed earlier. The rebar current distribution patterns along the slab main direction showed that, before their disconnection, rebars in the chloride-contaminated zone were often net anodes, contributing at times a total anodic current comparable to or exceeding the current supplied by the point anode. During that period, the rebar potential distribution along the slab main direction showed clearly that the rebars in the chloride contaminated zone, which exhibited potentials typical of actively corroding steel, were a substantial polarizing source for the rest of the system. The steel in the chloride zone of the slabs had potentials similar to, or even more negative than, the typical potential of the main anode, which in turn was more negative than that of the bars in the chloride-free concrete zones. When conducting depolarization tests, the overall potentials relaxed relatively little, toward terminal values influenced by those of the active rebars. Consequently, the overall depolarization levels were poor. These results indicate also that point anodes of this size and at the placement density used, and for the amount of steel present in the slabs, are not likely to provide substantial levels of conventional cathodic protection of an already corroding rebar assembly.

After disconnection of the active rebars in the 1st set tests, the anodes were indeed the most negative elements in the system, and the only source of cathodic polarization of the remaining, passive, bars. The steel depolarization levels for the Type C anodes, which were still quite active at that time, improved accordingly to average levels in excess of 100 mV for the rebar group closest to the anode. The 1st set of Type W anodes had already degraded considerably by that time and failed to achieve appreciable levels of polarization even for only the passive rebars.

For the 2nd set of anodes polarization involved always only the passive rebars, and overall rebar polarization was consequently improved from the beginning compared with that of the 1st set. Furthermore, the 2nd set of Type W anodes did not show the deficiency affecting the 1st set and steel polarization for those anodes improved accordingly.

The composite cathodic rebar polarization curve shown in Figure 33 shows features well establish by previous work, including an apparent Tafel region at low polarization levels followed by incipient indications of the establishment of a diffusion control regime at greater polarization levels. The main cathodic reaction has the characteristics of oxygen reduction, and the polarization/current function parameters match approximately those reported elsewhere for steel in moderately humid concrete [Sagüés 2003]. Further analysis of this curve is presented in the Modeling section (Chapter 5).

5. MODELING

5.1 Introduction

A one-dimensional numerical model was developed to study the behavior of galvanic anode systems for patch repair applications in reinforced concrete structures. The anode performance is measured by how far away from the patch perimeter (the "throwing distance" x_T) an amount of cathodic polarization meeting or exceeding a required minimum (the "prevention criterion" C_P) can be provided to the passive rebar surrounding the patch[3]. A generic patch configuration with a 1-D approximation was used in the modeling to calculate the throwing distance that could be achieved by a given number of anodes per unit perimeter of the patch area, concrete thickness, concrete resistivity, amount of steel and amount of polarization needed for cathodic prevention.

Several numerical models including finite element and boundary element methods have been applied in the past to reinforcing steel corrosion [Presuel-Moreno 2005B, Kranc 1994, Sagüés 1994]. The present model was based on the finite differences method using a regular spreadsheet program. Experimental data on the anodic polarization as a function of service time (PF curves), and the polarization information for the steel coupled to the anode presented in the previous sections, were used as input parameters in conjunction with other variables that will be introduced later. Results from the model allow determining the current and potential distribution on the cathode as a function of the distance from the anode element.

[3] The value of C_P is an input to the model, to be chosen based on the extent of chloride contamination in the concrete around the patch and how the chloride threshold depends on potential. This issue is discussed separately later on.

5.2 Anode - Rebar System Modeled

The simplified system chosen for implementation of the model consists of a reinforced concrete slab (which may represent a bridge deck, parking structure floor, or a part of a wall) having a patch zone in which all the concrete has been replaced as shown in Figure 36. The patch is assumed to be roughly circular with anodes placed at uniform intervals w (anode center-to-center distance) just inside the patch perimeter. It is assumed for simplicity that x_T is not large compared with the dimensions of the patch, so radial spread of the galvanic current is modest. The rebar mat (or mats) in the slab is treated as roughly corresponding to a uniform amount of steel surface to be polarized per unit area of the external concrete footprint. Thus, the problem can be considered on first approximation as a 1-D current distribution calculation. Further simplifications involve assuming uniform concrete resistivity, concrete thickness and rebar polarization properties. The latter include a time-and potential-independent anodic passive dissolution current density and a time independent cathodic reaction (oxygen reduction) current density equal to that determined experimentally on the rebars in the yard slab tests, but constricted by a limiting current density of fixed value. The polarization function (and its dependence on service time, t, or total charge delivered, Q) of the point anode correspond to that observed experimentally for each of the two types of anode investigated. The current needed to polarize the region of steel inside the patch area is neglected for simplicity. A variation of that treatment was conducted as well to take into account for the presence of that steel and is presented later on.

The base conditions outlined above then correspond to an anode placed at the end of a linear concrete beam, with the galvanic current running lengthwise and a distributed sink current density on the steel given by the local concrete potential and the polarization function of the steel. At the anode end of the beam the potential is a function of the end potential and the polarization function of the anode. The nomenclature to be used is listed in Table 2.

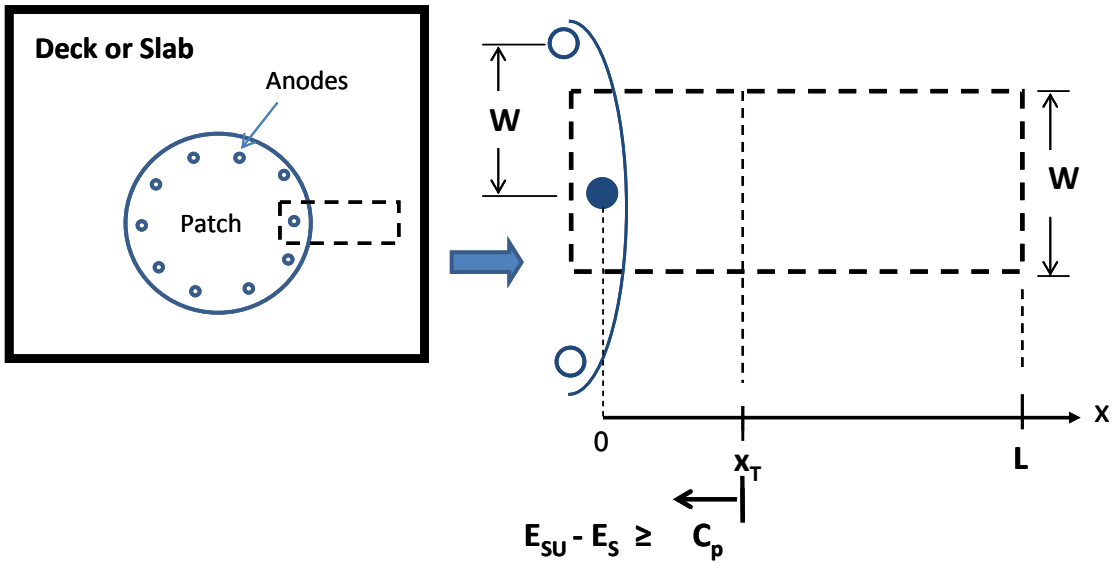

Figure 36 - Plan view of idealized system chosen for implementation of the model

5.3 Principles and Assumptions

Calling E_{SU} the steady state potential that the passive rebar in the surrounding zone would achieve in the absence of any galvanic coupling with the rebar in the patch, and $E_S(x,t)$ the rebar potential at service time t and a distance x away from the patch perimeter, then the performance condition is given by

$$E_{SU} - E_S(x_T,t) = C_P \quad (3)$$

All electrode potentials are given in the CSE scale.

As discussed earlier, within certain limits, anode aging may sometimes be better described not in terms of service time but rather by the total amount Q of charge delivered since the moment of placement in service. In such case the performance condition can be alternatively given as

$$E_{SU} - E_S(x_T,Q) = C_P \quad (4)$$

In the following, a formalism on Q will be presented for completeness alongside equations based on time as the aging parameter. However, calculations and examples will be limited for brevity to the case of time as the aging parameter.

The desired projection model output is therefore the value of x_T , for the chosen values of C_P and t (or Q), as function of the other system conditions which serve as model inputs.

Following the treatment described elsewhere [Presuel-Moreno 2005B] for similar conditions, at any given distance x charge conservation under the above assumptions requires that the concrete potential satisfies:

$$d^2E_C/dx^2 = - \rho S_F t_C^{-1} i_S \quad (5)$$

The following boundary conditions apply:
At the patch perimeter (anodes placed there), by Ohm's law:

$$I_A=w t_C \rho^{-1} dE_C/dx |_{x=0} \quad (6)$$

At the outer slab edge (no current leaving the slab):

$$dE_C/dx = 0|_{x=L} \quad (7)$$

The net steel current is assumed to depend only on potential, $i_S(E_S)$. It is noted that given $i_S(E_S)$, setting $i_S=0$ yields the value of E_{SU}. The anode current is assumed to depend on both potential and aging condition, $I_A(E_A, t)$ (or $I_A(E_A,Q)$).

Accounting for the presence of the current constriction resistances, and by using the configuration parameters $k_1= \rho S_F t_C^{-1}$and $k_2= S_F w$, the ruling equation and anode-end boundary condition become:

$$d^2E_C/dx^2 = - k_1 i_S (E_C - R_S i_S) \quad (8)$$

$$I_A(E_C + R_A I_A) = k_2 k_1^{-1} dE_C/dx |_{x=0} \quad (9)$$

Thus, giving as inputs k_1, k_2, L, R_S and R_A as well as the functional relationships $i_S(E_S)$ and $I_A(E_A, t)$ (or $I_A(E_A,Q)$), solution of Equation (5) with the boundary conditions in Eqs. (6 to 9) yields $E_C(x, t)$ (or $E_C(x, Q)$) as output. The use of the parameters k_1 and k_2 permits obtaining solutions that are roughly scalable for all systems having the same values of those parameters, and the same anode and steel polarization properties. Generality is precluded however if, for example, the factors that determine local resistance vary sufficiently from system to system. Post-processing of that output then yields the value of the throwing power x_T for any chosen criterion C_P at the specified anode aging condition, therefore achieving the objective of the performance projection model.

The sign convention used in writing the system equations is to declare $i_S < 0$ when i_S is a net cathodic current. That choice permits keeping the customary polarity designation when evaluating the results, with electrode potentials referred to the electrolyte and absolute values of activation-polarized anodic/cathodic current densities respectively increasing/decreasing with potential. Interpretation of the findings is thus facilitated compared with other alternatives [Kranc 1994].

5.4 Implementation of the Model

5.4.1 Model Inputs

5.4.1.1 Overall Dimensions and Global Concrete Properties

The ranges of values for model inputs $k_1$and k_2 were chosen to bracket typical dimensional and concrete resistivity conditions that may be encountered

in the field. L was fixed at 200 cm which approaches a semi-infinite condition compared with the throwing power values that may be usually expected; the solution is in that case conservatively evaluated and with low sensitivity to the precise value of L.

5.4.1.2 Local Resistance

The following are rough estimates of the current constriction resistances of rebar and anode, intended to refine to some extent the throwing power calculations. More accurate solutions would necessitate use of a multidimensional model, but such step may be premature considering the limited extent of the performance data base available at present.

Model inputs R_S and R_A were estimated from geometric considerations and from the input values of k_1 and k_2 (Table 3). For R_S the approach corresponding to the current flow between two concentric cylinders was assumed to apply on first approximation. In such case the length-specific current constriction resistance R_{SUL} is given by [Sagüés 1994]:

$$R_{SUL}=\rho\ (2\pi)^{-1}\ \ln\ (t_C/\Phi_S) \qquad (10)$$

where Φ_S is the rebar diameter (diameter of the inner cylinder) and t_C is an approximation to the diameter of the outer cylinder, in this case taken to be in the order of the characteristic thickness of the system. Taking into account the problem scaling, the term R_S in Eq. (8) is then

$$R_S=\pi\ \Phi_S\ R_{SUL} \qquad (11)$$

Complications in estimating R_A stem from the metallic anode being surrounded by consecutive shells corresponding to corrosion products, proprietary anode pellet mortar, anode placement mortar/concrete if different

from the slab concrete, and finally the slab concrete itself. Moreover, current distribution can be highly complicated if the metallic surface of the anode is not uniformly activated. In such case the polarization function $I_A(E_A, t)$, even if determined by instant-Off measurements, may itself contain a considerable ohmic component per arguments described in detail by Sagüés [1994] and as discussed elsewhere in this report. Assuming that only the uniform part of the current constriction effect needs to be considered, the value of R_A may be estimated on first approximation as corresponding to that for the space between a sphere of effective diameter Φ_A in an spherical medium of diameter in the order of t_C and resistivity equal to that of the slab concrete [Landolt 2007], so that

$$R_A \sim ½ \rho\pi^{-1} [(\Phi_A)^{-1} - t_C^{-1}] \quad (12)$$

Assuming that the anode pellet mortar is highly conductive and that any ohmic effects due to corrosion product accumulation are already built into $I_A(E_A, t)$, then the effective anode diameter Φ_A is considered to be in the order of the characteristic outer dimension of the anode mortar pellet, $\Phi_A \sim ½$ (pellet width + pellet thickness). A rounded-off value representative of both anode types evaluated was used (Table 3).

5.4.1.3 Polarization Function – Steel

The function $i_S(E_S)$ for the model realizations explored below is chosen to be representative of the behavior of the steel used in the test yard slabs. The function is abstracted starting from the combined data set of instant-Off potential measurements as function of rebar current given earlier in Figure 33. The abstraction consists of assuming for the cathodic reaction an increasing current density with decreasing potential following simple Tafel kinetics, until a nominal limiting current density value i_L is reached. For more negative potentials the current is fixed at i_L thus creating a simplified combined activation-concentration limited cathodic polarization curve. The anodic reaction on the rebar is assumed

to correspond to a potential-independent passive dissolution current density i_P. Thus when $i_{0S}\ 10^{((E_S-E_{0S})/\beta_{CS})} <= i_L$:

$$i_S = i_{0S}\ 10^{((E_S-E_{0S})/\beta_{CS})} - i_P \quad (13)$$

and when otherwise:

$$i_S = i_L - i_P \quad (14)$$

Where i_{0S}, E_{0S} and β_{CS} are the nominal exchange current density, nominal equilibrium potential and nominal Tafel slope respectively for the species undergoing the cathodic reaction. The values of i_P, i_{0S} , E_{0S} [4] and β_{CS} were determined by least square fitting to the data shown in Figure 33 (Table 3), treating the portion of the polarization diagram spanned by the data as if the cathodic reaction were simply activation-polarized. The resulting abstracted function is shown by the solid line in Figure 33. Application of the chosen parameter set resulted in a visually plausible fit function. However, it is cautioned that the fit procedure is prone to produce alternative parameter sets with nearly similar fit quality, so the set chosen for these calculations should be viewed only as a representative example of the steel polarization function parameters.

The value of i_L is a preset parameter. A comparatively large value (i_L = 2 μA/cm^2) was chosen to represent cases where cathodic diffusional limitation was unlikely (e.g. concrete atmospherically exposed at moderate relative humidity regimes [Sagüés 2003]). Smaller i_L values were chosen based on previous findings [Sagüés 2003] to represent moist conditions.

[4] The values of i_{0S} , E_{0S} are not independent for the purposes of these calculations [Kranc 1992] so E_{0S} was specified arbitrarily.

5.4.1.4 Polarization Function - Anode (PF)

As indicated earlier, the following application is limited to the use of time as the anode aging parameter. The functions $I_A(E_A, t)$ from instant-Off measurements for individual anodes at various t have been shown when presenting the PF results in Section 3. Tests with various abstraction representations showed that a function of the form shown in Eq.(15) yielded a reasonably fit to the experimental potential-current curves of individual anodes under nearly all circumstances. Eq. (15) is written with service time as the age parameter, but it is expected that on first approximation a comparable form could be used with Q as the aging parameter.

$$E_A(I_A,t)\ V^{-1} = E_{A0}(t)\ V^{-1} + (I_A/I_{A0}(t))^{n(t)} \qquad (15)$$

Here E_{A0} is the unpolarized potential of the anode, and I_{A0} is the anode current that, when delivered, results in 1V of anode polarization over E_{A0} (effectively corresponding to an anode potential close to that of isolated passive rebar, where the anode provides essentially no protection). The exponent n indicates how steeply the anode output approaches that level as current demand approaches that limit. It is emphasized that Eq.(15) is a convenient empirical fit function and no relationship with fundamental causes is implied. The parameters E_{A0}, I_{A0} and n were obtained by least square fit from the polarization curve of each individual anode at various ages (Table 3). Those parameters exhibited significant variability for the replicate specimens of a given type of anode at a given age, reflecting the unit-to-unit variability in behavior noted earlier. For the purposes of obtaining a generic age-dependent anode performance curve, the combined trends of E_{A0}, I_{A0} and n with age for all anode specimens of a given type were displayed graphically and a representative simplified variation function with age was abstracted in each case. Convenient empirical relationships thus found, again not necessarily reflecting basic issues were:

$$E_{A0}(t) = E_B + a\ (t/t_u) \quad (16)$$

$$I_{A0}(t) = I_B\ (t/\ t_u)^{\ b} \quad (17)$$

$$n(t) = n_B\ (t/t_u)^{\ c} \quad (18)$$

Where t_u is the time unit (e.g. months).

Those relationships reflect the observation that the unpolarized potential tended to increase roughly linearly with time, while both the limit condition current and the steepness of approach to it tended to increase with time, but at a rate that decayed as time progressed (which resulted in parameters b and c being significantly <1).

5.4.2 Implementation of the Model - Computational Procedure

Numeric solutions of the ruling equation with boundary conditions were obtained by the finite differences method using a 20-element array and an iterative Jacobi technique with a relaxation factor between consecutive calculations chosen to achieve stability and prompt convergence of the solution. Separate calculations were performed for each value of time t. The functions $i_S(E_S)$ and $I_A(E_A, t)$ were entered as numeric arrays, which permitted manipulation to obtain reciprocal functions by lookup and interpolation as well as easily obtaining values of expressions such as $i_S\ (E_C\text{-}R_S\ i_S)$ or $I_A(E_C\text{+}R_A\ I_A)$. Entry by numeric array also provided flexibility to accommodate if desired functions other than the analytical expressions given in the previous section. General model parameters for calculated cases are given in Table 4.

5.4.3 Model Application Scope

The model is not intended for precise design purposes, but rather as an exploratory tool to obtain insight and identify broad operating conditions. As such sweeping simplifications were made such as the use of a one-dimensional representation, an approach that could be vastly improved if sufficiently accurate data on component properties became available. The x_T model output is obtained by interpolation between consecutive spatial nodes, so reported values should be viewed as only approximate estimates with only marked changes meriting note. In these calculations the spatial node array is not intended to replicate the placing of individual rebars. Thus values of x_T are reported nominally with cm resolution for comparison purposes, with the understanding that in an actual rebar grid the polarization pattern would be strongly influenced by the local geometry. Further model development is expected in continuation work [Dugarte 2010].

5.4.4 Sensitivity Analysis

A sensitivity analysis was performed to establish how model results may be affected by variations in the choice of assumed steel polarization parameters. The parameters selected for this analysis were the nominal Tafel slope for cathodic reaction on steel (β_{CS}), and the anodic passive current density on steel surface (i_P), both of which may be affected by considerable uncertainty. As a slave variable, the nominal exchange current density for the cathodic reaction of steel (i_{0S}) was chosen coupled to the variations in i_P and β_{CS} so that the value of E_{SU} always remained fixed at the same value used for the baseline model computations. That way the calculations evaluated sensitivity to the polarizability of the steel without the added complication of changes in the unpolarized steel potential. The value of β_{CS} was varied from its central scenario conditions value of 138 mV downwards to 100 mV (an approximate low end of commonly reported

values [Glass 2000, Sagüés 2003]), and in to opposite direction, but by the same amount, to 176 mV to span a plausible range of conditions. The parameter i_P was varied from its central scenario choice of 2.6 E-08 A/cm^2 to ½ and 2 times that value (1.3 E-08 and 5.2E-08 A/cm^2 respectively) to account for an appreciable uncertainty range. All calculations were performed with k_1=1kΩ and k_2 =50 cm, for 10 mo age of both types of anode. Only cases with zero current to the patch region were explored.

Table 2 - Nomenclature of model variables and parameters.

t (s)	amount of time since anode placement and energizing
Q (coul)	integrated electric charge delivered by the anode since placement and energizing
x (cm)	distance away from perimeter of the patch (where anodes are placed)
x_T (cm)	throwing power
C_P (V)	cathodic prevention criterion value
L (cm)	distance from perimeter of the patch to outer edge of the concrete slab.
t_C (cm)	concrete slab thickness
w (cm)	anode center-to-center placement distance along patch perimeter
S_F(cm^2-cm^{-2})	steel placement density (amount of steel surface area per surface area of concrete slab footprint)
Φ_S (cm)	rebar diameter
Φ_A (cm)	effective anode diameter
ρΩ-cm)	concrete resistivity
i_S (A-cm^{-2})	net current density on steel surface
i_P (A-cm^{-2})	anodic passive current density on steel surface
i_C (A-cm^{-2})	cathodic current density at the steel surface
I_A (A)	galvanic current delivered by anode
E_C (V)	potential of the concrete away from the immediate proximity of the steel surface or the metallic surface of the anode.
E_S (V)	potential of the concrete at a point immediately adjacent to the steel surface
E_{SU} (V)	unpolarized steel potential

Table 2 (Continued)

E_A (V)	potential of the mortar at a point immediately adjacent to the metallic surface of the anode
R_{SUL} (Ω-cm)	effective length-specific current constriction resistance of concrete at the steel surface
R_S (Ω-cm^2)	effective area-specific current constriction resistance of concrete at the steel surface
R_A (Ω)	effective current constriction resistance of concrete around the active zone(s) of the metallic portion of the anode.
k_1 (Ω)	configuration parameter: $k_1 = \rho S_F t_C^{-1}$
k_2 (cm)	configuration parameter: $k_2 = S_F w$
i_{0S} (A-cm^{-2})	nominal exchange current density, cathodic reaction on steel
E_{0S} (V)	nominal equilibrium potential, cathodic reaction on steel
β_{CS} (V)	nominal Tafel slope, cathodic reaction on steel
i_L (A-cm^{-2})	nominal limiting current density, cathodic reaction on steel
E_{A0} (V)	unpolarized anode potential
E_B, a(V)	E_{A0} time dependence parameters
E'_B, a'(V)	E_{A0} Q dependence parameters
I_{A0} (A)	anode current demand resulting in 1V polarization
I_B (A), b	I_{A0} time dependence parameters
I'_B (A), b'	I_{A0} Q dependence parameters
n	anode potential steepness of variation with current demand
n_B, c	n time dependence parameters
n'_B, c'	n Q dependence parameters
t_u (e.g. mo)	time unit for parameter abstraction
Q_u (e.g. Coul)	charge unit for parameter abstraction

Table 3 - PF, steel and other parameters for model cases.

Anode	E_B (V)	a (V)	I_B (A)	b	n_B	c
C	-1.16	0.0057	2.0E-03	-0.43	2.7	-0.03
W	-0.85	0.0085	5.4E-02	-1.7	0.81	0.33

Steel:	Parameters used as base for k_1, k_2 cases and for constriction resistances
i_{0S} = 2.03 E-9 A-cm^{-2}	Φ_A = 5 cm
E_{0S} = -0.00 V_{CSE} *	tc = 20 cm
β_{CS} = 0.138 V	L = 200 cm
i_P = 2.59 E-8 A-cm^{-2}	S_F = 1
i_L = 2 E-6 A-cm^{-2}	
E_{SU}= -0.153 V_{CSE} **	
Φ_S = 2.2 cm	
*Nominal value	
**Value resulting from the other inputs	

Table 4 - General model parameters for calculated cases.

k_1 (kΩ)	3.33 , 1.00, 3.00
k_2 (cm)	25, 50, 75
C_P (V)	0.10, 0.15, 0.20
T (months)	1, 4 , 10, 13
Anode Current to Steel in Patch	0, ½

5.4.5 Model Validation

Validation of the model projections by comparison against a well characterized actual system was performed and results are presented in Appendix 1. There, the model was applied to compute the extent of polarization delivered to the passive rebars in the yard slabs by the sacrificial point anodes at various ages. The results supported the validity of the approach used here.

5.5 Model Results

Figure 37 presents model results for the C anodes, showing the throwing distance x_T as function of k_1 and using the cathodic prevention criterion value C_P as a secondary parameter, for a fixed value of k_2=50 cm and for anode ages of 1, 4, 10 and 13 months respectively. Those ages were chosen to correspond to the times for which PF data were collected in the yard slabs. Also for the C anodes Figure 38 shows as a function of time, and for a fixed value of k_1=1kΩ, the effect of variations in the value of k_2 on the throwing distance. Figures 39 and 40 show similarly displayed results for the W anodes. In all cases, the polarization amount can be converted into steel current density by reference to Figure 33; the results are i_S = 0.11, 0.29 and 0.70 μA/cm^2 for C_P = 100, 150 and 200 mV respectively. It is noted that for these model calculations the area of steel inside the patch was considered to be relatively small, and the current needed to polarize this area was neglected. The resulting projections are consequently somewhat optimistic, and the derating effect of current flowing into the patch is discussed afterwards.

The results can be best interpreted by recalling that a value of k_1=1kΩ, at the center of the horizontal axis in Figures 37 and 39, corresponds to a reinforced concrete slab of thickness t_C=20 cm (8 in), a steel density factor S_F=1 and a concrete resistivity ρ = 20 kΩ-cm, baseline conditions that may be considered typical of many bridge deck or parking structure conditions. The other

k_1 values for which results are given, 0.33 and 3.3 kΩ correspond for the same t_C and S_F combination to concrete resistivities of 6.7 and 60 kΩ-cm, or severe and mild corrosion propensity conditions respectively. Since S_F was chosen as unity for theses examples, the parameter value k_2= 50 cm corresponds to a placement density of one anode for every 50 cm of patch perimeter, which may be considered to be a reasonable practical value. Finally, C_P values of 0.1, 0.15 and 0.2 V represent depolarization criteria for cathodic prevention that are increasingly more conservative [Presuel-Moreno 2005B]. In Figures 38 and 40 and for the above combinations, variations of k_2 to values of 25 cm and 75 cm represent anode spacing near the tighter or wider extremes respectively of expected practical applications.

Figure 41 presents the results from the sensitivity analysis. Changes in β_{CS} in either direction from the central scenario resulted in moderate relative changes (by about a factor of 2 or less) in the value of the projected throwing distance for the 100 mV polarization criterion. The effect was comparably moderate for the 150 mV criterion when the excursion was toward greater values of β_{CS}, but if β_{CS} was reduced to 100 mV the resulting lower rebar polarizability became effectively prohibitive. For the most demanding criterion, 200 mV, excursion of β_{CS} toward 176mV increased x_T above the zero or nearly zero values at the central scenario, but not enough to exceed 10 cm. Analogous to the effect of variations in β_{CS}, changes in i_P had moderate impact on the 100 mV criterion throwing distance, and stronger relative effect for the cases of the more demanding criterion values. Overall, the sensitivity calculations showed that relatively wide changes in key steel polarization parameters induced no dramatic change in the highest projected values of x_T for the age condition examined. Large relative changes in x_T were projected for the more demanding polarization criteria cases, but the absolute values in those cases tended not to be large.

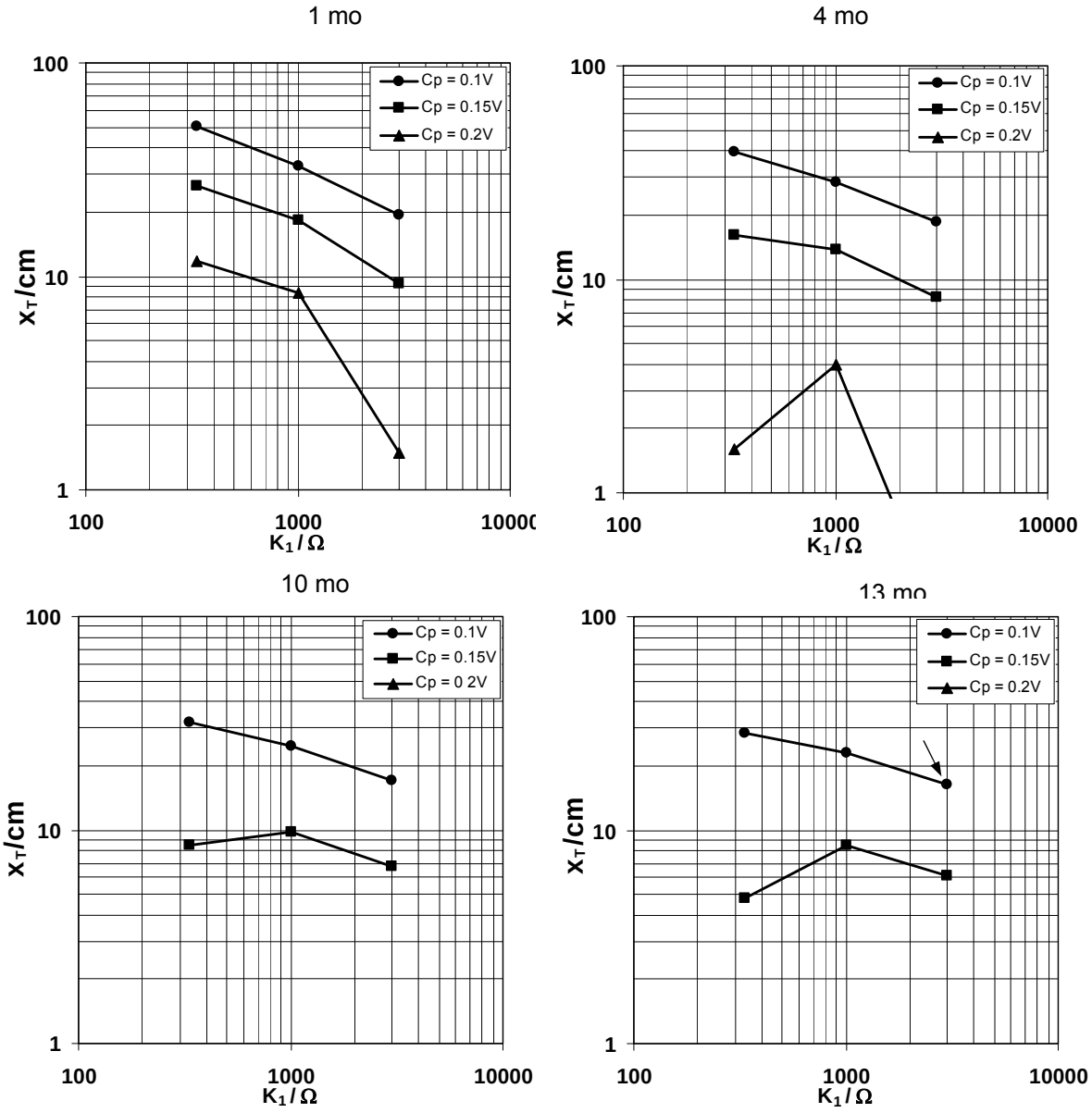

Figure 37 - Model projections of throwing distance for C anodes at the indicated service times. All graphs are for k_2 = 50 cm, C_P as shown. Absent symbol/line: polarization not achievable or x_T < 1 cm.

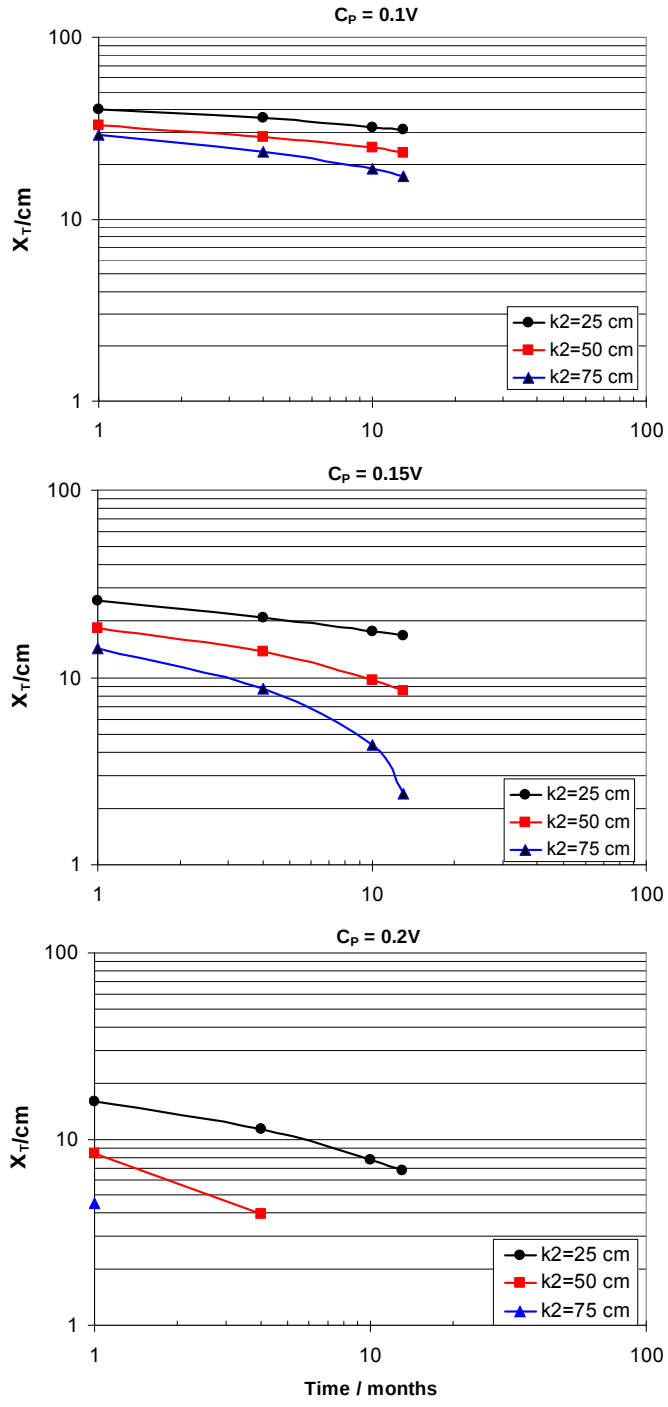

Figure 38 - Model projections of throwing distance for C anodes, as a function of service time. Legends indicate values of k_2 (cm). Absent symbol/line: polarization not achievable or x_T < 1 cm.

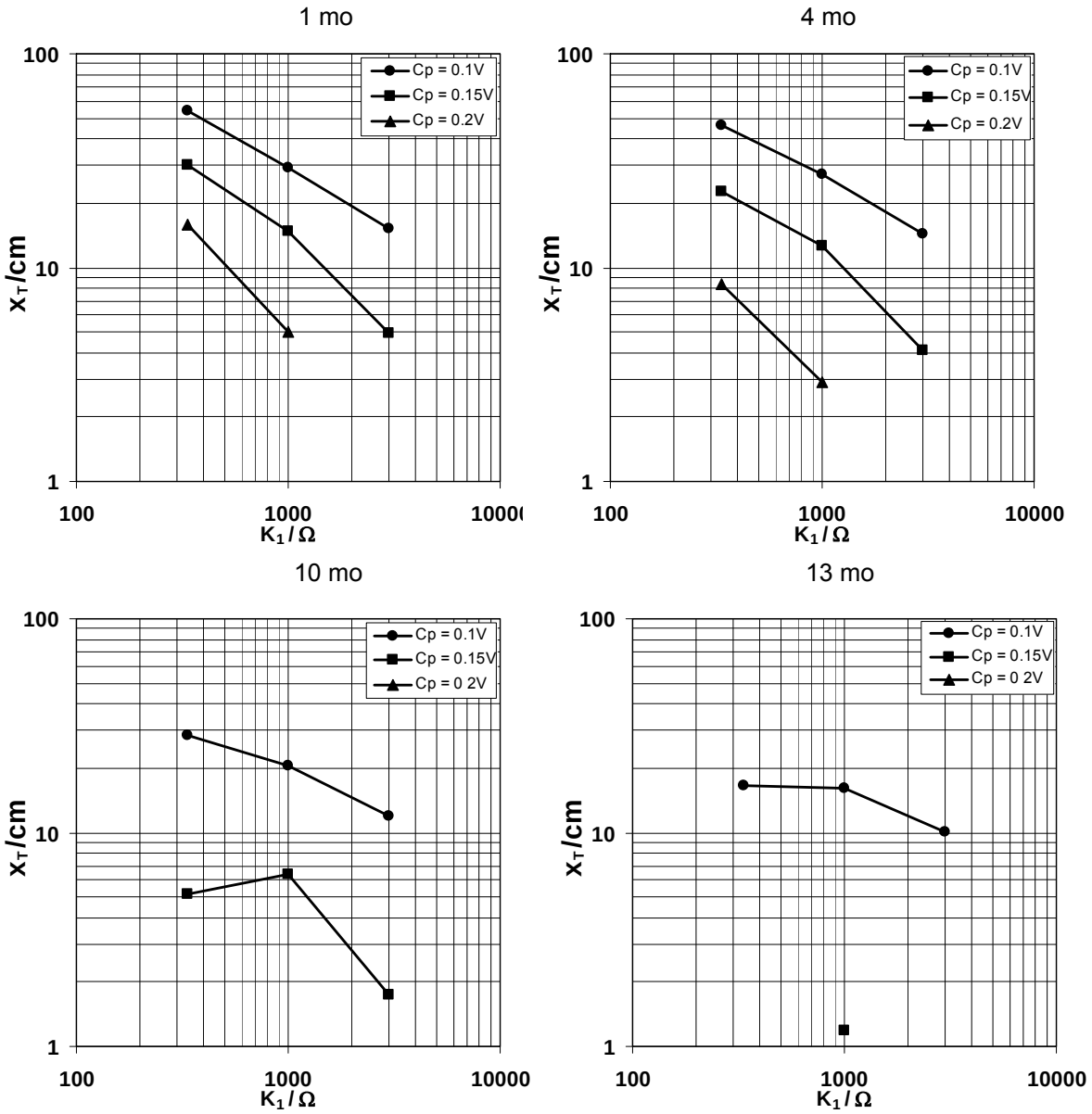

Figure 39 - Model projections of throwing distance for W anodes at the indicated service times. All graphs are for k_2 = 50 cm, C_P as shown. Absent symbol/line: polarization not achievable or x_T < 1 cm.

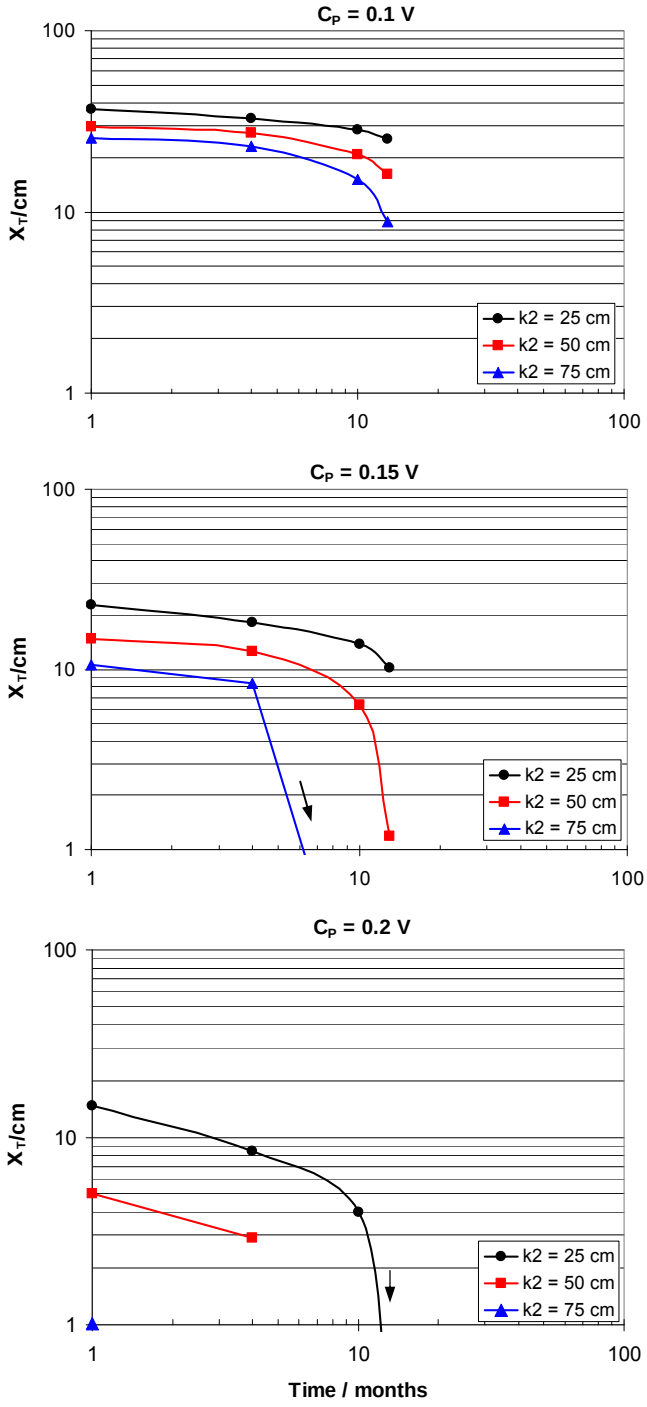

Figure 40 - Model projections of throwing distance for W anodes, as a function of service time. Legends indicate values of k_2 (cm). Absent symbol/line: polarization not achievable or x_T < 1 cm.

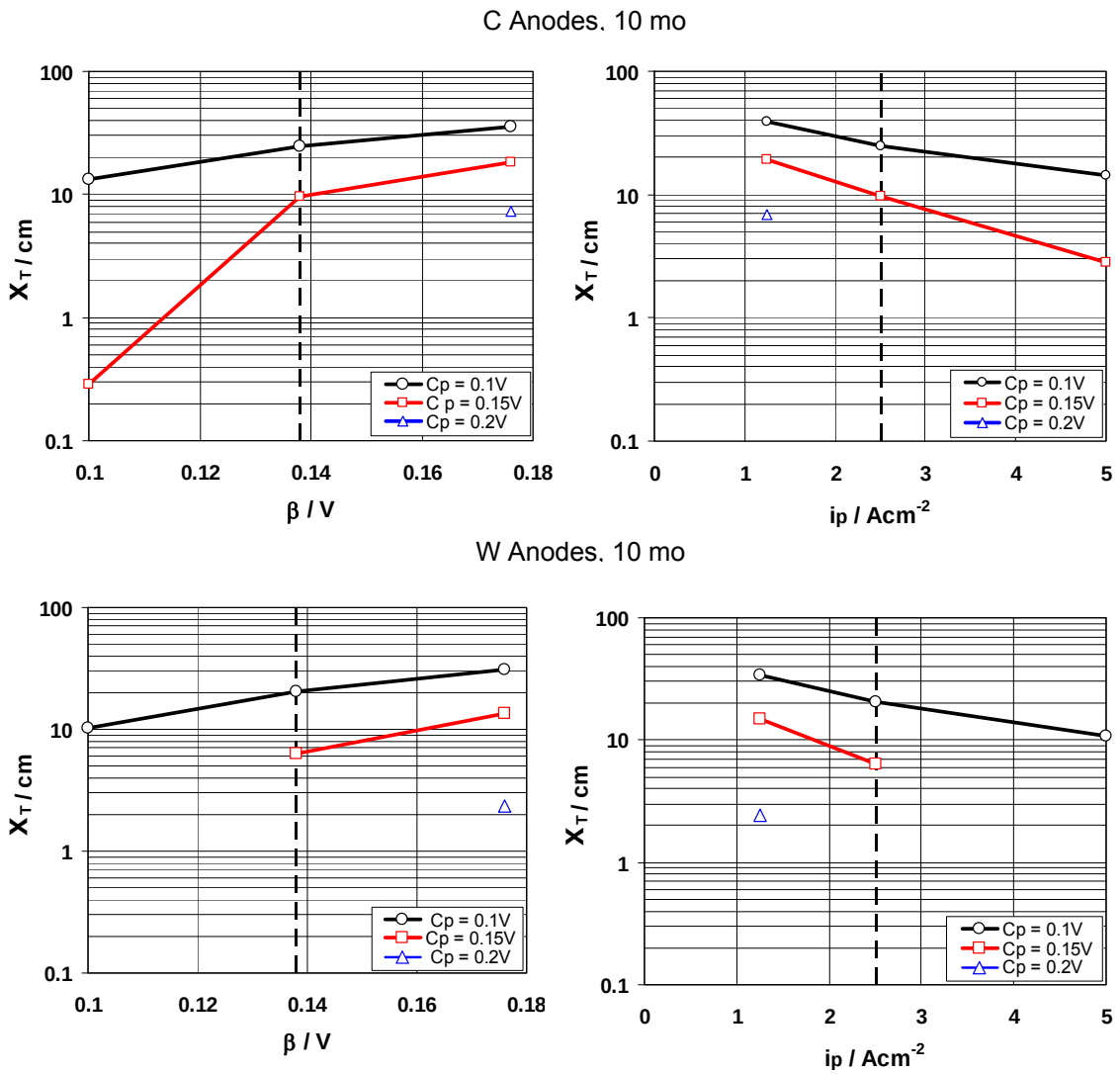

Figure 41 - Sensitivity analysis of model projections to the choice of β_{CS} and i_P, for 10 mo anode age. Dashed lines denote the central scenario. Absent symbol/line: polarization not achievable or x_T < 0.1 cm.

5.6 Model Discussion

Using the C anode cases as an example, and for the above assumed baseline conditions, the 1-month projections indicate an appreciable throwing distance, 33 cm for a 100 mV polarization criterion. For that polarization level reducing the anode spacing to 25 cm elevated x_T to 40 cm, while it still reached 29 cm even for the 75 cm wide anode placement case. The projected throwing distance for k_2=50 cm however degraded to less than 10cm when the wide anode spacing and a more conservative polarization criterion (200 mV) was used. A throwing distance of less than 10 cm may be considered to be quite ineffectual as it is in the order of rebar spacing in many applications. The other scenarios in the same figures can be similarly evaluated for insight.

The projected throwing distance decreased with service time to various extents as shown in figures 38 and 40, depending strongly on the polarization prevention criterion used. Thus, continuing with the above example, for baseline conditions and 13 mo age the projected 100 mV throwing distance for the 50 cm anode spacing was reduced to 23 cm. For the same anode spacing Increasing the polarization criterion to 150 mV lowered the projected throwing distance to less that 10 cm, and the model projected that the 200 mV criterion was no longer reachable. The 200 mV criterion could be met at 13 mo by reducing the anode spacing to 25 cm, but the projected throwing distance was poor (<10 cm).

The projections for the W anodes (Figures 39 and 40) resulted in x_T values that were comparable to those of the C anodes at early ages, but generally smaller later on, in keeping with the relative anode polarization behavior of the anodes in the yard slab tests as noted earlier. Otherwise, the same general trends and observations noted for the C anodes apply here as well.

As indicated earlier, the projections would become more pessimistic when current demand by the steel in the patch area is considered. The extent of this

effect was addressed by evaluating model projections for the case where the region inside the patch required half of the galvanic current from the anode, so that the anode current is distributed equally between the patch area and the surrounding concrete. The results are presented in Table 5 for the baseline condition with k_1=1kΩ and a 50 cm anode spacing. As expected the projected performance degraded compared to the cases where the entire anode current flowed outside the patch. The extent of degradation depended particularly on the polarizability of the anode. Thus the projected effect was relatively small early on when the added current demand caused only a relatively small shift of the anode potential toward more positive values. However, the shift would be more pronounced as later anode ages are considered, where a consequently steeper polarization curve applies. At age 13 months the projections indicated a substantial reduction in the throwing distance to about ⅓ to ½ of the value obtained when no current to the patch was assumed depending on anode type. In an actual system the patch zone may be small compared to its surroundings, so the galvanic current partition and resulting effect in polarization would be somewhat in between the two extreme situations (no current vs. ½ of the current going to the patch) considered in Table 5.

Table 5 - Effect of current demand by the patch zone.

C Anode		Base Cases (No current to patch)	Alternative (½ current to patch)
Age	C_P / V	X_T /cm	X_T /cm
1 mo	0.1	33	26
	0.15	18	11
	0.2	8	1
4 mo	0.1	28	19
	0.15	14	5
	0.2	4	–
10 mo	0.1	25	14
	0.15	10	–
	0.2	–	–
13 mo	0.1	23	12
	0.15	8	–
	0.2	–	–

W Anode		Base Cases (No current to patch)	Alternative (½ current to patch)
Age	C_P / V	X_T /cm	X_T /cm
1 mo	0.1	29	22
	0.15	15	8
	0.2	5	–
4 mo	0.1	27	19
	0.15	13	5
	0.2	3	–
10 mo	0.1	21	10
	0.15	6	–
	0.2	–	–
13 mo	0.1	16	3
	0.15	1	–
	0.2	–	–

Projections over periods of time longer than 13 months are subject to considerable uncertainty as those would be beyond the testing period that yielded the PF data used as input to these model calculations. However, the trends from Figure 23 and the performance derating information as function of total charge in Figures 16 and 17 suggest that both types of anodes may settle, under conditions resembling those in the test yard slabs, into quasi-steady state operating currents in the order of ~0.1 mA after another year or two of operation. The corresponding charge delivery would be~3.2 k Coul/year. Barring the effects of any other aging mechanism (such as dissipation of pellet activator compound into the surrounding concrete), and based on the arguments made in previous section, anode operation at that rate might continue over about a decade of years range before approaching excessive consumption levels. Due to the relative shape of the anode and rebar polarization curves, under the conditions modeled here the anodes tend to operate near the limit current condition defined by the upward leg of the PF. As shown in Figure 15, at age 13 months that current for both C and W anodes is in the order of ⅓ to ½ mA. As noted before,

by 13 months age the projected throwing distance had begun to shorten considerably especially for the more demanding polarization criteria. The effect on x_T of further lowering the anode current by twofold or more toward ~0.1 mA may be inferred from the projected decrease of x_T as anode spacing increased in comparable proportions (effectively lowering the anode current available per unit of patch perimeter) and also from the results of halving the anode current shown in Table 5. Such comparison suggests that as anode currents decay into the order of 0.1 mA the throwing distance for satisfying the 100 mV polarization criterion would become two or more times smaller than those projected for 13 mo, yielding quite poor projected performance. By the same argument, the more demanding polarization criteria (150 mV, 200 mV) would result in even poorer or nil projected long performance.

In summary, the model projections together with the aging information detailed in Chapter 3 suggest that anode performance in the likely scenarios discussed above, as measured by the throwing distance, may seriously degrade after only a few years of operation even if a 100 mV corrosion prevention criterion were assumed.

It has been proposed in the technical literature that, even with small polarization levels, significant corrosion control benefits can accrue from sustaining cathodic current densities with low values ranging from 0.2 μA/cm^2 to as little as 0.02 μA/cm^2 on passive steel [Pedeferri 1996, Sergi 2008]. The lower end of that range may not be relevant to atmospherically exposed concrete, for which a low end of 0.05 μA/cm^2 has been cited instead [Pedeferri 1996]. Those low end values would correspond to polarization levels in the order of only 34 to 65 mV for 0.02 and 0.05 μA/cm^2 respectively (Figure 33), with consequently greater throwing distances than those obtained for the 100 mV cases. It is noted however that the 0.2 μA/cm^2 high end of the range does not improve prognosis relative to the situations addressed earlier, as it corresponds in the present

model to a C_P value approaching 150 mV (Figure 33). That case has already been addressed above, and yielded generally poor performance projections.

There are indeed benefits from long term application of cathodic currents, in particular from an increase in pH near the surface of the rebar and also a decrease in chloride content if contamination already exists [Glass 1997, 2007]. Those effects are to be expected at substantial cathodic current densities. However, the extent of benefits at the very low polarization levels that correspond to the low end of the current density-based criteria awaits sufficient experimental demonstration. Should future research develop adequate supporting evidence, the less conservative criterion requirements may merit further consideration.

A contrary argument, for a more conservative corrosion prevention criterion, may be made based on the analysis by Presuel-Moreno [2005A] summarized in Figure 42. As indicated there, polarization to as much as 400 mV below the normal open circuit potential (which is some -0.1 V vs SCE, or ~-0.18 V CSE) of passive steel in atmospherically exposed concrete may be required for an order-of- magnitude increase in the chloride corrosion threshold. If that were the case, cathodic polarization in the order of 100 mV would only achieve a marginal threshold increase. In the light of such conservative scenario, the model projections would question the ability of point anodes of the size investigated here to provide a useful corrosion prevention effect. The precise dependence of corrosion threshold on potential of the passive steel is a critical issue in interpreting the results of the present investigation. However, as evidenced from the scatter of available data in Figure 42 there is much uncertainty as to the extent of that effect. The issue is much in need of resolution by development of reliable data in future investigations.

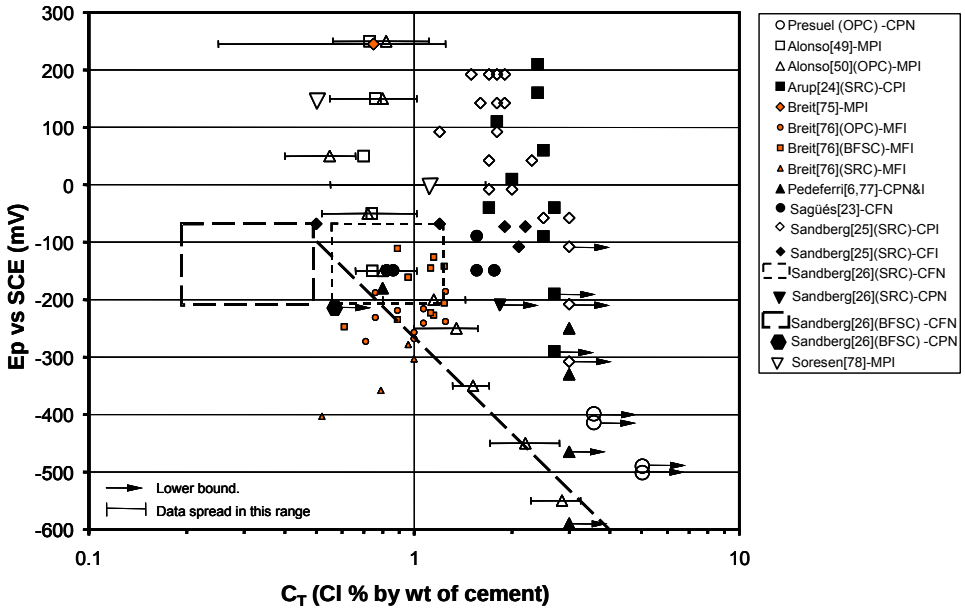

Figure 42 - Summary of information toward establishing a cathodic prevention polarization criterion*.

* Each symbol represents an instance of documented corrosion threshold for passive steel held in concrete at the potential indicated. Arrows indicate that the chloride threshold was equal or higher than the corresponding value. The dashed line yields the proposed cathodic prevention potential for a given level of protection. Potentials are in the saturated calomel electrode scale; potentials vs CSE are 77 mV lower than the value indicated. See Presuel-Moreno [2005A] for the references cited in the figure.

CONCLUSIONS

a. Galvanostatic tests under controlled humidity and test yard slabs with reinforced concrete for both types of anodes revealed PFs with comparable features. The PFs showed relatively little anodic polarization from an open circuit potential at low current levels, followed by an abrupt increase in potential as the current approached an apparent terminal value. This limiting current for a new anode was in the order of 1.5 mA and 2.0 mA for C and W anodes respectively. For aged anodes (13 months service) it was in the order of ~0.6 mA and 0.4 mA for C and W anodes respectively. The curves resemble the behavior expected from a system that is approaching a diffusion-controlled limiting current density, or alternatively having a sizable ohmic resistance polarization component.

b. For a given test condition and anode service history, the PCFs showed significant variability among units of the same type within a given set of anodes delivered by the suppliers. For one of the anode types (W anodes), the 1st set tested performed notable worse as a group than the 2nd set (delivered 3 years later) suggesting an initial manufacturing problem. For the 2nd set of anodes the unit-to-unit performance variability among each type was much less.

c. Aging of the anodes by delivering current in service was manifested by a continually decreasing current output in the test yard slabs. As implied by Slow Cyclic Polarization test results, those changes reflected an evolution of the PF generally toward more positive OC potentials and, more importantly, to the onset of elevated polarized potentials at increasingly lower current levels. The value of OC potential for a new anode (1 month)

was in the order of ~-1.15 V and -0.85 V for C and W anodes respectively. When the anode was 13 months old the OC potential decayed to ~-1.09 V and -0.75 V for C and W anodes respectively.

d. Coupling of the anodes to rebar at the time of casting in concrete containing 1.5% Cl^- by weight of cement was not sufficient to prevent corrosion initiation of the steel rebars in that zone. Testing for about 480 days in reinforced concrete slabs containing those corroding rebars in addition to passive rebars showed that the point anodes induced only modest to negligible polarization of the steel assembly. That effect was ascribed to the low polarizability of the actively corroding rebars.

e. Upon disconnection of the actively corroding rebars while evaluating the first set of anodes, one of the anode types produced cathodic polarization levels exceeding 100 mV in the passive rebars that were in close proximity to the anode. The other anode type (suspected of deficiency in the first set evaluated) had already exhausted much of its polarizing ability in the preceding interval and produced only negligible effects on the surrounding passive steel.

f. A continuation test with a second set of anodes of each type, coupled with only passive rebar, showed substantial polarization levels (100 mV to 200 mV) of rebar in the proximity of either type of anode. Current delivery decreased with service time but appreciable polarization levels were still achieved in nearby rebars after ~500 days of operation

g. Most anode units of both types in the 1st set tested showed on average significant current delivery decrease after delivering a cumulative anodic charge that was only about 10% to 20% of the maximum theoretical amount (Q_T). Values of Q_T were ~ 324 k Coul and 133 k Coul for 1st set C and W anodes respectively. Anodes in the 2nd set tested showed less

aging effects over the duration of the test, which was conducted until reaching up to about 25% of the theoretical limit. Estimates based on the extent of derating observed in the test interval suggest that in the absence of other degradation effects, anodes of this type may be able to function adequately up to about ¼ to ⅓ of the theoretical consumption limit.

h. Quantitative polarization functions of the steel rebar were found to agree with the results of previous investigations. A steel PF abstraction was used as input for modeling projections of anode performance in a generic reinforced concrete system.

i. A numerical abstraction of the PF graphs for the anode representative of the anodic behavior at various stages of anode aging was obtained using a mathematical function that reasonable fit to the experimental data. This function was written with service time as the age parameter.

j. Improved performance of the 2nd over the 1st set of anodes was clearly observed. However, anodes from 2nd set were connected to passive rebar only, and enhanced performance may have resulted also from the low resistivity (nominally ~5000 Ω-cm) medium cast around the 2nd set anodes.

k. Modeling of a generic patch configuration with a one-dimensional approximation was used to calculate the throwing distance that could be achieved by a given number of anodes per unit perimeter of the patch, concrete thickness, concrete resistivity, amount of steel and amount of polarization needed for cathodic prevention. The model projections together with the aging information determined experimentally suggest that throwing distance in likely application scenarios may seriously degrade within a few years of operation, even if a relatively optimistic 100 mV corrosion prevention criterion were assumed. The model was

validated by comparison against the experimental results from the test yard slabs.

l. Less conservative, current density-based corrosion prevention criteria have been proposed in the literature that would result in improved throwing distance projections under some conditions yet to be substantiated. However, other investigations suggest that a significantly more conservative corrosion prevention criterion than 100 mV polarization may be necessary instead. The latter case would question the ability of the point anodes to provide a useful corrosion prevention effect for reinforcement around the patch.

REFERENCES

Alonso, C., Castellote, M. and Andrade, C., “Dependence of Chloride Threshold with the Electrical Potential of Reinforcements,” in 2nd Int. RILEM Workshop on Testing and Modeling the Chloride Ingress into Concrete, PRO 19 (Cachan, France: RILEM Publications, (2000), p. 415.

Alonso, C., Castellote, M. and Andrade, C. "Chloride threshold dependence of pitting potential of reinforcements". Electrochim. Acta 47, 21(2002), p. 3, 469.

Bennett, J. and Talbot, C., “Extending the Life of Concrete Patch Repair with Chemically Enhanced Zinc Anodes”, Paper No. 02255, Corrosion/2002, NACE International, Houston, (2002).

Bennett, J. and McCord, W., “Performance of Zinc Anodes Used to Extend the Life of Concrete Patch Repairs”, Paper No. 06331, Corrosion/2006, NACE International, Houston, (2006).

Bentur, A., Diamond, S. and Berke, N.S., “Steel Corrosion in Concrete: Fundamental and Civil Engineering Practice” (New York, NY: E&FN SPON, 1997), p. 30.

Berke, N.S. and Hicks, M.C., “ Estimating the Life Cycle of Reinforced Concrete Decks and Marine Piles using Laboratory Diffusion and Corrosion Data”, in Corrosion Forms and Control for Infrastructure, ASTM STP 1137, Victor Chaker, Ed., ASTM, Philadelphia, (1992), p. 207.

Bertolini, L., Esener, B, Pedeferri, P. and Polder, R., “Corrosion of steel in concrete: prevention, diagnosis, and repair”, Wiley-VCH, (2004).

Breit, W., “Critical chloride content – Investigation of steel in alkaline chloride solutions” Materials Corrosion 49 (1998), p. 539.

Broomfield, J.P., “Corrosion of Steel in Concrete: Understanding, Investigation and Repair”, Taylor & Francis, (1997).

Castro, P., Sagüés, A.A., Moreno, E.I., Maldonado, L., and Genescá, J. “Characterization of Activated Titanium Solid Reference Electrodes for Corrosion Testing of Steel in Concrete”, Corrosion 52, 8 (1996), p. 609.

Dugarte, M. and Sagüés, A.A., “Polarization of sacrificial point anodes for cathodic prevention of reinforcing steel in concrete repairs - part 1: experimental findings”**.** To be published (2010).

Dugarte, M. and Sagüés, A.A., “Polarization of sacrificial point anodes for cathodic prevention of reinforcing steel in concrete repairs - part 2: Modeling”**.** To be published (2010).

Fontana, M.G. (1986), “Corrosion Engineering”, 3rd edition, McGraw-Hill Inc.

FunahashI M. ; Bushman J. B. , "Technical review of 100 mV polarization shift criterion for reinforcing steel in concrete " Corrosion, (1991), vol. 47, p. 376-386

Frankel, G.S., "Pitting corrosion of metals: a review of the critical factors", J. Electrochem. Soc. Vol. 145 (1998), p. 2186-2198.

FHWA-RD-01-156. “Corrosion Costs and Preventive Strategies in the United States”, (2002).

Glass, G. and Chadwick, J., “An Investigation into the Mechanisms of Protection Afforded by a Cathodic Current and the Implication for Advances in the Field of Cathodic Protection”, Corrosion Science, Vol. 36(1994), No. 12, p. 2193-2209.

Glass G. K. and Buenfeld N. R., “Theoretical basis for designing reinforced concrete cathodic protection systems”, British Corrosion Journal Vol. 32, (1997), p. 179-184.

Glass, G.K., Hassanein, A. M. and Buenfeld, N. R., “CP Criteria for Reinforced Concrete in Marine Exposure Zones”, Journal of Mat. in Civil Eng., Vol. 12, No. 2, May (2000), p. 164-171

Glass, G. K., Reddy, B. and Clark, L. A.,"Making concrete immune to chloride induced corrosion", Proceedings of the Institution of Civil Engineers, Construction Materials, 160 (4) (2007), p. 155-164.

Glass, G., Roberts, A., “Hybrid corrosion protection of chloride-contaminated concrete”, Const. Mat. 161 (2008), Issue CM4, p. 163 -172.

Gouda, V. K. and Halaka, W.Y., “Corrosion and Corrosion Inhibition of Reinforcing Steel: II. Embedded in Concrete” *Brit. Corros. J.* 5, 9 (1970), p. 198.

Hausmann, D. A., “Steel Corrosion in Concrete. How Does it Occur?” Mater. Prot. 6, 11 (1967), p. 19.

Hurley, M.F. and Scully, J.R., "Threshold chloride concentrations of selected corrosion-resistant rebar materials compared to carbon steel", Corrosion Vol. 62 (2006), p. 892.

Izquierdo, D., Alonso, C., Andrade, C. and Castellote, M., “Potentiostatic determination of chloride threshold values for rebar depassivation: Experimental and statistical study”, Electrochimica Acta, Volume 49, 2004, p. 2731-2739.

Jones, D. A. (1996), “Principles and Prevention of Corrosion”, 2nd edition, Prentice- Hall, Inc.

Kaesche, H. "Corrosion of Metals", Springer, Berlin (2003).

Kranc, S. and Sagüés, A. “Detailed Modeling of Corrosion Macrocells on Steel Reinforcing in Concrete”, Corrosion Science, Vol. 43, (2001), p. 1355.

Kranc, S.C and Sagüés, A.A., "Computation of Reinforcing Steel Corrosion Distribution in Concrete Marine Bridge Substructures", Corrosion, Vol. 50 (1994), p.50.

Landolt, D. "Corrosion and Surface Chemistry of Metals", CRC Press (2007)

Li, L. and. Sagüés, A.A., "Chloride Corrosion Threshold of Reinforcing Steel in Alkaline Solutions - Open-circuit Immersion Tests", Corrosion, Vol. 57 (2001), p.19.

Li, L. and Sagüés, A.A., "Chloride Corrosion Threshold of Reinforcing Steel in Alkaline Solutions – Cyclic Polarization Behavior" Corrosion 58, 4 (2002), p. 305.

Mac-Berthouex, P., Brown, L.C., “Statistics for environmental engineers”, CRC Press, (2002)

Macdonald, D.D., "The point defect model for the passive state", J. Electrochem. Soc. Vol. 139 (1992), p. 3434.

Myrdal, R., "Phenomena that Disturb the Measurement of Potentials in Concrete", Paper No. 0339, Corrosion/1996, NACE International, Houston, 1996

Page, C.L. and Sergi, G., “Developments in Cathodic Protection Applied to Reinforced Concrete”, Journal of Mat. in Civil Eng., Vol. 12, (2000), p. 8-15.

Pedeferri, P., “Cathodic protection and Cathodic Prevention” Constr. Build. Mater. Vol. 10, No. 5 (1996), p. 391.

Pour-Ghaz, M., Isgor, O.B, Ghods, P., “The effect of temperature on the corrosion of steel in concrete. Part 1: Simulated polarization resistance tests and model development”, Corrosion Science 51 (2009), p. 415–425.

Presuel-Moreno, F.J., Sagüés, A.A. and Kranc, S.C., "Steel Activation in Concrete Following Interruption of Long Term Cathodic Polarization", Corrosion 61 (2005A), p. 428-436.

Presuel-Moreno, F.J, Kranc, S.C., and Sagüés, A. A., “Cathodic Prevention Distribution in Partially Submerged Reinforced Concrete”, Corrosion, Vol. 61 (2005B). p. 548-558.

Raupach, M., “Chloride-induced macrocell corrosion of steel in concrete-theoretical background and practical consequences”, Cons. and Bldg. Mat., Vol. 10, Issue 5, Durability of Reinforced Concrete Structures, July (1996), p. 329-338.

Sagüés, A.,"Electrochemical Impedance of Corrosion Macrocells on Reinforcing Steel in Concrete", Paper No. 132, pp. 28 , Corrosion/90, National Assoc. of Corr. Engs., Houston, (1990).

Sagüés, A.A. and S.C. Kranc, S.C.“Model for a Quantitative Corrosion Damage Function for Reinforced Concrete Marine Substructure”, Rehabilitation of Corrosion Damaged Infrastructure, Proceedings, Symposium 3, 3rd. NACE Latin-American Region Corrosion Congress, NACE International, Houston, (1998), p.268.

Sagüés, A.A., Pech-Canul, M.A., and Al-Mansur, A.K.M., “Corrosion macrocell behavior of reinforcing steel in partially submerged concrete columns”, Corr. Sci. Vol. 45 (2003), p. 25-30.

Sagüés, A.A, Balakrishna, V. and Powers, R.G, “An approach for the evaluation of performance of point anodes for corrosion prevention of reinforcing steel in concrete repairs”, Paper 1-083, International Federation for Structural Concrete (FIB) symposium: “Structural concrete and time: La Plata, Argentina., September 28-30, 2005.

Sagüés, A., Kranc, S. and Lau, K. "Service Life Forecasting for Reinforced Concrete Incorporating Potential-Dependent Chloride Threhslold", Paper No. 09213, Corrosion /09, NACE International, Houston, (2009A), p. 22.

Sagüés, A.A., Kranc S.C. and Lau, K., “Modeling of Corrosion of Steel in Concrete with Potential-Dependent Chloride Threshold", NACE International, Houston, (2009B).

Sergi, G. and Page, C., "Sacrificial anodes for cathodic prevention of reinforcing steel around patch repairs applied to chloride-contaminated concrete". In: Mietz, J. et al (eds.), Corrosion of Reinforcement in Concrete, IOM Communications, London, European Federation of Corrosion Publications, No. 31(2001), p. 93-100.

Sergi, G., Simpson, D. and Potter, J. "Long-term performance and versatility of zinc sacrificial anodes for control of reinforcement corrosion", Proceedings of Eurocorr 2008, The European Corrosion Congress “Managing Corrosion for Sustainability”, Edinburgh 7-11 September 2008.

Szklarska-Smialowska, Z., “The Pitting Corrosion of Metals”, Houston, TX: NACE International, (1986), p. 202-212.

Torres-Acosta, A. and Sagüés, A. “Concrete Cracking by Localized Steel Corrosion - Geometric Effects”, ACI Materials Journal, Vol. 101 (2004), p.501

Virmani, Y.P, Clear, K. and Pasko, T., "Time-to-Corrosion of Reinforcing Steel in Concrete Slabs," FHWA-RD-76-70, Federal Highway Administration, Washington, DC (1983).

Whitmore, D. and Abbott, S., “Using Humectants to Enhance the Performance of Embedded Galvanic Anodes”, Paper No. 03301, Corrosion/2003, NACE International, Houston, (2003).

APPENDICES

Appendix A: Computation of Polarization Distribution in a Reinforcing Steel Member – Model Validation

A.1 Objective and Approach

While based on sound principles, the 1-D model that was used in Chapter 5 to estimate the extent of cathodic polarization provided to a generic repair configuration involved numerous simplifications and assumptions in the interest of practical implementation. Validation of the model projections by comparison against a well characterized actual system is therefore highly desirable. The test yard slabs have a simple reinforcement and concrete configuration suitable for such comparison. In this section, the model was applied to compute the extent of polarization delivered to the passive rebars in the yard slabs by the sacrificial point anodes at various ages.

The model was adapted with minimum changes to simulate the actual physical system. The same computational array used for the model calculations was implemented but the number of consecutive nodes was changed to 12 to exactly match the existing number of rebar segments in the slabs. Under those conditions Eq. 8 in finite difference form is the same as that of a circuit network with resistance between concrete nodes corresponding to the actual concrete resistance between planes centered on consecutive rebars, and potentials equal to those of the concrete on the nodes, as illustrated in Figure 43.

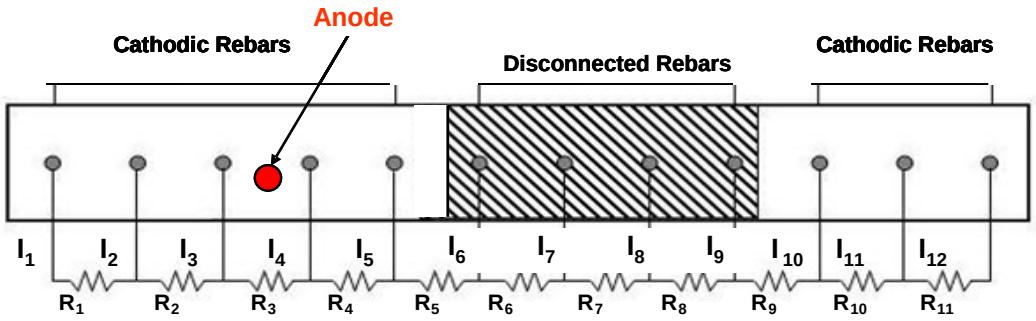

Figure 43 - Circuit network equivalent for model validation. Configuration modeled corresponds to the testing of the 2nd set of anodes. I_6 to I_9 = 0.

The model in Chapter 5 was implemented with one anode placed at the grid node corresponding to the repair patch end. For the validation calculations it was chosen to represent the case where the 2nd set of anodes was tested, so the anode position was located between rebars No. 3 and 4. This condition was modeled by associating nodes 3 and 4 each with one fictitious half-anode. For such half-anode, the PF has for a given potential one half of the current of the actual anode, and the current constriction resistance is twice as large as that of the actual anode. Those provisions offer internal consistency since the parallel combination of both halves would then behave electrically equivalent to one full anode. Also as during the evaluation of the 2nd set of anodes, where rebars 6 though 9 were disconnected, the corresponding nodes were assigned zero sink current. The boundary conditions at each end were specified similar to that of the remote end in the model in Chapter 5 (Eq.7).

A.2 Procedure

The validation calculations were made to correspond to conditions during the testing of the 2nd set of both types of anodes at ages 4 and 13 months. The following model inputs were used:

a. PF for both ages calculated using the global fit equations 15 to 18 with parameters listed in Table 3.
b. Concrete resistivity for the chloride-free and chloride-rich zones. The values used, 25 kΩ-cm and 12.5 kΩ-cm respectively corresponded to the average of the temperature-corrected data for the period between days 1045 and 1550 in Figure 34, representative of the conditions prevalent at the two selected 2nd set anode ages.
c. Steel polarization function as abstracted per Eq. (13) from the data in Figure 33, with parameters listed in Table 3.
d. Slab dimensions per Figure 7.
e. Steel placement density = 0.0906 computed from rebar nominal size and slab dimensions.

The model inputs were used to calculate the secondary expressions for rebar and anode current constriction resistances, and numeric solution was conducted in the same manner as indicated earlier.

The model outputs for the purposes of validation comparisons were, for each rebar No. i that was connected to the anode at anode age t:

a. The values of the potential Es (i,t)
b. The values of the net cathodic rebar current I(i,t)

The difference P(i,t) = Esu – Es (i, t) for each rebar[5] was calculated as a secondary output from the above and reported as the projected steel polarization in each case.

[5] It is recalled the Esu is the value of the potential of unpolarized (open circuit) passive rebar.

A.3 Results and Discussion

The model output values of P(i,t) and I(i,t) were compared with the 4h steel depolarization values and individual temperature corrected rebar currents, averaged for each group of 3 slabs, measured at the respective anode ages. Tables 6 and 7 presents all the model results and the corresponding experimental data used for C and W anodes respectively. It is emphasized that other than adapting for system configuration and concrete resistivity the parameter inputs used in the model calculations were the same as those used for the overall calculations in Chapter 5, and that no parameter adjustment took place to normalize or condition the fit between the computed and measured amounts.

The results are shown in graphic form in Figures 44 and 45 for the C anodes at ages 4 and 13 mo respectively, and similarly in Figures 46 and 47 for the W anodes. Comparisons are made only for the rebars that were connected to the anodes at the time, since the others (No. 6-9) were in the open circuit condition and not forming part of the overall galvanic macrocell. Their open circuit potential values corresponded to a mixed potential determined in the anodic component by active steel dissolution in chloride contaminated concrete, a condition not addressed by the model so no comparisons for potential were made for those rebars. Moreover, since those rebars were placed crosswise to the main electrolytic current flow and of small dimensions compared to the concrete bulk, they represented only a minor disruption of the current distribution pattern so any residual effect on the rest of the system was ignored.

In all cases the pattern shapes of model steel polarization and galvanic current distribution matched well those observed experimentally. Those patterns included maxima at or between rebars No. 3 and 4 which are on either side of the anode, and decay away from the anode in comparable proportions including substantially smaller amounts for the rebars at the other end of the slab. The model also replicated for both types of anodes the pattern of decreasing extent of polarization as anode age increased from 4 to 13 months.

Appendix A: (Continued)

Table 6 - Model output and experimental data for C anodes at ages 4 and 13 months.

C anodes 4 mo									
Depolarization(V)									
Rebar #		1	2	3	4	5	10	11	12
C Exp	1	0.117	0.135	0.175	0.157	0.166	0.063	0.054	0.054
C Exp	3	0.162	0.189	0.229	0.195	0.180	0.091	0.101	0.081
C Exp	5	0.136	0.130	0.193	0.174	0.166	0.098	0.086	0.082
C Exp	Average	0.138	0.151	0.199	0.175	0.170	0.084	0.080	0.072
C Model		0.155	0.177	0.219	0.219	0.178	0.108	0.092	0.085

Current (uA)									
Rebar #		1	2	3	4	5	10	11	12
C Exp	1	55	99	272	248	91	75	28	13
C Exp	3	48	86	208	258	133	26	15	14
C Exp	5	38	70	152	243	95	27	10	13
C Exp	Average	47	85	211	250	106	43	18	14
C Model		94	138	286	286	139	39	28	24
C anodes 13 mo									
Depolarization(V)									
Rebar #		1	2	3	4	5	10	11	12
C Exp	1	0.097	0.113	0.151	0.135	0.129	0.060	0.059	0.057
C Exp	3	0.156	0.176	0.187	0.180	0.166	0.087	0.086	0.087
C Exp	5	0.146	0.168	0.210	0.176	0.163	0.109	0.095	0.093
C Exp	Average	0.133	0.152	0.183	0.164	0.153	0.085	0.080	0.079
C Model		0.123	0.138	0.168	0.167	0.136	0.085	0.074	0.068

Current (uA)									
Rebar #		1	2	3	4	5	10	11	12
C Exp	1	48	84	202	164	95	71	20	10
C Exp	3	34	59	116	136	89	21	12	10
C Exp	5	27	55	97	143	76	22	6	10
C Exp	Average	36	66	138	148	87	38	13	10
C Model		52	68	117	116	66	24	18	16

Appendix A: (Continued)

Table 7 - Model output and experimental data for W anodes at ages 4 and 13 months.

W anodes 4 mo									
Depolarization(V)									
Rebar #		1	2	3	4	5	10	11	12
W Exp	1	0.148	0.166	0.213	0.165	0.158	0.079	0.078	0.070
W Exp	3	0.164	0.175	0.235	0.166	0.168	0.092	0.078	0.066
W Exp	5	0.148	0.162	0.202	0.159	0.180	0.075	0.090	0.085
W Exp	Average	0.153	0.168	0.217	0.163	0.169	0.082	0.082	0.073
W Model		0.142	0.161	0.198	0.198	0.160	0.098	0.085	0.078

Current (uA)									
Rebar #		1	2	3	4	5	10	11	12
W Exp	1	55	99	272	248	91	75	28	13
W Exp	3	48	86	208	258	133	26	15	14
W Exp	5	38	70	152	243	95	27	10	13
W Exp	Average	47	85	211	250	106	43	18	14
W Model		74	103	198	198	103	31.56	23.59	20.35

W anodes 13 mo									
Depolarization(V)									
Rebar #		1	2	3	4	5	10	11	12
W Exp	1	0.146	0.166	0.188	0.163	0.145	0.075	0.082	0.087
W Exp	3	0.119	0.130	0.151	0.112	0.110	0.049	0.039	0.035
W Exp	5	0.140	0.142	0.159	0.154	0.140	0.090	0.095	0.088
W Exp	Average	0.135	0.146	0.166	0.143	0.131	0.071	0.072	0.070
W Model		0.105	0.116	0.139	0.138	0.114	0.072	0.063	0.059

Current (uA)									
Rebar #		1	2	3	4	5	10	11	12
W Exp	1	30	42	85	88	46	28	6	7
W Exp	3	33	43	55	72	53	41	-20	12
W Exp	5	30	36	77	64	67	9	4	3
W Exp	Average	31	40	72	74	55	26	-4	7
W Model		36	45	69	68	43	18	14	13

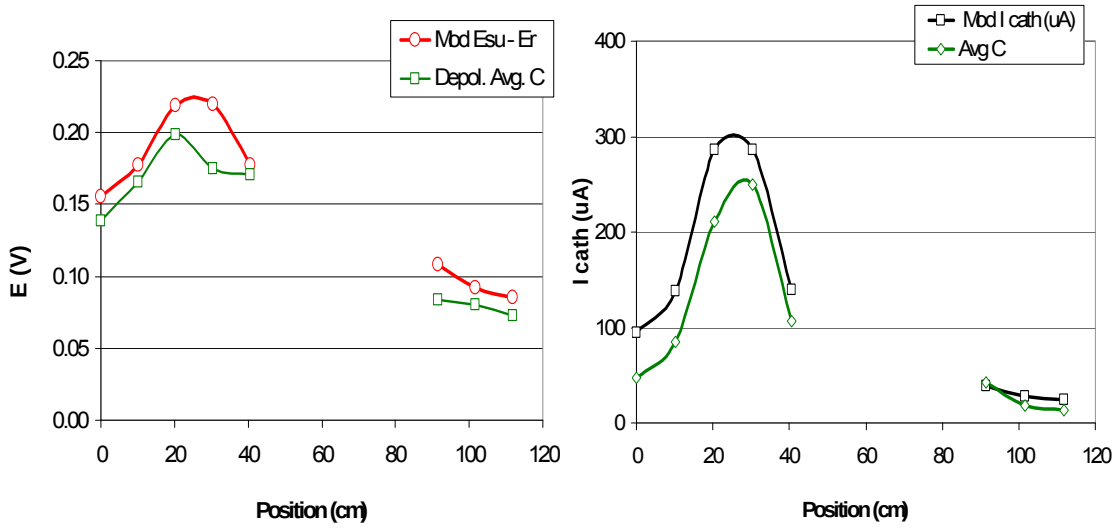

Figure 44 - Experimental and modeled values of polarization and cathodic current for rebars connected to the main Type C anode 2nd Set (4 months anode age). Rebar positions measured from the slab edge next to Rebar No.1.

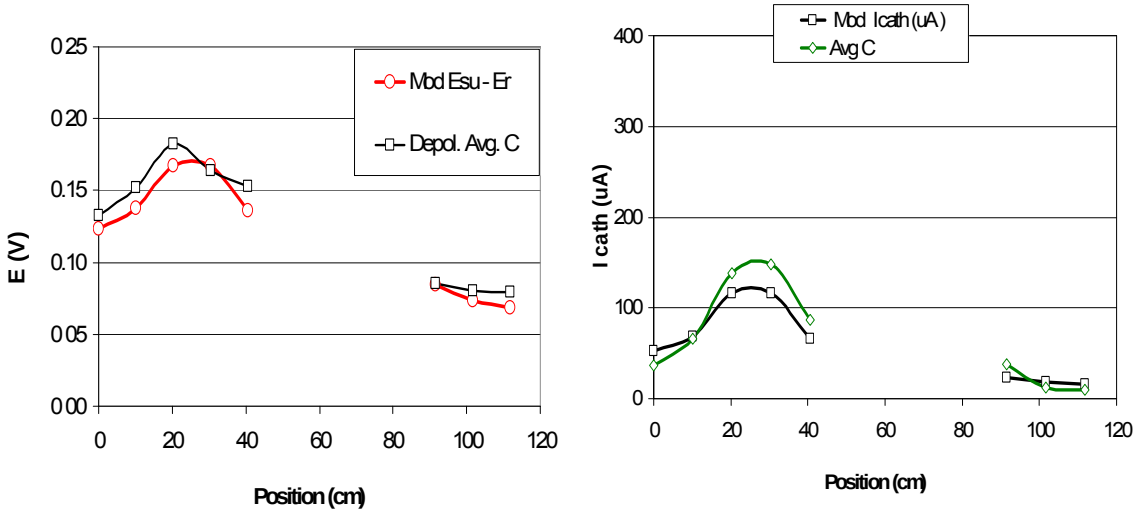

Figure 45 - Experimental and modeled values of polarization and cathodic current for rebars connected to the main Type C anode 2nd Set (13 months anode age). Rebar positions measured from the slab edge next to Rebar No.1.

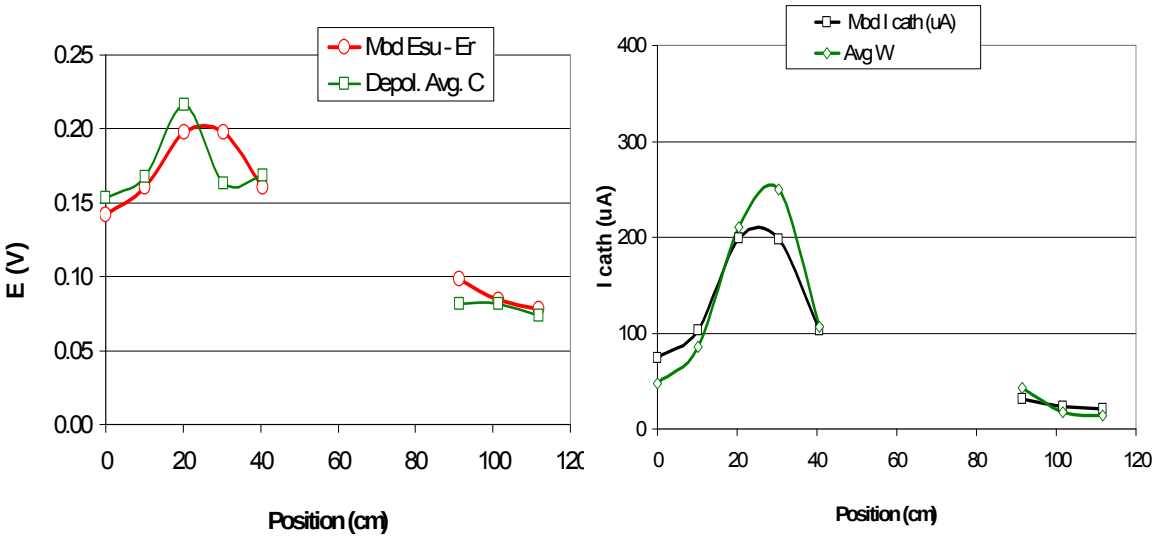

Figure 46 - Experimental and modeled values of polarization and cathodic current for rebars connected to the main Type W anode 2nd Set (4 months anode age). Rebar positions measured from the slab edge next to Rebar No.1.

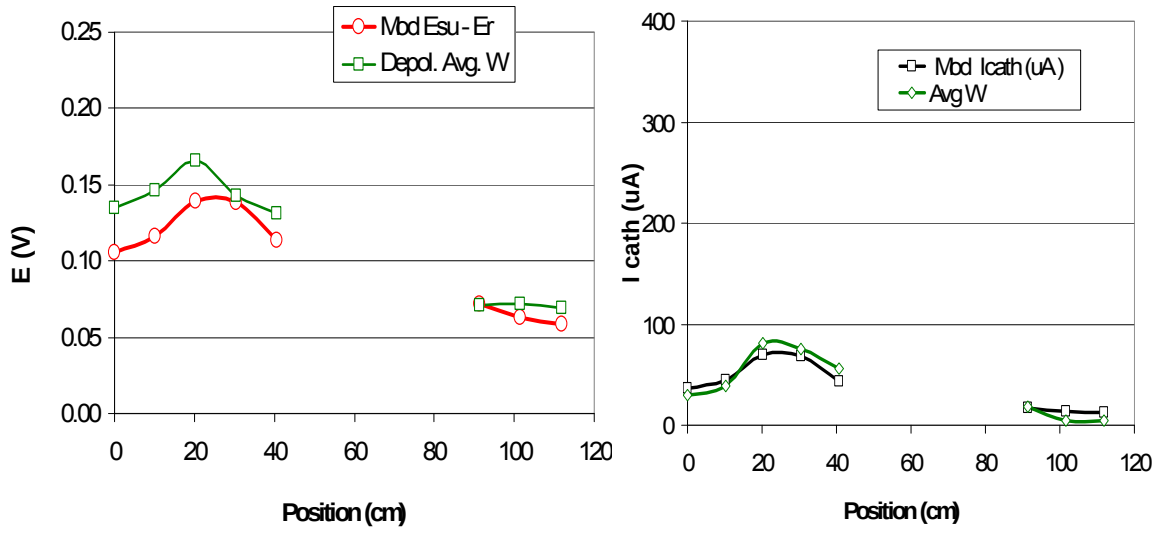

Figure 47- Experimental and modeled values of polarization and cathodic current for rebars connected to the main Type W anode 2nd Set (13 months anode age). Rebar positions measured from the slab edge next to Rebar No.1.

Quantitative agreement between model and experimental observations is readily assessed in the graphic comparison in Figures 48 and 49 for C and W anodes respectively, where the model and experimental values are plotted as function of each other and contrasted against an ideal 1:1 agreement line. In keeping with the Tafel-like behavior of the cathodic reaction over much of the range of interest, comparisons between model and experimental polarization results were considered in terms of potentials differences, while comparisons of currents were made in terms of ratios given the near exponential current-potential relationship over the same range. In addition, the extent of agreement was evaluated numerically as shown in Table 8. There for each anode type and age condition examined the differences of model minus experimental polarization values of the 8 rebars (average of 3 slabs) were computed, and an average and standard deviation obtained. Similar calculations were performed for the ratios of model to experimental cathodic current. The results showed that model and experimental polarizations were typically on average within < 20 mV of each other, with standard deviation <20 mV. Likewise, model cathodic currents were typically within a multiplying/dividing factor of 1.5 of those obtained experimentally.

Table 8 - Deviations between model output and experimental data.

Anode / Age	Pmodel - Pexp		I cath model / I cath exp	
	Average	St Dev	Average	St Dev
C / 4 mo	0.021	0.011	1.460	0.349
C / 13 mo	-0.009	0.007	1.060	0.370
W / 4 mo	0.002	0.017	1.13	0.32
W / 13 mo	-0.02	0.012	1.41	0.83

The quantitative comparison showed agreement between model and experimental behavior that was generally close, comparable to the variability observed between the experimental results of replicate slabs in Tables 6 and 7. Together with the agreement with spatial polarization patterns and time evolution behavior documented above, these findings support the validity and applicability of the model.

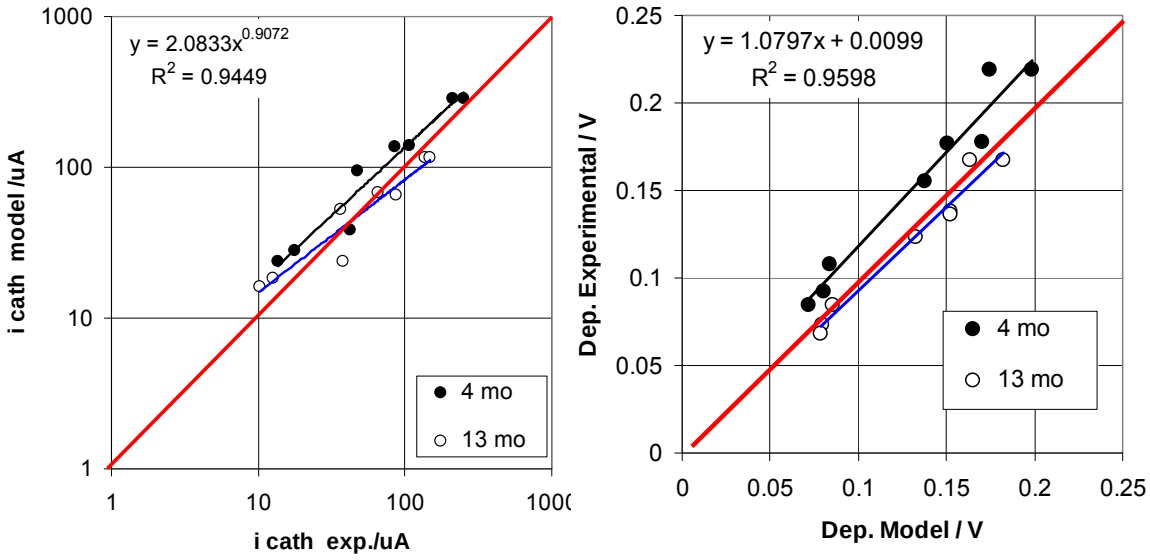

Figure 48 - One-on-one comparison of model output and experimental values for C anodes. 4 mo (black circles) and 13 mo (open circles).

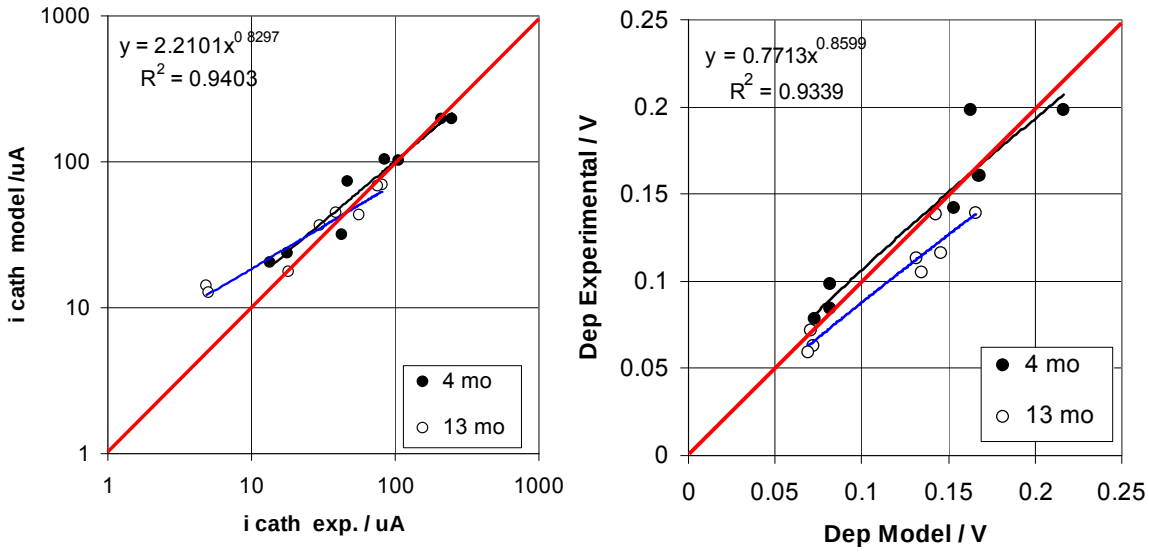

Figure 49 - One-on-one comparison of model output and experimental values for W anodes. 4 mo (black circles) and 13 mo (open circles).

It is noted that the deviation between model and experimental results had often a moderate but clearly systematic component that varied in extent and direction with the anode age considered. This is not surprising considering that the anode polarization functions used, and their time dependence parameters (Eqs. 15 to 18) resulted from a global fit to the behavior of the group of three anodes evaluated in each set over the total test period. Moreover, the cathodic polarization function was also a global fit which had time invariant parameters and fixed concrete resistivity value for each slab zone was used in the model for all the calculations. Such global fits and flat approximations are expected to reasonably reproduce overall trends, but are less likely to precisely capture the instantaneous behavior of the system, therefore giving rise to modest systematic offsets such as those observed here.

In the foregoing the potential model output was considered only as a deviation from the unpolarized condition and compared to experimental results from the 4-hour depolarization measurements which may underestimate to some extent the values that could be obtained after longer disconnection times. Moreover, since the cathodic rebar assembly remained interconnected after the anode was disconnected, some residual macrocell currents between individual rebars may have been still present after only 4 hours. Consequently, comparisons by the same methods used above were made using instead the individual instant-off rebar potentials determined experimentally and those predicted by the model. The extent of agreement between model and experimental values was comparable to that obtained when comparing polarization values, suggesting that the effects of those residual conditions were highly consequential in this case.

A.4 Conclusion

Comparison between model calculations and experimental observations generally supported the validity of the modeling approach for the conditions examined.

ABOUT THE AUTHOR

Margareth Dugarte graduated *Summa cum laude* from Universidad Del Norte (Colombia) in 2004 with a Bachelor's Degree in Civil Engineering. She entered the Ph.D. program in the Civil Engineering Department at the University of South Florida in fall 2005.

While in the Ph.D. program, Ms Dugarte worked as a Graduate Research Assistant in the Corrosion Engineering Laboratory for almost 5 years, she was directly involved in a research project funded by the Florida Department of Transportation. She also worked in several occasions as Teaching Assistant for undergraduate classes.

She has also participated several times in Student research poster presentations at international Conferences, where her hard work was recognized as a recipient of the prestigious Mars Fontana Award at the NACE International Corrosion/2007 conference. She also has published 3 papers in refereed international conference proceedings. She is a student member of the National Association of Corrosion Engineers and the Electrochemical Society.